

UNCLASSIFIED

AD 427273

DEFENSE DOCUMENTATION CENTER

FOR

SCIENTIFIC AND TECHNICAL INFORMATION

CAMERON STATION, ALEXANDRIA, VIRGINIA



UNCLASSIFIED

NOTICE: When government or other drawings, specifications or other data are used for any purpose other than in connection with a definitely related government procurement operation, the U. S. Government thereby incurs no responsibility, nor any obligation whatsoever; and the fact that the Government may have formulated, furnished, or in any way supplied the said drawings, specifications, or other data is not to be regarded by implication or otherwise as in any manner licensing the holder or any other person or corporation, or conveying any rights or permission to manufacture, use or sell any patented invention that may in any way be related thereto.

427273

RTD-TDR-63-4009

64-7

CATALOGED BY DDC
AS AD No. _____

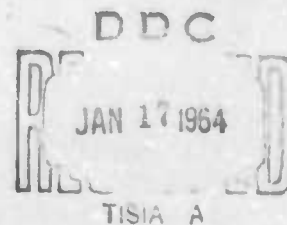
427273

**AN ANALYSIS OF THE EFFECT OF IONIZATION
ON THE LAMINAR FLOW OF A DENSE GAS IN A CHANNEL**

HENRY R. VELKOFF

TECHNICAL DOCUMENTARY REPORT No. RTD-TDR-63-4009

OCTOBER 1963



AIR FORCE AERO PROPULSION LABORATORY
RESEARCH AND TECHNOLOGY DIVISION
AIR FORCE SYSTEMS COMMAND
WRIGHT-PATTERSON AIR FORCE BASE, OHIO

Project No. 3141

NOTICES

When Government drawings, specifications, or other data are used for any purpose other than in connection with a definitely related Government procurement operation, the United States Government thereby incurs no responsibility nor any obligation whatsoever; and the fact that the Government may have formulated, furnished, or in any way supplied the said drawings, specifications, or other data, is not to be regarded by implication or otherwise as in any manner licensing the holder or any other person or corporation, or conveying any rights or permission to manufacture, use, or sell any patented invention that may in any way be related thereto.

Qualified requesters may obtain copies of this report from the Defense Documentation Center (DDC), (formerly ASTIA), Cameron Station, Bldg. 5, 5010 Duke Street, Alexandria 4, Virginia

This report has been released to the Office of Technical Services, U.S. Department of Commerce, Washington 25, D.C., in stock quantities for sale to the general public.

Copies of this report should not be returned to the Aeronautical Systems Division unless return is required by security considerations, contractual obligations, or notice on a specific document.

FOREWORD

This report was prepared by the Air Force Aero Propulsion Laboratory of the Research and Technology Division of the Air Force Systems Command. Dr. Henry R. Velkoff served as project scientist. The work reported herein was accomplished under Project 3141, "Electric Propulsion Technology."

This work is a continuation of a sequence of programs aimed at exploring the basic nature and practical applications of the interactions of electrostatic fields with fluids. The general area has been entitled, "Electrofluid-mechanics." Prior research in this area has included (a) a basic review of possible phenomena, reported in ASD-TR-61-642; (b) a study of electrostatic effects on free convection, reported in ASD-TDR-62-650; (c) a study of electrostatic effects on condensation of vapors, reported in RTD-TDR-63-4008; and (d) an exploratory study of the effects of ions on laminar flow, reported in ASD-TDR-63-842. This report seeks to explain a phenomenon observed in the latter work, ASD-TDR-63-842. This research was accomplished from May 1963 to September 1963.

The author wishes to express his appreciation to those of the Aero Propulsion Laboratory who aided in this program, particularly Mr. Michael Pennucci for his steadfast assistance in performing the many computations necessary in this analysis.

ABSTRACT

An analysis was performed on the actions of ions in a laminar flow stream. The analysis seeks to provide an explanation for the unusually high pressure drops found during a preceding experimental program involving laminar flow of ionized gas with an applied electrostatic field. The analysis revealed that very high pressure drops could be expected and that velocity profile distortions would occur. Good correlation with test data was achieved. A new nondimensional parameter, called the charge number, was introduced. Charge number is related to the Knudsen number and is the controlling parameter for ion action in the gas stream. The conclusion from this work is that ions bound electrically to a flow stream set up an internal field on the stream, and then tend to resist the motion of the stream. This action causes profile distortions and increases effective fluid friction.

This report has been reviewed and is approved.



ROBERT E. SUPP
Asst. Chief, Aerospace Power Division
Air Force Aero Propulsion Laboratory

TABLE OF CONTENTS

	PAGE
Introduction	1
Hypothesis	2
Ion-Flow Interaction	2
Electric-Field and Fluid-Flow Equations	4
Assumptions for Channel Flow	5
Analysis	11
Nondimensional Equations	11
Flat Plate Equations	11
Cylindrical Geometry Equations	13
Equation with Mean Value of Body Force	13
Solution of the Mean Value Equation	14
Equations for Round Tube with Central Wire	17
Charge Density in the Channel	18
Loeb Solution	18
Stuetzer Solutions	19
Charge and Current Density	20
Magnitude of the Influence of Charge Number	22
Solutions for Channel Flow With Charge Present	24
Case I. Parallel Plates, ρ_c Constant	24
Case II. Parallel Plates, ρ_c Variable	26
Case III. Round Tube, ρ_c Constant	27
Case IV. Concentric Tube, ρ_c Constant	28
Case V. Round Tube, ρ_c Variable	29
Case VI. Concentric Tube, ρ_c Variable	31
Other Cases	32

TABLE OF CONTENTS (Continued)

	PAGE
Correlation and Discussion	34
Friction Factor Curves	34
Comparison of Velocity Profiles	35
Comparisons of Friction Factor	36
Effects of Mobility and Nonuniformity of Charge Density	36
Summary	38
Conclusions	40
References	41
Appendix I. Nondimensional Parameters	69
Appendix II. Curves for Calculating Case V and Case VI Velocity Profiles ...	73
Appendix III. Pressure Drop Data and Modified Corona Wire Test	81
Appendix IV. Comparison with Stuetzer's Paper	85

LIST OF ILLUSTRATIONS

FIGURE		PAGE
1	Effect of Ionization on Friction Factor of a Round Duct with Air at One Atmosphere, Positive Corona, Test Data	42
2	Effect of Ionization on Velocity Profiles in Terms of Pressure Tube with Concentric Wire, Positive Corona, Test Data	43
3	Effect of Ionization on Heat Transfer with Air at One Atmosphere in a Round Tube, Positive Corona, Test Data	44
4	Round Tube Channel with Central Wire	45
5	Parallel Plate Flow Channel	45
6	Charge Densities in a Round Tube	46
7	Case I. Theoretical Flat Plate Velocity Distribution, $\rho_c = \text{Constant}$	47
8	Case III. Theoretical Round Tube Velocity Distribution, $\rho_c = \text{Constant}$..	48
9	Theoretical Concentric Tube Velocity Distribution Case IVb and IVc, $\rho_c = \text{Constant}$ in Tube	49
10	Theoretical Concentric Tube Velocity Distribution Case IV, $\rho_c = \text{Constant}$ in Tube	49
11	Case V. Variation of Velocity Distribution at Constant Pressure Drop and with $\rho_c \propto \eta^{-\frac{1}{2}}$	50
12	Case V. Velocity Profiles for Round Tube	51
13	Case VI. Velocity Profile for Concentric Tube	52
14	Velocity Profile for $\rho_c \propto \eta^{-2}$	53
15	Effect of Charge Number on i_D . Mean Value Approach	54
16	Variation of Friction Factor with Charge Number	55
17	Typical velocity Distributions at $w_m = 1 \text{ ft/sec.}$	56
18	Typical Profiles in Terms of Pressure	57
19	Velocity Profile Without Ionization. Concentric 0.0005-Inch Wire. $w_m = 2.35 \text{ ft/sec}$	58
20	Velocity Profile Data, $N_{Re} = 1200$	58
21	Velocity Profile Data, $N_{Re} = 1190$	59

LIST OF ILLUSTRATIONS (Continued)

FIGURE		PAGE
22	Velocity Profile Data, $N_{Re} = 1450$	60
23	Velocity Profile Data, $N_{Re} = 1745$	61
24	Velocity Profile Data, $N_{Re} = 2070$	62
25	Exploratory Test Data Showing Variation of f_D with Charge Number for Air	63
26	Variation of f_D with Charge Number for Air	64
27	Variation of f_D with Charge Number for Oxygen	65
28	Variation of f_D with Charge Number for Carbon Dioxide	66
29	Effect of Charge Number on f_D for Nitrogen	67
II-1 thru II-10	Universal Curves for Calculating Velocity Profiles, Cases V and VI	74-79
III-1	Pressure Drop vs. Corona Current, Exploratory Sequence for Oxygen, Wire Positive	82
III-2	Pressure Drop vs. Corona Current Exploratory Sequence for Air, Wire Positive	82
III-3	Pressure Drop vs. Corona Current for CO_2 , Wire Positive	83
III-4	Pressure Drop vs. Corona Current for Stored CO_2 , Modified Positive Wire	84

LIST OF SYMBOLS

A	area
A_1	constant defined by Equation (168)
α	selected constant
B_1	constant defined by Equation (169)
\bar{c}	mean speed of molecules, meters/sec
D	total derivative operator
D_1	parameter defined by Equation (171)
D_0	parameter defined by Equation (172)
D_R	parameter defined by Equation (173)
D_H	hydraulic diameter, $4A/\text{wetted perimeter}$
\bar{E}	electrical field strength, volts/meter
E_j	electrical field in direction indicated by subscript
\bar{F}	body force in fluid stream, newtons/cubic meter
F_z	body force in z direction
F_{zm}	mean value of F_z
f_B	Blasius friction factor
f_D	Darcy friction factor, $f_D = 4f_B$
g	gravitational constant
\bar{H}	magnetic field strength
h	half height of flat channel
I_n	imaginary Bessel function of order n
\hat{i}	unit vector in x direction
i	index indicating direction
i	current, amperes
i_y	current in y direction
i_z	current in z direction

LIST OF SYMBOLS (Continued)

\bar{J}	current density, amperes/sq meter
J_y	current density in y direction
J_z	current density in z direction
J_w	current density in r or y direction at the wall
\hat{j}	unit vector in y direction
j	index indicating direction
K	ion mobility - meters squared/volt-sec
K_n	imaginary Bessel function of order n
\hat{k}	unit vector in z direction
L	reference length
ℓ	length
M_a	Mach number
M	Hartmann number
m	mass of molecule
m_i	mass of ion
N	molecular number density, molecules/cubic meter
N_i	ion number density, ions/cubic meter
N_{Re}	Reynolds number
N_{Pc}	charge number
N_{Rc}	charge Reynolds number
N_{Kn}	Knudsen number
P_e	term defined by Equation (81)
Δp	pressure drop in pipe, test data
p	pressure, newtons/sq meter
p^*	dimensionless pressure, $\frac{p}{\left(\rho \frac{u_w^2}{2}\right)}$
q	charge of an ion, coulombs

LIST OF SYMBOLS (Continued)

R_g	perfect gas constant
R	inside radius of round tube
r	direction along radius
r_c	distance to edge of corona
r_w	wire radius
T	temperature
t	time
u	velocity in x direction
u^j	velocity in j^{th} direction
u_i^j	ion velocity in j^{th} direction
u_R^j	relative velocity of ion in j^{th} direction
V	applied potential, volts
v	velocity along r or y coordinate
v_i	ion velocity along r or y coordinate
v_R	relative velocity of ion
W	dimensionless velocity
$W. P.$	wetted perimeter
w	velocity in z direction
w_m	mean stream velocity in channel
w_{max}	maximum velocity in z direction
x	coordinate direction
y	axis normal to flow
z	coordinate direction along axis of channel
α	parameter defined by Equation (147)
β_i	parameter defined by Equation (170)
γ_i	parameter, $\left(\frac{R^2}{\mu K} \right) \left(\frac{\epsilon J_w}{KR} \right)^{1/2}$

LIST OF SYMBOLS (Continued)

ϵ	permittivity, farads/meter
ϵ_0	permittivity of free space, 8.85×10^{-12} farads/meter
ζ	dimensionless distance $\frac{z}{h}$ or $\frac{z}{R}$
η	dimensionless distance, either $\frac{r}{R}$ or $\frac{y}{h}$
η_0	value of η near the centerline
λ	mean free path of molecules, meters
λ_i	mean free path of ions
λ_1	variable, $\lambda_1 = \frac{4}{3} \alpha \eta^{3/4}$
μ	kinematic viscosity
μ_e	permeability of medium
μ_E	apparent electroviscosity
ξ	variable defined as $\xi = \frac{4}{3} \gamma_1^{1/2} \eta^{3/4}$
ρ	fluid density, Kg/cubic meter
ρ_c	charge density, coulombs/cubic meter
ρ_{cm}	mean charge density, $\rho_{c0} = \rho_{cm}$
ρ_c^*	dimensionless charge, ρ_c / ρ_{cm}
σ	electrical conductivity, mhos/meter

INTRODUCTION

During an exploratory investigation into the effects of ionization on the flow of gases in a channel, unusually high pressure drops were observed when ionization was present in the channel. Complete details of that investigation may be found in Reference 1. In that work, gases, such as air, were passed through a 1-1/4-inch-diameter pipe in which a 0.004-inch-diameter wire was located concentrically. A high voltage applied to the wire resulted in a corona discharge that provided ions in the gas stream. Under the action of the field, pressure drops in the pipe were doubled, velocity profiles were distorted, and heat transfer was doubled. Typical data shown in Figures 1, 2, and 3 illustrate the type of changes observed with the ion-gas interaction. Figure 1 shows that data for a given value of current fall on lines that are parallel to, but displaced above, the theoretical $64 / N_{Re}$ line. This indicates that the flow tends to retain its laminar character even under the influence of the field. Figure 1 also indicates that little influence is exerted in the turbulent flow regime.

The velocity profile data of Figure 2 are given in terms of the total pressure as measured with a glass total head probe. The velocity profiles without field applied illustrate the distortions due to the presence of the wire alone. When the ions traverse the stream, very large changes in the shape of the profiles are evident. Although the data presented are not precise in the vicinity of the wall, the general pattern indicates a flattening of the profile and a corresponding steepening of the gradient at the wall. This action is in the correct direction to cause increases in pressure drop, or Δp , as shown in Figure 1. Data on heat transfer shown in Figure 3 provides further evidence of the effect of ions on fluid behavior.

Several possible mechanisms that could account for the phenomenon are discussed in Reference 1. It was concluded that none of those mechanisms accurately described the phenomenon, nor did they fit the data presented. This report puts forth a hypothesis which attempts to explain the nature of the phenomenon. A series of models based upon selected approximations is presented to describe the pressure drop increase and to indicate possible effects on the velocity profile. Comparisons are then drawn between the models and the data.

HYPOTHESIS

Two approaches will be taken in considering the actions of the ions on the stream. The first is based upon physical insight to the problem and the second is a more formal mathematical approach.

ION-FLOW INTERACTION

In considering the physical aspects of the problem, it is helpful to utilize several highly idealized models as well as the concentric tube actually used in the tests. As shown in Figure 4, the gas flows down the channel in the z direction. The electrical field is applied between the wire and the tube wall. Ions created by the corona discharge drift from the wire to the wall under the action of the field, and at the same time tend to be dragged downstream with the flow. The order of magnitude of the velocity normal to the flow can be obtained from the mobility equation for ions in a gas (Ref. 2):

$$v_i = \kappa E_r \quad (1)$$

where v_i is the ion velocity normal to the stream,

κ is the mobility of the ion, and

E_r is the electrical field strength.

For the case under consideration, typical values are:

$$\kappa = \frac{2.0 \times 10^{-4} \text{ m}^2}{\text{volt-sec}}$$

and

$$E = 5 \times 10^5 \text{ volts/m.}$$

Thus, v_i is of the order of 100 m/sec.

In the case of laminar flow with air at standard conditions, $w_m = 1$ m/sec, where w_m is the mean stream velocity. If the ion is dragged downstream with the flow, it will acquire approximately this value of axial drift velocity. The net effect of this condition is that the ion travels almost directly across the channel under the influence of the applied field.

If the above description is assumed valid, then it does not appear possible for the ions to interact with the flow stream. Another interpretation, however, is also possible. If the ions were to drift at all, then this would imply that some of them would be carried out of the pipe at the end. Such an action would violate the condition of current continuity, that is, the ions leaving the wire must collect on the outer electrode in order to complete the electrical circuit. If this condition is met, then the ions must try to stay within the confines of the pipe. To do so, some type of internal field must exist to cause the ions to move in opposition to the flow. As a first order approximation, it can be assumed that the ions resist being dragged by the axial velocity of the stream, and as a limiting case would tend to move directly across the stream without any net w velocity. For this limiting case, the ions, on the average, would tend to remain stationary relative to a given position along the pipe as they move in the radial direction under the action of the applied field. The velocity of the ion is given by:

$$u_i^j = u^j + u_R^j \quad (2)$$

where u^j is the stream velocity in j^{th} direction,

u_i^j is the ion velocity in the j^{th} direction, and

u_R^j is the ion velocity relative to the stream velocity.

The mobility equation for an ion, in general form, is:

$$u_R^j = K E^j \quad (3)$$

and in the radial direction is:

$$\begin{aligned} v_i &= v + v_R \\ &= v + K E_r \end{aligned} \quad (4)$$

But the average stream velocity in the r direction, v , is zero. Hence,

$$v_i = K E_r,$$

which is Equation (1). In the case of the axial motion

$$w_i = w + w_R \quad (5)$$

$$w_i = w + K E_z \quad (6)$$

If the ion drifts with the stream, then w_R is zero and $w = w_i$, and no field exists. If, however, the other limiting case applies, w_i goes to zero since the ions remain stationary relative to the walls. In this case:

$$\begin{aligned} w_i &\rightarrow 0 \\ w &= -K E_z \end{aligned}$$

This equation indicates that an internal field may be established in the gas stream which is a function of the stream velocity and mobility:

$$E_z = f\left(\frac{w}{K}\right) \quad (7)$$

As a limiting case,

$$E_z = -\frac{w}{K} \quad (8)$$

An estimate of the order of magnitude of the electrical fields involved can be determined by using Equation (8) and assuming typical values for K and w ,

Let:

$$K = 2.0 \times 10^{-4} \text{ m}^2 / \text{volt-sec} \quad \text{and} \quad w = 1 \text{ m/sec.}$$

Then:

$$E_z = -\frac{w}{K}$$

$$E_z = -50 \text{ volts/cm.}$$

Thus, the induced fields are small relative to the applied radial fields.

If the usual assumptions for laminar Hagen-Poiseuille flow are made, the Navier-Stokes equations become:

$$\mu \nabla^2 w = -\frac{\partial p}{\partial z} + F_z \quad (9)$$

where p is the pressure, F_z is the body force in the z direction, and μ is the viscosity of the gas. Assuming the only active body force is due to charge action in the stream,

$$F_z = \rho_c E_z \quad (10)$$

where ρ_c is the scalar charge density:

$$\mu \nabla^2 w - \frac{\partial p}{\partial z} + \rho_c E_z = 0. \quad (11)$$

Substituting Equation (8),

$$\mu \nabla^2 w - \rho_c \frac{w}{K} = \frac{\partial p}{\partial z}. \quad (12)$$

This equation can be solved once a charge density distribution is known using the usual assumption that $\partial p / \partial z$ is a constant for fully established steady-state pipe flow. This equation represents the limiting case for $w_i = 0$.

Before considering solutions to this equation, a more extensive consideration will be given to the effect of current continuity on the ion motion phenomenon. The equations applicable to the problem at hand are a combination of electric-field and fluid-flow equations (Ref. 3). The problem attacked here is that of the isothermal flow case; the energy equation is not included since the energy of corona discharge is so small (Ref. 1).

ELECTRIC-FIELD AND FLUID-FLOW EQUATIONS

$$p = \rho g R_g T \quad (13)$$

$$\frac{\partial p}{\partial t} + \frac{\partial}{\partial x_j} (\rho u_j) = 0 \quad (14)$$

$$\rho \frac{Du_j}{Dt} = -\frac{\partial p}{\partial x_j} + \mu \nabla^2 u_j + \frac{\mu}{3} \frac{\partial \Delta}{\partial x_j} + F_j \quad (15)$$

$$\Delta = \frac{\partial u_j}{\partial x_j} \quad (16)$$

$$F_j = \rho_c E_j + \mu_e (\bar{J} \times \bar{H}) + \frac{\epsilon_0}{2} \rho \nabla \left[E^2 \left(\frac{\partial \epsilon}{\partial \rho} \right)_T \right] - \frac{\epsilon_0 E^2}{2} \left(\frac{\partial \epsilon}{\partial T} \right)_\rho \nabla T \quad (17)$$

$$\nabla \times \bar{H} = \bar{J} + \frac{\partial \epsilon \bar{E}}{\partial t} \quad (18)$$

$$\nabla \times \bar{E} = -\frac{\partial \mu_e \bar{H}}{\partial t} \quad (19)$$

$$\frac{\partial \rho_c}{\partial t} + \frac{\partial J^j}{\partial x_j} = 0 \quad (20)$$

$$J^j = i^j + \rho_c u_i^j = \sigma [E_j + \mu_0 (\bar{u} \times \bar{H})] + \rho_c u_i^j \quad (21)$$

$$\nabla \cdot \bar{H} = 0 \quad (22)$$

$$\nabla \cdot \bar{E} = \frac{\rho_c}{\epsilon} \quad (23)$$

$$u_R^j = K E^j \quad (3)$$

ASSUMPTIONS FOR CHANNEL FLOW

The following assumptions are made:

1. The stream velocities are very low, of the order of 0 to 2 meters/second, and $M_0 \rightarrow 0$.
2. The fluid is incompressible.
3. Flow is steady-state; no local time derivatives exist.
4. Flow is fully established in the channel; the entrance region will not be considered.
5. There are no gravitational body forces; in the isothermal case, this is considered a valid assumption.
6. No magnetic effects are present. No external magnetic fields are applied, and the currents involved are so small as to make induced magnetic fields negligible. No time-changing electrical or magnetic fields are present.
7. The nonuniform gradient terms are small relative to any charge motion effects. This is particularly true for a nonpolar gas, but it may not be always true for polar liquids when highly nonuniform gradients are present.
8. The electrical conductivity, σ , of the gas is extremely small. It is assumed that all current is due to the ion motion.

With these assumptions, the field and flow equations become:

$$\frac{\partial u_j}{\partial x_j} = 0 \quad (24)$$

$$\rho u^k \frac{\partial u^j}{\partial x^k} = - \frac{\partial p}{\partial x_j} + \mu \nabla^2 u_j + F_j \quad (25)$$

$$F_j = \rho_c E_j \quad (26)$$

$$\nabla \times \bar{E} = 0 \quad (27)$$

$$\frac{\partial \rho_c}{\partial t} + \frac{\partial J^j}{\partial x^j} = 0 \quad (28)$$

$$J^j = \sigma E^j + \rho_c u_i^j \quad (29)$$

$$\nabla \cdot \bar{E} = \frac{\rho_c}{\epsilon} \quad (30)$$

$$u_R^j = \kappa E^j \quad (3)$$

Considering Equations (30) and (26):

$$\begin{aligned} \rho_c &= \epsilon \nabla \cdot \bar{E} \\ F_j &= \rho_c E_j = \epsilon E_j \nabla \cdot \bar{E} \\ F_j &= \epsilon E_j \left(\frac{\partial E^k}{\partial x^k} \right) \end{aligned} \quad (31)$$

For cartesian coordinates:

$$\begin{aligned} \bar{F} &= \hat{i} \left[\epsilon E_x \left(\frac{\partial E_x}{\partial x} + \frac{\partial E_y}{\partial y} + \frac{\partial E_z}{\partial z} \right) \right] \\ &+ \hat{j} \left[\epsilon E_y \left(\frac{\partial E_x}{\partial x} + \frac{\partial E_y}{\partial y} + \frac{\partial E_z}{\partial z} \right) \right] \\ &+ \hat{k} \left[\epsilon E_z \left(\frac{\partial E_x}{\partial x} + \frac{\partial E_y}{\partial y} + \frac{\partial E_z}{\partial z} \right) \right] \end{aligned} \quad (32)$$

Thus, the body force can be expressed explicitly if either the charge density distribution or the field is known. In the case of two-dimensional flow between flat plates with a two-dimensional field, Equation (32) becomes:

$$F_y = \frac{\epsilon}{2} \frac{\partial E_y^2}{\partial y} + \epsilon E_y \frac{\partial E_z}{\partial z} \quad (33)$$

$$F_z = \epsilon E_z \frac{\partial E_y}{\partial y} + \frac{\epsilon}{2} \frac{\partial E_z^2}{\partial z} \quad (34)$$

The terms on the trace represent the gradient of the ordinary electrostatic pressure rise. The other terms indicate the possible cross influences. In particular, if any E_z field at all exists in the flow, the $\partial E_y / \partial y$ term may be large enough to be significant.

With no sources of ions throughout the stream, a quasi-steady-state process exists. Then Equation (28) becomes:

$$\frac{\partial J^j}{\partial x^j} = 0. \quad (28a)$$

For example, consider the parallel plate case again. Using Equations (28a) and (29) with $\sigma = 0$,

$$\frac{\partial J^j}{\partial x^j} = \frac{\partial \rho_c u_i^j}{\partial x^j} = 0. \quad (35)$$

For the two-dimensional case:

$$\frac{\partial \rho_c v_i}{\partial y} + \frac{\partial \rho_c w_i}{\partial z} = 0. \quad (36)$$

As an analogous case to the flow of ions from the wire to the wall, assume that the corona discharge takes place at the flat channel wall and the ions drift across the space to the other wall. In this case, the net ion current, i , will be given by:

$$i = J_y A \quad (37)$$

where A = the cross section of the flat plate over which the fluid flows.

$$i = \rho_c v_i A. \quad (38)$$

Although ρ_c and v_i vary with y , i is a constant. Substituting Equation (38):

$$\frac{i}{A} \frac{\partial \rho_c v_i A}{\partial y} + \frac{\partial \rho_c w_i}{\partial z} = 0. \quad (39)$$

Therefore:

$$\frac{\partial \rho_c w_i}{\partial z} = 0 \quad (40)$$

$$\rho_c w_i = f(y) \quad (41)$$

$$\rho_c w + \rho_c w_R = f(y) \quad (42)$$

$$\rho_c (w + KE_z) = f(y). \quad (43)$$

For fully established flow,

$$w = f_1(y) \text{ only.} \quad (44)$$

For ρ_c constant,

$$E_z = f_2(y). \quad (45)$$

Let:

$$w = \sum_{n=0,1}^{\infty} a_n y^n \quad (46)$$

$$E_z = \sum_{n=0,1}^{\infty} b_n y^n \quad (47)$$

From Equation (29),

$$J^j = \rho_c (u^j + u_R^j) + \sigma E^j \quad (29)$$

For $\sigma \rightarrow 0$

$$J^j = \rho_c (u^j + u_R^j) \quad (48)$$

Substituting Equation (3):

$$J^j = \rho_c (u^j + KE^j) \quad (49)$$

In the y direction:

$$J_y = \rho_c v + \rho_c KE_y \quad (50)$$

Since $v = 0$ in channel flow:

$$J_y = \rho_c v_R = \rho_c KE_y \quad (51)$$

This is the equation of current density for the case of corona discharge in a gas with parallel electrodes. In the z direction:

$$J_z = \rho_c w + \rho_c KE_z \quad (52)$$

The physical conditions on the test require that no net current flows out the ends of pipe:

$$I = \int_A J_z dA = 0 \quad (53)$$

$$\int_A \left(\frac{\rho_c w}{k} + \rho_c E_z \right) dA = 0 \quad (54)$$

Therefore:

$$\int_A (\rho_c E_z) dA = - \frac{1}{k} \int_A \rho_c w dA \quad (55)$$

Consider two-dimensional channel flow with a channel of height $2h$; Equation (55) then becomes:

$$\int_{-h}^h \rho_c E_z dy = - \frac{1}{k} \int_{-h}^h \rho_c w dy$$

Letting

$$\eta = \frac{y}{h}$$

$$h \int_{-1}^1 \rho_c E_z d\eta = - \frac{h}{K} \int_{-1}^1 \rho_c w d\eta .$$

Rewriting, Equations (46) and (47) become:

$$w = \sum A_n \eta^n ; E_z = \sum B_n \eta^n$$

and letting ρ_c be constant:

$$\int_{-1}^1 \sum (A_n + K B_n) \eta^n d\eta = 0$$

$$\sum_{n=0,1,2}^{\infty} (A_n + K B_n) \frac{\eta^{n+1}}{n+1} \Big|_{-1}^1 = 0 .$$

If this function were evaluated over an indefinite interval instead of over the specific interval -1 to 1, then such an expression would lead to the conclusion that each of the coefficients would have to be zero. If this were the case, then:

$$\sum A_n \eta^n = - \sum K B_n \eta^n$$

and

$$E_z = - \frac{w}{K} .$$

Because of the definite integral, the sum becomes:

$$\sum_{n=0,2,4}^{\infty} 2 \left(\frac{A_n + K B_n}{n+1} \right) = 0 .$$

With the conditions available, it is not possible to evaluate the coefficients A_n in terms of B_n . It does not appear possible to uniquely determine the coefficients of the power series.

Considering Equation (55), we can see that Equation (8),

$$E_z = - \frac{w}{K}$$

satisfies the equation identically and consequently it is a permissible relationship. It is not likely, however, that it is a unique relationship.

The Navier-Stokes equations for fully established flow become:

$$\mu \nabla^2 w - \frac{\partial p}{\partial z} + \rho_c E_z = 0 . \quad (11)$$

Solving for $\rho_c E_z$ and substituting into Equation (54), we find:

$$\int_A \left(\nabla^2 w - \frac{\rho_c}{\mu K} w - \frac{1}{\mu} \frac{\partial p}{\partial z} \right) dA = 0. \quad (56)$$

One condition for the flow which satisfies the current condition is:

$$\nabla^2 w - \frac{\rho_c}{\mu K} w - \frac{1}{\mu} \frac{\partial p}{\partial z} = 0. \quad (12)$$

This equation may be considered to offer a first approximation to the influence of the ions on the flow stream. As mentioned above for Equation (8), however, this is not necessarily a unique condition.

Equation (55) can lead to an insight into the phenomenon involved. From the definition of the mean value of a function:

$$\frac{1}{A} \int_A \rho_c E_z dA = (\rho_c E_z)_m \quad (57)$$

$$\frac{1}{A} \int_A \rho_c \frac{w}{K} dA = \left(\frac{\rho_c w}{K} \right)_m. \quad (58)$$

The mean value of the body force, Equation (26), becomes,

$$F_{zm} = - \frac{1}{K} (\rho_c w)_m. \quad (59)$$

Substituting into Equation (11),

$$\mu \nabla^2 w - \frac{\partial p}{\partial z} - \frac{1}{K} (\rho_c w)_m = 0. \quad (60)$$

In summary, it appears that as a first approximation the equation of motion for the flow with ions present in a field can be given by:

$$\mu \nabla^2 w - \frac{\rho_c}{K} w - \frac{\partial p}{\partial z} = 0. \quad (12)$$

In addition, based upon the mean value of the body force, the equation of motion can be given by:

$$\mu \nabla^2 w - \frac{1}{K} (\rho_c w)_m - \frac{\partial p}{\partial z} = 0 \quad (60)$$

where $(\rho_c w)_m$ is a constant value. Finally, it is logical to assume that:

$$E_z = f\left(\frac{w}{K}\right)$$

and Equations (8) and (59) indicate two permissible forms of the relationship.

ANALYSIS

Equations (12) and (60) for the case of channel flow in a constant area duct with incompressible flow become ordinary linear differential equations. Equation (12) contains a variable coefficient, ρ_c , while Equation (60) has only constant coefficients.

NONDIMENSIONAL EQUATIONS

Before proceeding with the solutions to these equations, they will be put into non-dimensional form.

Let:

$$W = \frac{w}{w_m}; \quad (61)$$

$$\eta = \frac{r}{R} \quad \text{for the cylindrical case, and} \quad (62)$$

$$\eta = \frac{y}{h} \quad \text{for the parallel plate,} \quad (63)$$

where w_m is the mean stream velocity,

R is the inside radius of the tube, and

h is the half height of the channel.

For channel flow:

$$\nabla^2 w = \frac{\partial^2 w}{\partial y^2} \quad \text{for parallel plates}$$

and

$$\nabla^2 w = \frac{d^2 w}{dr^2} + \frac{1}{r} \frac{dw}{dr} \quad \text{for a round tube.}$$

FLAT-PLATE EQUATIONS

Equation (12) becomes:

$$\frac{d^2 W}{d\eta^2} - \frac{\rho_c h^2}{\mu K} W = \frac{h^2}{\mu w_m} \left(\frac{\partial p}{\partial z} \right). \quad (64)$$

The term $\frac{h^2}{\mu w_m} \left(\frac{\partial p}{\partial z} \right)$ can be rewritten as:

$$\frac{h^2}{\mu w_m} \frac{\partial p}{\partial z} = \frac{NR_0}{2} \frac{\partial p^*}{\partial \zeta} \quad (65)$$

where

$$p^* = \frac{p}{\frac{\rho w_m^2}{2}} \quad (66)$$

$$\zeta = \frac{z}{h} \quad (67)$$

$$NR_\theta = \frac{\rho w_m D_H}{\mu} \quad (68)$$

$$D_H = \frac{4A}{W.P.} \cong 4h \quad (69)$$

$$-\frac{d^2 W}{d\eta^2} - \frac{\rho_c h^2}{\mu K} W = \frac{NR_\theta}{2} \frac{\partial p^*}{\partial \zeta} \quad (70)$$

All terms of Equation (70) are dimensionless.

Since W is dimensionless, then $\rho_c h^2 / \mu K$ must be dimensionless as well. It represents the unique contribution of the ions on the flow, and is the characteristic number for this type of flow.

Let:

$$\rho_c^* = \frac{\rho_c}{\rho_{c_m}} \quad (71)$$

Therefore

$$\frac{\rho_c L^2}{\mu K} = \left(\frac{\rho_{c_m} L^2}{\mu K} \right) \rho_c^* \quad (72)$$

Define:

$$N\rho_c = \frac{\rho_{c_m} L^2}{\mu K} \quad (73)$$

where ρ_{c_m} is the mean value of charge and

L is the characteristic dimension of the flow.

This dimensionless number represents the ratio of the charge forces to the viscous forces in the flow.

For flat plates, Equation (73) becomes:

$$N\rho_c = \frac{\rho_{c_m} h^2}{\mu K}$$

Substituting into Equation (64):

$$-\frac{d^2 W}{d\eta^2} - N\rho_c \rho_c^* W = \frac{NR_\theta}{2} \frac{\partial p^*}{\partial \zeta} \quad (74)$$

This indicates that the flow depends upon two independent parameters, the flow charge number and the Reynolds number. It should be kept in mind that ρ_c^* can be a variable.

CYLINDRICAL GEOMETRY EQUATIONS

Substituting into Equation (12), we find:

$$\frac{d^2 W}{d\eta^2} + \frac{1}{\eta} \frac{dW}{d\eta} - \left(\frac{\rho_c R^2}{\mu K} \right) W = \frac{R^2}{\mu w_m} \frac{\partial p}{\partial z} \quad (75)$$

or:

$$\frac{d^2 W}{d\eta^2} + \frac{1}{\eta} \frac{dW}{d\eta} - N_{\rho_c} \rho_c^* W = N_{R_e} \frac{\partial p^*}{\partial \zeta} \quad (76)$$

where

$$N_{R_e} = \frac{\rho w_m D}{\mu} \quad (66)$$

$$p^* = \frac{p}{\frac{\rho w_m^2}{2}}$$

$$\zeta = \frac{z}{R} \quad (77)$$

$$N_{\rho_c} = \frac{\rho_{cm} R^2}{\mu K} \quad (78)$$

The same two independent dimensionless parameters are involved as before. The terms in Equations (65) and (75),

$$\frac{h^2}{\mu w_m} \frac{\partial p}{\partial z} \quad \text{and} \quad \frac{R^2}{\mu w_m} \left(-\frac{\partial p}{\partial z} \right),$$

are constant during integration.

EQUATION WITH MEAN VALUE OF BODY FORCE

Equation (60) can be put into nondimensional form.

Flat Plates

$$\frac{d^2 W}{d\eta^2} - \frac{(\rho_c w)_m}{\rho_{cm} w_m} N_{\rho_c} = \frac{N_{R_e}}{2} \frac{\partial p^*}{\partial \zeta} \quad (79)$$

Round Tubes

$$\frac{d^2 W}{d\eta^2} + \frac{1}{\eta} \frac{dW}{d\eta} - \frac{(\rho_c w)_m}{\rho_{cm} w_m} N_{\rho_c} = N_{R_e} \frac{\partial p^*}{\partial \zeta} \quad (80)$$

SOLUTION OF THE MEAN VALUE EQUATION

Considerable insight into the action of the charge on the stream can be gleaned from an analysis of the approximate mean value equations. Consider Equation (79). It can be written in the form:

$$\begin{aligned}\frac{d^2 W}{d\eta^2} &= \frac{h^2}{\mu w_m} \left(\frac{\partial p}{\partial z} \right) + \frac{(\rho_c w)_m h^2}{\mu K w_m} \\ &= \frac{h^2}{\mu w_m} \left(\frac{\partial p}{\partial z} + \frac{(\rho_c w)_m}{K} \right)\end{aligned}$$

Define:

$$\frac{\Delta P_0}{\Delta z} = \frac{\partial p}{\partial z} + \frac{(\rho_c w)_m}{K} \quad (81)$$

Therefore:

$$\frac{d^2 W}{d\eta^2} = \frac{h^2}{\mu w_m} \frac{\Delta P_0}{\Delta z}$$

Since the term on the right-hand side is a constant, the solution is that of Hagen-Poiseuille flow:

$$W = - \frac{h^2}{2\mu w_m} \frac{\Delta P_0}{\Delta z} (1 - \eta^2) \quad (82)$$

$$w = - \frac{h^2}{2\mu} \frac{\Delta P_0}{\Delta z} (1 - \eta^2) \quad (83)$$

$$\begin{aligned}w_{\max} &= - \frac{h^2}{2\mu} \frac{\Delta P_0}{\Delta z} \\ w_m &= - \frac{1}{3} \frac{h^2}{\mu} \frac{\Delta P_0}{\Delta z} \quad (84)\end{aligned}$$

Substituting for $\frac{\Delta P_0}{\Delta z}$ from Equation (81):

$$\begin{aligned}w_m &= \frac{1}{3} \frac{h^2}{\mu} \left(\frac{\partial p}{\partial z} + \frac{(\rho_c w)_m}{K} \right) \\ w + \frac{1}{3} \frac{h^2}{\mu} \frac{(\rho_c w)_m}{K} &= - \frac{1}{3} \frac{h^2}{\mu} \frac{\partial p}{\partial z} \quad (85)\end{aligned}$$

This equation indicates that for a given mean flow velocity, the pressure drop will increase with the amount of charge present. To more clearly show the effects, consider the case of constant charge density. Assume ρ_c is constant. Then:

$$(\rho_c w)_m = \rho_c w_m$$

Equation (85) becomes:

$$w_m = - \frac{\frac{1}{3} \frac{h^2}{\mu} \left(-\frac{\partial p}{\partial z} \right)}{\left(1 + \frac{1}{3} \frac{\rho_c h^2}{\mu K} \right)} \quad (86)$$

Equation (85) indicates that for a given available pressure drop, the flow velocity will decrease as the charge density increases. This action is in agreement with the test data obtained.

Consider, next, Equation (80) for the round tube:

$$\frac{d^2 W}{d\eta^2} + \frac{1}{\eta} \frac{dW}{d\eta} = \frac{R^2}{\mu w_m} \frac{\partial p}{\partial z} + \frac{(\rho_c w)_m R^2}{\mu K w_m} \quad (87)$$

Defining:

$$\begin{aligned} \frac{\Delta P_e}{\Delta z} &= \frac{\partial p}{\partial z} + \frac{(\rho_c w)_m}{K} \\ \frac{d^2 W}{d\eta^2} + \frac{1}{\eta} \frac{dW}{d\eta} &= \frac{R^2}{\mu w_m} \frac{\Delta P_e}{\Delta z} \end{aligned} \quad (88)$$

The solution of this equation leads to:

$$W = \frac{R^2}{4\mu w_m} \frac{\Delta P_e}{\Delta z} (1 - \eta^2) \quad (89)$$

$$w_{max} = - \frac{R^2}{4\mu} \frac{\Delta P_e}{\Delta z} \quad (90)$$

$$w_m = - \frac{R^2}{8\mu} \frac{\Delta P_e}{\Delta z} \quad (91)$$

Substitution of Equation (87) leads to:

$$w_m + \frac{R^2}{8\mu} \frac{(\rho_c w)_m}{K} = - \frac{R^2}{8\mu} \frac{\partial p}{\partial z} \quad (92)$$

which is similar to Equation (85).

For the case of constant charge density:

$$w_m = - \frac{\frac{R^2}{8\mu} \frac{\partial p}{\partial z}}{\left(1 + \frac{\rho_c R^2}{8\mu K} \right)} \quad (93)$$

which is similar to the form of Equation (85) for flow between infinite parallel plates.

Expressing these relationships in terms of the charge number, N_{ρ_c} :

For Flat Plates

$$w_m = - \frac{\frac{h^2}{3\mu} \frac{\partial p}{\partial z}}{\left(1 + \frac{N\rho_c}{3}\right)} \quad (94)$$

For Round Tubes

$$w_m = - \frac{\frac{R^2}{8\mu} \frac{\partial p}{\partial z}}{\left(1 + \frac{N\rho_c}{8}\right)} \quad (95)$$

The Blasius friction factor is defined as follows:

$$f_B = \frac{\tau_w}{\frac{\rho w_m^2}{2}} \quad (96)$$

where τ_w is the fluid shear stress at the wall. The friction factor can also be defined in terms of the pressure drop in the channel.

For Round Tubes

$$f_B = 2 \frac{\left(\frac{R^2}{\mu} \frac{\partial p}{\partial z}\right)}{N_{Re} \times w_m} \quad (97)$$

$$N_{Re} = \frac{\rho w_m D}{\mu}$$

For Infinite Parallel Flat Plates

$$f_B = \frac{\frac{h^2}{\mu} \frac{\partial p}{\partial z}}{w_m N_{Re}} \quad (98)$$

$$N_{Re} = \frac{\rho w_m D_H}{\mu}$$

The friction factor ordinarily used in engineering work is the Darcy friction factor, which is defined as:

$$f_D = 4 f_B \quad (99)$$

Both versions of friction factors are used in this report.

Based upon Equations (94) and (95), the friction factors for flow with charge, assuming ρ_c is a constant, become:

For Flat Plates

$$f_B = \frac{24}{NR_e} \left(1 + \frac{N\rho_c}{3} \right) \quad (100)$$

$$f_D = \frac{96}{NR_e} \left(1 + \frac{N\rho_c}{3} \right) \quad (100a)$$

For Round Tubes

$$f_B = \frac{16}{NR_e} \left(1 + \frac{N\rho_c}{8} \right) \quad (101)$$

$$f_D = \frac{64}{NR_e} \left(1 + \frac{N\rho_c}{8} \right) \quad (101a)$$

EQUATIONS FOR ROUND TUBE WITH CENTRAL WIRE

The case of a round tube with a central wire will lead to a change in the velocity profile from the parabolic shapes indicated in Equation (89). In the tests conducted, the wire was 0.004 inch in diameter. This distance (0.004 inch) is three orders of magnitude greater than the mean free path of gas molecules at normal temperature and pressure conditions. Consequently, the wire will appear as a stationary surface to the macroscopic flow stream. Under this condition the velocity profile without ions present is:

$$w = -\frac{1}{4\mu} \frac{\partial p}{\partial z} (R^2 - r_w^2) \left[\frac{\ln \frac{R}{r}}{\ln \frac{R}{r_w}} - \frac{(R^2 - r^2)}{(R^2 - r_w^2)} \right] \quad (102)$$

$$w_m = -\frac{1}{8\mu} \frac{\partial p}{\partial z} (R^2 - r_w^2) \left[\frac{1}{\ln \frac{R}{r_w}} - \frac{R^2 + r_w^2}{R^2 - r_w^2} \right] \quad (103)$$

$$f_D = \frac{64}{NR_e} \left(\frac{R - r_w}{R + r_w} \right) \left[\frac{R^2 + r_w^2}{R^2 - r_w^2} - \frac{1}{\ln \frac{R}{r_w}} \right]^{-1} \quad (104)$$

For the case of ρ_c constant, with the central wire and $R \gg r_w$:

$$f_D = \frac{64}{NR_e} \frac{\left(1 + \frac{N\rho_c}{8} \right)}{\left(1 - \frac{1}{\ln \frac{R}{r_w}} \right)} \quad (105)$$

For the test conditions, $R = .625$ inch and $r_w = 0.002$ inch:

$$f_D = \frac{64 (1.21)}{NR_e} \left(1 + \frac{N\rho_c}{8} \right) \quad (106)$$

CHARGE DENSITY IN THE CHANNEL

In order to determine the significance of the charge number on the flow, it is necessary to determine the charge density, its magnitude, and its distribution in the channel. There are two general approaches for determining the distribution of charge of a corona discharge in a dense gas.

LOEB SOLUTION

Loeb and Brown indicate a method suitable for determining the distribution of charge between coaxial electrodes (Refs. 4, 5). Their method assumes that with small corona currents, the space charge will be very low, and the distortion of the field lines will be negligible. Parts of Loeb's analysis, for coaxial electrodes, will be reproduced here.

The motion of the ions involved in the corona current is assumed to act essentially independent of the flow velocity. The problem, then, is reduced to determining the current motion in a radial direction only:

$$i = 2 \pi r \rho_c v_R \ell \quad (107)$$

where ℓ is the length along the pipe. Assume $\ell = \text{unity}$. Substituting Equation (3):

$$i = 2 \pi r \rho_c K E_r \quad (108)$$

$$E_r = \frac{V - \pi \rho_c (R^2 - r_w^2)}{r \ln \left(\frac{R}{r_w} \right)} - 2 \pi \rho_c r \quad (109)$$

$$i = \frac{2 \pi K V}{\ln \frac{R}{r_w}} \rho_c - \left[\frac{2 \pi^2 K (R^2 - r_w^2)}{\ln \left(\frac{R}{r_w} \right)} + 4 \pi^2 r^2 K \right] \rho_c^2 \quad (110)$$

For small charge density, Loeb assumes that the second term can be dropped. Then:

$$i \approx \frac{2 \pi K V}{\ln \left(\frac{R}{r_w} \right)} \rho_c \quad (111)$$

$$\rho \approx \frac{i}{2 \pi K V} \ln \frac{R}{r_w} \quad (112)$$

Loeb points out that this approximation holds in a region outside of the intense corona surrounding the wire. The radius of the intense corona region at a pressure of one atmosphere is of the order of 10^2 mean free paths. At standard conditions, this distance is of the order:

$$\begin{aligned} \Delta r &= 0 (10^{-3}) \text{ cm} \\ r_c &= r_w + \Delta r \\ &\approx 0.003 \text{ inch} = 0.0076 \text{ cm} \end{aligned} \quad (113)$$

where r_c is the radius at the edge of the corona. In terms of η and a tube radius of 0.625 inch,

$$\eta_c \approx 0.005 \quad (114)$$

Thus, under these assumptions, the space charge density will be essentially constant between the electrodes.

STUETZER SOLUTIONS

Another approach for obtaining charge density distributions is presented in summary form by Stuetzer in Reference 6. The space charge effects are included in this approach, and it is assumed that the field at the intense corona goes to zero because the discharge is space-charge limited. Only his results are presented here for ready reference.

Coaxial Electrodes

$$\rho_c = \left[\frac{\epsilon i}{2\pi R K l} \cdot \frac{r}{(r^2 - r_c^2)} \right]^{\frac{1}{2}} \quad (115)$$

$$E_r = \left[\frac{i r}{2\pi R l \epsilon K} \left(1 - \frac{r_c^2}{r^2} \right) \right]^{\frac{1}{2}} \quad (116)$$

Parallel Plate Electrodes

$$\rho_c = \left[\frac{i \epsilon}{2KA(y - y_0)} \right]^{\frac{1}{2}} \quad (117)$$

$$E_y = \left[\frac{2i(y - y_0)}{A \epsilon K} \right]^{\frac{1}{2}} \quad (118)$$

where A is the cross section normal to ion current flow, and y_0 is the distance to the edge of the intense corona.

In the region away from the intense corona, $r > r_c$ and the following approximation for Equation (115) results in:

$$\begin{aligned} \rho_c &= \left[\frac{i \epsilon}{2\pi R K l} \right]^{\frac{1}{2}} \left(\frac{1}{r} \right)^{\frac{1}{2}} \\ &= \left[\frac{J_w \epsilon}{RK} \right]^{\frac{1}{2}} \left(\frac{R}{r} \right)^{\frac{1}{2}} \end{aligned} \quad (119)$$

where J_w is the current density at the wall.

The average charge density for a region $r_0 > r_c$ is:

$$\rho_{c_{avg}} = \int_{r_0}^R \left(\frac{i \epsilon}{2\pi R K l} \right) \frac{1}{r^{3/2}} 2\pi r dr \quad (120)$$

$$= \frac{4}{3} \left(\frac{J_w \epsilon}{RK} \right)^{\frac{1}{2}} \frac{R^{1/2} (R^{3/2} - r_0^{3/2})}{R^2} \quad (121)$$

$$\rho_{c_0} \approx \frac{4}{3} \left(\frac{\epsilon J_W}{RK} \right)^{\frac{1}{2}} \quad (122)$$

CHARGE AND CURRENT DENSITY

To calculate the actual magnitude of the charge densities used in the tests, the actual test configurations must be considered, and the mobilities of the ions must be known.

Exploratory Sequence

$$l = 72 \text{ inches} = 1.828 \text{ meters}$$

$$R = 0.625 \text{ in} = 0.01587 \text{ meters}$$

Revised Test Sequence

$$l = 67 \text{ inches} = 1.70 \text{ meters}$$

$$R = 0.625 \text{ in.} = 0.01587 \text{ meters}$$

Table 1. Mobility of Ions

(From Reference 2)

GAS	K (meters ² / volt-sec)	
	K ⁻	K ⁺
Air (dry)	2.1×10^{-4}	1.36×10^{-4}
Air (very pure)	2.5×10^{-4}	1.8×10^{-4}
CO ₂ (dry)	$.98 \times 10^{-4}$	$.94 \times 10^{-4}$
H ₂ O at 100°C	$.95 \times 10^{-4}$	1.00×10^{-4}
N ₂	1.84×10^{-4}	1.27×10^{-4}
N ₂ (very pure)	1.45×10^{-4}	1.28×10^{-4}
O ₂	1.8×10^{-4}	1.31×10^{-4}

It must be recognized that ion mobilities are not precise quantities. The values shown are greatly affected by age, contaminants, moisture, and to some extent by the field strength. As in most corona wind analyses, however, we have assumed that K is constant (Refs. 7, 8).

For both sequences of tests reported in Reference 1, the current density and the charge densities based upon Equations (112) and (122) are given by:

Exploratory Tests

$$J_W = 5.49 \text{ I} \quad (123)$$

Constant charge density, Equation (112)

$$\rho_c = 0.48 \text{ I} \frac{\text{I}}{VK} \quad (124)$$

For Equation (122)

$$\rho_{c_0} = 7.4 \times 10^{-8} \left(\frac{\text{I}}{K} \right)^{\frac{1}{2}} \quad (125)$$

Final Tests

$$J_W = 5.88 \text{ I} \quad (126)$$

Equation (112):

$$\rho_c = 0.516 \frac{\text{I}}{VK} \quad (127)$$

Equation (122):

$$\rho_{c_0} = 7.65 \times 10^{-8} \left(\frac{\text{I}}{K} \right)^{\frac{1}{2}} \quad (128)$$

where J_y is given in amp/m²,
 I is given in amperes,
 ρ_c is given in coul/m³, and
 V is given in volts.

To calculate the charge number density, it is necessary to multiply the equations of charge density by the number of charges per coulomb:

$$1 \text{ coulomb} = 1.602 \times 10^{19} \text{ charges.} \quad (129)$$

For a typical case, assume the following values, based upon test data:

$$\text{I} = 1 \text{ milliamp}$$

$$V = 6500 \text{ volts}$$

$$K = 2 \times 10^{-4} \text{ m}^2 / \text{volt} \cdot \text{sec}$$

For the exploratory tests, these conditions lead to:

Equation (124)

$$\rho_c = 5.92 \times 10^9 \text{ charges / cc.}$$

Equation (125)

$$\rho_{c_0} = 2.56 \times 10^9 \text{ charges / cc.}$$

For this set of conditions, values for Equations (115) and (119) are plotted in Figure 6 along with the average values calculated. It can be seen that, except for the region close to the wire, Equation (119) gives a good approximation to the space-charge-limited variation. Although the two average values of charge density are not the same, they are in good agreement from an order-of-magnitude standpoint.

One of the parameters used in the analysis is:

$$\begin{aligned} \gamma_i &= \left(\frac{R^2}{\mu K} \right) \left(\frac{\epsilon J_W}{KR} \right)^{\frac{1}{2}} \\ &= \frac{R^2}{\mu K} \rho_{c_{wall}} \end{aligned} \quad (130)$$

The other factors used in the analysis are related to γ_i as follows:

From Equation (122)

$$\gamma_i = \frac{3}{4} \left(\frac{R^2}{\mu K} \right) \rho_{c_0} \quad (131)$$

From Equation (119)

$$\rho_c = \frac{3}{4} \rho_{c_0} \left(\frac{1}{\eta} \right)^{\frac{1}{2}} \quad (132)$$

From Equations (131) and (73) for the round tube and variable charge density, and since

$$\begin{aligned} \rho_{c_m} &= \rho_{c_0} \\ \gamma_i &= \frac{3}{4} N \rho_c \end{aligned} \quad (133)$$

MAGNITUDE OF THE INFLUENCE OF CHARGE NUMBER

A typical value for the charge number can be calculated as follows. For air at standard conditions:

$$\begin{aligned} K &= 2.0 \times 10^{-4} \text{ m}^2 / \text{volt} - \text{sec} \\ \mu &= 1.783 \times 10^{-5} \text{ kg} / \text{m} - \text{sec} \\ R &= 1.587 \times 10^{-2} \text{ m} \\ \frac{R^2}{\mu K} &= 7.06 \times 10^4 \text{ m}^3 / \text{coul.} \end{aligned}$$

From Equation (125) for the exploratory tests and a current of $i = 10^{-3}$ amp:

$$\begin{aligned}\rho_{c_0} &= 7.4 \times 10^{-5} \times \sqrt{5} \\ &= 16.5 \times 10^{-5} \text{ coul / m}^3\end{aligned}$$

Therefore:

$$N_{\rho_c} = \frac{R^2}{\mu K} \rho_{c_0} = 11.7$$

That this is a surprisingly large number can be seen from a consideration of the equation for friction factor:

$$f_D = \frac{64}{NR_0} \left(1 + \frac{N_{\rho_c}}{8} \right) \quad (101a)$$

$$f_D = \frac{64}{NR_0} (2.46) \quad (134)$$

Assuming the charge density given by Equation (124) and $i = 10^{-3}$ amp leads to:

$$f_D = \frac{64}{NR_0} (3.89) \quad (135)$$

Thus, the magnitude of the charge number is sufficient to cause increases in friction factor which are similar to those found in the test data. From consideration of Equations (73), (101), and (125), it can be seen that the increase in friction factor depends on the square root of the corona current:

$$f_D = \frac{64}{NR_0} \left(1 + ci^{\frac{1}{2}} \right) \quad (136)$$

where c is a constant.

Equations (100), (101), and (134) predict that the curves for friction factor should be parallel to the $64/NR_0$ line for flow without ionization. Values computed from these equations and the test results plotted in Figure 1 are strikingly similar. Although the absolute values of f_D as given by Equation (134) do not agree precisely with the test data, the degree of correlation achieved is surprisingly good. It must be borne in mind that these expressions for friction factor are based upon a mean value approximation to the body force which was used in the solution of the differential equation and that the mean value approximation leaves the shape of the velocity profile unchanged as the ions flow through the gas. Test data, however, show a marked influence on the velocity profiles. Consequently, to evaluate the possible effects of the charge on the profiles as well as on the pressure drops, it is necessary to consider the equations in which the body force varies.

SOLUTIONS FOR CHANNEL FLOW WITH CHARGE PRESENT

Six separate cases for flow through a channel are considered. They include variations in the flow boundary conditions and two different assumptions of charge density distribution, as follows:

Case I. Infinite parallel plates with constant charge density, ρ_{c_0} .

Case II. Infinite parallel plates with variable charge density given by Equation (117).

Case III. Round tube geometry with constant charge density, ρ_{c_0} , assuming the wire does not influence the flow.

Case IV. Round tube geometry with constant charge density, ρ_{c_0} , assuming the flow is at rest at or near the wire.

Case V. Round tube geometry with variable space charge, assuming the wire does not affect the flow.

Case VI. Round tube geometry with variable space charge, assuming the flow is at rest at or near the wire.

CASE I. PARALLEL PLATES, ρ_c CONSTANT

This is the simplest idealized case to consider. We have assumed that a uniform charge exists between two infinite parallel electrodes. Equations (64) or (74) are applicable.

Consider Equation (74):

$$\frac{d^2 W}{d \eta^2} - N \rho_c \rho_c^* W = \frac{NR_0}{2} \frac{\partial \rho^*}{\partial \zeta} \quad (74)$$

Since

$$\rho_c^* = \frac{\rho_c}{\rho_{cm}} = 1$$

for this case:

$$\frac{d^2 W}{d \eta^2} - N \rho_c W = \frac{NR_0}{2} \frac{\partial \rho^*}{\partial \zeta} = \frac{h^2}{\mu w_m} \left(\frac{\partial \rho}{\partial z} \right) \quad (137)$$

This equation can be solved directly with the boundary conditions of.

$$y = 0, \quad \frac{dW}{dy} = 0, \quad (138)$$

$$y = h, \quad W = 0, \quad (139)$$

$$W = - \left(\frac{h^2}{\mu w_m} \right) \frac{\partial \rho}{\partial z} \frac{1}{N \rho_c} \left[1 - \frac{\cosh \sqrt{N \rho_c} \eta}{\cosh \sqrt{N \rho_c}} \right] \quad (140)$$

As $\rho_c \rightarrow 0$, this expression becomes:

$$w = -\frac{1}{2} \frac{h^2}{\mu w_m} \left(\frac{\partial p}{\partial z} \right) (1 - \eta^2) \quad (84)$$

which is the equation for flow without ionization.

It is of interest to compare the form of Equation (140) with the Hartmann equation of magnetohydrodynamics. From Reference 9:

$$w = -\frac{1}{w_m} \left[\frac{E}{\mu_e H_0} + \frac{\frac{\partial p}{\partial z}}{\mu_e^2 \sigma H_0^2} \right] \left[1 - \frac{\cosh M \eta}{\cosh M} \right] \quad (141)$$

where H_0 is the applied magnetic field,

μ_e is the permeability of the medium, and

M is the Hartmann number.

The term in the left set of brackets of Equation (141) is a constant for a given set of parameters. Likewise, the terms preceding the bracket of Equation (140) are constant. We can readily see that the two profiles are of the same general form. In MHD, this flow leads to a flattening of the velocity profiles. It can be expected, therefore, that Equation (140), which deals with charge motion, leads to a similar flattening. This flattening is apparent in Figure 7, where two values of the charge parameter, N_{ρ_c} , for Equation (140) are plotted. The value $N_{\rho_c} = 8.9$ corresponds to a charge density of approximately 12.5×10^{-5} coul/m³ and a channel height equal to $D = 1.25$ inches. The mean value of the flow velocity is:

$$w_m = -\left(\frac{h^2}{\mu} \right) \frac{\partial p}{\partial z} \frac{1}{N_{\rho_c}} \left[1 - \frac{\tanh \sqrt{N_{\rho_c}}}{\sqrt{N_{\rho_c}}} \right] \quad (142)$$

Using Equation (98):

$$\begin{aligned} f_D &= \frac{32 \frac{h^2}{\mu} \frac{\partial p}{\partial z}}{w_m N_{R_0}} \\ &= \frac{32 N_{\rho_c}}{N_{R_0}} \left[1 - \frac{\tanh \sqrt{N_{\rho_c}}}{\sqrt{N_{\rho_c}}} \right]^{-1} \quad (143) \\ \rho_c &\rightarrow 0 \\ f_D &\rightarrow \frac{96}{N_{R_0}} \end{aligned}$$

which is the value for ordinary flow. The friction factor expression, Equation (142), will be displayed later in comparison with the other cases.

CASE II. PARALLEL PLATES, ρ_c VARIABLE

This is a case in which the charge density is assumed to vary in accordance with Equation (117). A flat ion source is assumed to lie on the $y=0$ plane, coplanar with the walls, as shown in Figure 5. In this idealized case, it is assumed that the planar ion source does not impede the flow at the centerline.

$$\frac{d^2 W}{d\eta^2} - \rho_c^* \rho_c W = \frac{h^2}{\mu w_m} \frac{\partial \rho}{\partial z} \quad (144)$$

Utilizing Equation (112):

$$\rho_c \cong \left[\frac{\epsilon i}{2 K A h} \right]^{\frac{1}{2}} (\eta)^{-\frac{1}{2}} \quad (145)$$

for $y > y_0$

$$N_{\rho_c} \cdot \frac{\rho}{\rho_{cm}} = \frac{h^2}{\mu K} \left[\frac{\epsilon J_W}{2 h} \right]^{\frac{1}{2}} \eta^{-\frac{1}{2}} \quad (146)$$

Let

$$\frac{h^2}{\mu K} \left[\frac{\epsilon J_W}{2 h} \right] = \alpha^2 \quad (147)$$

Equation (144) becomes:

$$\frac{d^2 W}{d\eta^2} - \alpha^2 \frac{W}{\eta^{1/2}} = \frac{h^2}{\mu w_m} \frac{\partial \rho}{\partial z} \quad (148)$$

The solution, following Reference 10, becomes:

$$W = \frac{h^2}{\mu w_m} I_{2/3}(\lambda_1) \eta^{1/2} \left[\int_1^\eta \frac{I_{2/3}(\lambda_1) \eta^{1/2} d\eta}{[I_{2/3}(\lambda_1)]^2 \eta} - \int_1^\eta \frac{I_{2/3}(\lambda_1) \eta^{1/2} d\eta}{[I_{2/3}(\lambda_1)]^2 \eta} \right]_{\eta=1} \quad (149)$$

where

$$\lambda_1 = \frac{4}{3} \alpha \eta^{3/4} \quad (150)$$

$I_{2/3}(\lambda_1)$ is the imaginary Bessel function. The boundary conditions are: (a) that the solution must remain finite, and (b) at:

$$\eta = 1, \quad W = 0.$$

The integrals in this case are not evaluated further, since this case is not of direct importance to the evaluation of the test data. The solution, Equation (149), does serve to illustrate the complexity of the form, however, even when simplifying assumptions are used.

CASE III. ROUND TUBE, ρ_c CONSTANT

In this case, round tube geometry is considered, assuming constant space charge, ρ_{c0} . It is assumed that the wire does not influence the flow; hence at $r = 0, w \neq 0$. Starting with Equations (75) and (76):

$$\frac{d^2 W}{d\eta^2} + \frac{1}{\eta} \frac{dW}{d\eta} - N\rho_c \rho_c^* W = N R_0 \frac{\partial p^*}{\partial \xi} \quad (76)$$

For constant charge density, ρ_{c0} :

$$N\rho_c \rho_c^* = N\rho_c \quad (151)$$

Equation (76) becomes:

$$\frac{d^2 W}{d\eta^2} + \frac{1}{\eta} \frac{dW}{d\eta} - N\rho_c W = \frac{R^2}{\mu w_m} \frac{\partial p}{\partial z} \quad (152)$$

With boundary conditions that permit the solution to remain finite, and at

$$\eta = 0, W = 0.$$

The solution of this equation is:

$$W = - \frac{R^2}{\mu w_m} \left(\frac{\partial p}{\partial z} \right) \frac{1}{N\rho_c} \left[1 - \frac{I_0(\sqrt{N\rho_c} \eta)}{I_0(\sqrt{N\rho_c})} \right] \quad (153)$$

This equation is similar to that for the parallel plate case and the Hartmann flow, except that the hyperbolic functions are replaced by the Bessel functions. Figure 8 illustrates the flattening of the profile due to the presence of charge in the stream. $N\rho_c = 8.9$ represents a charge density of approximately 12.5 coul/m^3 for the 1.25-inch-diameter tube and a current of approximately 580 microamperes under the test conditions.

The mean value of the flow velocity is:

$$w_m = - \frac{R^2}{\mu} \frac{\partial p}{\partial z} \frac{1}{N\rho_c} \left[1 - \frac{I_1(\sqrt{N\rho_c})}{\sqrt{N\rho_c} I_0(\sqrt{N\rho_c})} \right] \quad (154)$$

As $\rho_c \rightarrow 0$, Equations (153) and (154) become identical to Equations (89) and (91) for flow without ionization, where $p = p_0$ for zero ionization.

Using Equation (97):

$$t_D = \frac{4 (N\rho_c)^{3/2} I_0(\sqrt{N\rho_c})}{N R_0 \left[\frac{\sqrt{N\rho_c}}{2} I_0(\sqrt{N\rho_c}) - I_1(\sqrt{N\rho_c}) \right]} \quad (155)$$

where I_0 and I_1 are imaginary Bessel functions (Ref. 11). Equation (155) indicates that t_D is a complex function of the charge density. It can be shown that as

$$\rho_c \rightarrow 0, f_D = \frac{64}{N_{R_e}}.$$

The variation of f_D will be presented later in this report.

CASE IV. CONCENTRIC TUBE, ρ_c CONSTANT

In this case, round tube geometry is considered, assuming constant space charge and that the wire does affect the flow. The boundary conditions are:

$$W = 0, \text{ at } \eta = 1$$

and the three different conditions near the wire are:

Case IVa. No charge present:

$$W = 0, \text{ at } \eta_0 = 0.004.$$

Case IVb. Based upon Equation (114):

$$W = 0, \text{ at } \eta_0 = 0.005.$$

Case IVc. Based upon the assumption that the corona region may be of the order of 10 wire diameters:

$$W = 0, \text{ at } \eta_0 = 0.04$$

The equation in this case is the same as for Case III, Equation (152):

$$\frac{d^2 W}{d\eta^2} + \frac{1}{\eta} \frac{dW}{d\eta} - N_{\rho_c} W = \frac{R^2}{\mu w_m} \left(\frac{\partial p}{\partial z} \right) \quad (152)$$

Case IVa. The solutions for this case without space charge are given in Equations (102), (103), and (104).

Case IVb. Where $\eta_0 = 0.005$:

$$W = \frac{R^2}{\mu w_m} \left(\frac{\partial p}{\partial z} \right) \frac{1}{N_{\rho_c}} \left[1 - 0.1442 I_0(\sqrt{N_{\rho_c}}) - 0.204 K_0(\sqrt{N_{\rho_c}}) \right] \quad (156)$$

$$\begin{aligned} w_m = & -\frac{2R^2}{\mu} \frac{\partial p}{\partial z} \frac{1}{N_{\rho_c}} \left[\frac{1}{2} - 0.1442 N_{\rho_c}^{-\frac{1}{2}} I_1(\sqrt{N_{\rho_c}}) \right. \\ & + 0.204 N_{\rho_c}^{-\frac{1}{2}} K_1(\sqrt{N_{\rho_c}}) + 0.1442 \left(\frac{0.005}{\sqrt{N_{\rho_c}}} \right) I_1(0.005 \sqrt{N_{\rho_c}}) \\ & \left. - 0.204 \left(\frac{0.005}{\sqrt{N_{\rho_c}}} \right) K_1(0.005 \sqrt{N_{\rho_c}}) \right] \quad (157) \end{aligned}$$

The friction factor can be obtained from:

$$f_D = \frac{8}{N_{R_0}} \frac{\left(\frac{R^2}{\mu} \frac{\partial p}{\partial z} \right)}{w_m} \quad (97)$$

where w_m is obtained from Equation (157) and K_0 and K_1 are imaginary Bessel functions of the second kind.

Case IVc. Where $\eta = 0.04$:

$$W = - \frac{R^2}{\mu w_m} \left(\frac{\partial p}{\partial z} \right) \frac{1}{N_{\rho_c}} \left[1 - 0.1436 I_0(\sqrt{N_{\rho_c}}) - 0.403 K_0(\sqrt{N_{\rho_c}}) \right] \quad (158)$$

$$\begin{aligned} w_m = & - \frac{2R^2}{\mu} \left(\frac{\partial p}{\partial z} \right) \frac{1}{N_{\rho_c}} \left[\frac{1}{2} - 0.1436 N_{\rho_c}^{-\frac{1}{2}} I_1(\sqrt{N_{\rho_c}}) \right. \\ & + 0.403 N_{\rho_c}^{-\frac{1}{2}} K_1(\sqrt{N_{\rho_c}}) + 0.1436 \left(\frac{0.04}{\sqrt{N_{\rho_c}}} \right) I_1(0.04 \sqrt{N_{\rho_c}}) \\ & \left. - 0.403 \left(\frac{0.04}{\sqrt{N_{\rho_c}}} \right) K_1(0.04 \sqrt{N_{\rho_c}}) \right] \quad (159) \end{aligned}$$

The friction factor can be calculated from:

$$f_D = \frac{8}{N_{R_0}} \left(\frac{R^2}{\mu} \frac{\partial p}{\partial z} \right) \cdot \frac{1}{w_m} \quad (97)$$

To obtain f_D , substitute w_m from Equation (157) into Equation (97).

Figure 9 illustrates the variation of the profiles with a change in η_0 for Cases IVb and IVc. Figure 10 illustrates Case IVa and Case IVc. The velocity profiles have been normalized by dividing the values by the maximum velocity. The effect of the charge can be seen by comparing the two curves for $\eta_0 = 0.04$.

CASE V. ROUND TUBE, ρ_c VARIABLE

In this case, the round tube geometry is considered, and the space charge is assumed to vary with radius according to Equation (119) or (132). Equation (76) is applicable to this case:

$$\frac{d^2 W}{d\eta^2} + \frac{1}{\eta} \frac{\partial W}{\partial \eta} - N_{\rho_c} \rho_c^* W = N_{R_0} \frac{\partial \rho^*}{\partial \xi} \quad (76)$$

From Equation (132):

$$\rho_c^* N_{\rho_c} = \frac{\rho_c}{\rho_{c_0}} N_{\rho_c} = \frac{3}{4} N_{\rho_c} \eta^{-\frac{1}{2}}$$

Using

$$\gamma_1 = \frac{3}{4} N \rho_c$$

Equation (76) then becomes:

$$\frac{d^2 W}{d \eta^2} + \frac{1}{\eta} \frac{dW}{d\eta} - \gamma_1 \frac{W}{\eta^{1/2}} = \frac{R^2}{\mu w_m} \left(\frac{\partial p}{\partial z} \right) \quad (160)$$

The boundary conditions for this case are chosen as:

$$W = 0, \quad \text{at } \eta = 1$$

and W remains finite at the origin.

A review of the test data on velocity profiles in Reference 1 indicates that when ion current flows, the profiles give the appearance that the flow may not stick at the central wire. The assumptions used in this case, for this reason, may be fairly realistic. The solution of Equation (160) is given as:

$$\begin{aligned} W = \frac{R^2}{\mu w_m} \left(\frac{\partial p}{\partial z} \right) \left(\frac{3}{4} \right)^{2/3} \gamma_1^{-1/3} \left\{ \frac{I_0(\xi)}{I_0\left(\frac{4}{3} \gamma_1^{1/2}\right)} \left[K_0\left(\frac{4}{3} \gamma_1^{1/2}\right) \int^{\frac{4}{3} \gamma_1^{1/2}} \xi^{5/3} I_0(\xi) d\xi \right. \right. \\ \left. \left. - I_0\left(\frac{4}{3} \gamma_1^{1/2}\right) \int^{\frac{4}{3} \gamma_1^{1/2}} \xi^{3/3} K_0(\xi) d\xi \right] + I_0(\xi) \int^{\xi^{5/3}} K_0(\xi) d\xi \right. \\ \left. - K_0(\xi) \int^{\xi^{3/3}} I_0(\xi) d\xi \right\} \quad (161) \end{aligned}$$

where

$$\xi = \frac{4}{3} \gamma_1^{1/2} \eta^{3/4} \quad (162)$$

It should be noted that although $K_0(\xi) \rightarrow \infty$ as $\xi \rightarrow 0$, the functions involved in Equation (161) are well behaved and reach a limit as $\xi \rightarrow 0$.

A series of functions of ξ is presented in Appendix II to aid in computing the velocity profiles. Figure 11 illustrates the effect of the variable charge density on the profiles for various values of average charge density. The peak value of the curves decreases with increasing charge because the curves are computed for a constant pressure drop. As the charge density increases, the mean flow velocity decreases. The flattening of the profile is evident. Figure 12 presents the data of Figure 11 normalized to the value at the centerline. In order to determine the mean velocity, the velocity profile curves were integrated. Consequently, only specific values of the average velocity were obtained. As the charge density, ρ_c , goes to zero, Equation (161) becomes identical to the form given in Equation (89) or (91) for ordinary flow in a round tube without charge effects.

$$N \rho_c = 0.56$$

$$w_m = 0.1095 \frac{R^2}{\mu} \frac{\partial p}{\partial z} \quad (163)$$

$$N\rho_c = 5.55$$

$$w_m = 0.0598 \frac{R^2}{\mu} \frac{\partial p}{\partial z} \quad (164)$$

$$N\rho_c = 12.4$$

$$w_m = -0.0399 \frac{R^2}{\mu} \left(\frac{\partial p}{\partial z} \right) \quad (165)$$

$$N\rho_c = 17.6$$

$$w_m = 0.0309 \frac{R^2}{\mu} \left(\frac{\partial p}{\partial z} \right) \quad (166)$$

The friction factors can be calculated from these equations for w_m and from Equation (97) for the round tube friction factor. The variation of r_D with charge density will be presented in a graph in a subsequent section of this report.

CASE VI. CONCENTRIC TUBE, ρ_c VARIABLE

In this case, the round tube geometry is considered, and the space charge is assumed to vary with radius according to Equation (119) or (132). It is assumed that the velocity goes to zero in the vicinity of the wire. For purpose of analysis, the boundary condition is taken at $r_c = r_w$. The same equation holds for this case as for Case V.

$$\frac{d^2 W}{d\eta^2} + \frac{1}{\eta} \frac{dW}{d\eta} - \gamma_1 \frac{W}{\eta^{1/2}} = \frac{R^2}{\mu w_m} \left(\frac{\partial p}{\partial z} \right) \quad (160)$$

With boundary conditions of:

$$\begin{aligned} \eta_0 &= 0.04, & W &= 0 \\ \eta &= 1, & W &= 0. \end{aligned}$$

the solution is given by:

$$W = A_1 I_0(\xi) + B_1 K_0(\xi) + \left(\frac{3}{4} \right)^{2/3} \gamma_1^{-1/3} \frac{R^2}{\mu w_m} \left(\frac{\partial p}{\partial z} \right) \left[I_0(\xi) \int \xi^{5/3} K_0(\xi) d\xi - K_0(\xi) \int \xi^{5/3} I_0(\xi) d\xi \right] \quad (167)$$

where the coefficients A and B are determined by application of the two boundary conditions:

$$A_1 = \beta_1 \frac{D_0 K_0 \left(\frac{4}{3} \gamma_1^{1/2} \right) - D_R K_0 \left(\frac{4}{3} \gamma^{1/2} \eta^{3/4} \right)}{D_1} \quad (168)$$

$$B_1 = \beta_1 \frac{D_R I_0 \left(\frac{4}{3} \gamma_1^{1/2} \eta^{3/4} \right) - D_0 I_0 \left(\frac{4}{3} \gamma_1^{1/2} \right)}{D_1} \quad (169)$$

where

$$\beta_1 = \frac{R^2}{\mu w_m} \left(\frac{\partial p}{\partial z} \right) \quad (170)$$

$$D_1 = I_0 \left(\frac{4}{3} \gamma_1^{1/2} \eta_0^{3/4} \right) K_0 \left(\frac{4}{3} \gamma_1^{1/2} \right) - I_0 \left(\frac{4}{3} \gamma^{1/2} \right) K_0 \left(\frac{4}{3} \gamma_1^{1/2} \eta_0^{3/4} \right) \quad (171)$$

$$D_0 = K_0 \left(\frac{4}{3} \gamma_1^{1/2} \eta_0^{3/4} \right) \int_0^{\frac{4}{3} \gamma_1^{1/2} \eta_0^{3/4}} \xi^{2/3} I_0(\xi) d\xi \\ - I_0 \left(\frac{4}{3} \gamma_1^{1/2} \eta_0^{3/4} \right) \int_0^{\frac{4}{3} \gamma_1^{1/2} \eta_0^{3/4}} \xi^{2/3} K_0(\xi) d\xi \quad (172)$$

$$D_R = K_0 \left(\frac{4}{3} \gamma_1^{1/2} \right) \int_0^{\frac{4}{3} \gamma^{1/2}} \xi^{2/3} I_0(\xi) d\xi \\ - I_0 \left(\frac{4}{3} \gamma_1^{1/2} \right) \int_0^{\frac{4}{3} \gamma^{1/2}} \xi^{2/3} K_0(\xi) d\xi \quad (173)$$

The value of η_0 is chosen as desired. If $\eta_0 = 0.04$, as indicated in the boundary conditions, this is inserted and the coefficients are determined.

For

$$\eta = 0.04,$$

$$\gamma_1 = 13.17, \quad N_{\rho_c} = 17.55$$

$$W = \frac{R^2}{\mu w_m} \left(\frac{\partial p}{\partial z} \right) \left[-1.1414 I_0(\xi) + 1.1298 K_0(\xi) \right. \\ \left. + I_0(\xi) \int \xi^{2/3} K_0(\xi) d\xi - K_0(\xi) \int \xi^{2/3} I_0(\xi) d\xi \right] \quad (174)$$

Figure 13 illustrates the velocity profile associated with Case VI. The assumed value for η_0 has a marked influence on the shape of the profile near the centerline. It is believed that the assumption of $r_c = 10 r_w$ is far too drastic, and that the value of $\eta_0 = 0.005$, as was used in Case IVb, may be somewhat more reasonable. The general influence of such a change in η_0 can be obtained from the curves in Figure 9 for the $\rho_c = \text{constant}$ case. Because of the large amount of work necessary for Case VI solutions, profiles for $\eta_0 = 0.005$ were not calculated.

The mean velocity for the flow in Case IV with $\eta_0 = 0.004$, can be obtained by integrating the velocity profile. The friction factor can be obtained by using this mean value in Equation (97).

OTHER CASES

Two other possible cases were studied in which the charge density varied with radius. The two variations considered are:

$$\rho_c = \rho_{cw} \frac{1}{\eta} = \left(\frac{e J_w}{R K} \right)^{1/2} \frac{1}{\eta} = \frac{3}{4} \rho_{ca} \frac{1}{\eta} \quad (175)$$

$$\rho_c = \rho_{c_{wall}} \frac{1}{\eta^2} = \frac{3}{4} \rho_{c_0} \frac{1}{\eta^2} \quad (176)$$

The differential equation for the density variation, Equation (175), is:

$$\frac{d^2 W}{d\eta^2} + \frac{1}{\eta} \frac{dW}{d\eta} - \frac{3}{4} N_{\rho_c} \frac{W}{\eta} = \frac{R^2}{\mu w_m} \left(\frac{\partial p}{\partial z} \right)$$

The differential equation for the case of Equation (176) is:

$$\frac{d^2 W}{d\eta^2} + \frac{1}{\eta} \frac{dW}{d\eta} - \frac{3}{4} N_{\rho_c} \frac{W}{\eta^2} = \frac{R^2}{\mu w_m} \left(\frac{\partial p}{\partial z} \right) \quad (177)$$

An elementary solution is possible for Equation (177):

$$W = - \frac{R^2 \left(\frac{\partial p}{\partial z} \right)}{\mu w_m \left[4 - \frac{3}{4} N_{\rho_c} \right]} \left\{ \eta \sqrt{\frac{3}{4} N_{\rho_c}} - \eta^2 \right\} \quad (178)$$

When $\rho_c \rightarrow 0$, Equation (178) reduces to that for ordinary Hagen-Poiseuille flow. The shape of the profile is given in Figure 14.

CORRELATION AND DISCUSSION

FRICTION FACTOR CURVES

The hypothesis presented in the previous section of this report puts forth the concept that the ions in the flow tend to set up an internal field within the flow. This internal field acts on the ions to provide a resisting body force within the flow. Based upon that hypothesis, two general forms for the charge-induced body force result. One is a mean value of the force given by:

$$F_{zm} = \frac{(\rho_c w)_m}{K} \quad (59)$$

Using this average value, a variation of friction factor for a round pipe is given by:

$$f_D = \frac{64}{N_{Re}} \left(1 + \frac{N_{\rho_c}}{8} \right) \quad (101a)$$

The second form for the body force is:

$$F_z = - \frac{w}{K} \rho_c \quad (179)$$

Using this form, we found several solutions for f_D in the previous section.

The curves of f_D using the mean value of the body force are presented in Figure 15. The equations for f_D for both flat plates and round tubes indicate that the friction factor should increase linearly with N_{ρ_c} . Since N_{ρ_c} is proportional to the square root of the corona current, then the increase in f_D should occur as $i^{1/2}$.

Curves for the variation of f_D based upon the variable body force, Equation (179), are shown in Figure 16. This figure includes almost all the cases considered in the previous section. As can be seen from both Figures 15 and 16, the theoretical predictions show the increase in friction factor to be much greater for the flat plate case than for the round tube cases. The round tube cases indicate that the effect of the variable charge density in a given tube configuration is to increase the rate of rise above the zero value. The effect of including the influence of the central wire or corona region on the flow is to displace the curves upward by approximately the amount of the zero current increase. Thus, the central boundary condition does not have a controlling influence on the pressure rise with current. This same point can be gleaned from the velocity profile data as well. Of significant importance is that all the theoretical lines indicate an approximately linear rise in the region of N_{ρ_c} under consideration, although the curves are actually not linear. This indicates that the more complex equations also predict that the increase in f_D should be proportional to the square root of the corona current in the region of interest.

The analysis of the actions of space charge utilized the simplifying assumption that for regions away from the wire:

$$r^2 \gg r_c^2$$

Consequently, r_c was dropped in Equation (115) for the charge density in the coaxial case. The analysis of Case V, which ignores the presence of the wire but uses the variable charge density assumption, may, consequently, be somewhat inaccurate in the region around r_c .

COMPARISON OF VELOCITY PROFILES

The velocity profiles in the flow stream vary depending on the assumptions made on the charge density and body force term. In the case of the mean value force, the velocity profiles given by Equation (82) or (89) are the same as for ordinary Hagen-Poiseuille flow. The profiles remain parabolas, and the charge acts only as a retarding influence on the flow. The action of the charge in this case can be considered as effectively increasing the viscosity. This approach was presented in Reference 1. From Equations (94) and (95), the effective electroviscosity could be given by:

Flat Plates

$$\mu_E = \mu \left(1 + \frac{N\rho_c}{3} \right) \quad (180)$$

Round Tubes

$$\mu_E = \mu \left(1 + \frac{N\rho_c}{8} \right) \quad (181)$$

Figure 17 presents a summary of the various velocity profiles for the round tube, assuming that the body force is variable in accordance with Equation (179). It can be seen for all the cases considered that, for a fixed mean flow velocity of 1 ft/sec, the profiles are severely distorted and somewhat flattened by the presence of the ionization. A strong tendency exists for the elimination of the large central velocities found in ordinary Hagen-Poiseuille flow. A steepening of the profiles at the walls of the tube can also be observed. This steepening should be expected to result in increased shear stress at the wall with a corresponding increase in pressure drop in the flow. Such an increase in pressure drop is what actually was observed.

Figure 18 presents typical profiles for a mean flow velocity of 1 ft/sec in terms of the pressure head which corresponds to the local velocity. This presentation affords a better comparison with the test data. The test data are given in Figures 2 and 19 through 24 (reproduced from Reference 1). A comparison of the values indicates the following: The test data indicate that without applied field, the presence of the wire definitely affects the flow at the lower Reynolds numbers. With ionization present, however, the presence of the wire does not seem to affect the profiles as much. In some cases (Figures 19, 23, and 24), the test data indicate that the velocity across the pipe is relatively uniform. Other runs, plotted in Figures 20, 21, and 22, indicate distinct variations of the profile in which the velocity tends to increase away from the centerline toward the wall. The theoretical curves of Figure 18 indicate a general flattening of the profiles. At higher NR_c , turbulence could be present and could contribute to the flattening found in the test data.

The Case V curves (Figures 17 and 18) indicate a trend of the profile to increase from the center of the pipe outward, even though this was not imposed as a boundary condition on the flow. As the ionization is increased, this gradient from the center outward increases. A similar profile shape can be seen in Figures 20 and 21. The profiles calculated upon the condition that the flow velocity near or at the wire goes to zero do not seem to be in as good agreement with the test data as are the cases where the wire effect is neglected in the analysis. No explanation for this is available at present. It would appear acceptable as a first approximation to neglect the presence of the fine wire and treat the flow problem as though the wire did not exist. In a general way, therefore, the test data

on profiles at the low Reynolds numbers verify the theoretical predictions that substantial distortions will occur with the presence of ions.

COMPARISONS OF FRICTION FACTOR

Comparison of the theoretical predictions for f_D and the test data are presented in Figures 25 through 29. Figure 25 presents a comparison of the value for theory and for air. These data are based upon the exploratory test sequence described in Reference 1. The exploratory test sequence utilized a very short starting length, and consequently the friction factors for the case of zero charge are higher than the theoretical

$$f_D = \frac{64}{N_{R_0}}$$

When this fact is considered, it can be seen that the data tend to show a linear increase in f_D with N_{p_c} at lower values of currents. Some falling off of f_D occurs at the higher values of current, which may possibly be due to localized discharge. The general agreement of slope and linearity is considered good. Only the curves for mean value force and Case III are shown for clarity.

Figure 26 presents a comparison of theoretical data with test data for air using the longer starting length configuration described in Reference 1. The data for all Reynolds numbers fall on a straight line. Although the magnitude of the increase is below that predicted by all the theories, the linearity achieved is encouraging. The value

$$K = 2.0 \times 10^{-4} \text{ m}^2 / \text{volt-sec},$$

often used for air, is used for both Figures 25 and 26 in the computation of charge number.

Figure 27 presents a comparison of theoretical data with test data for oxygen. Data for both positive and negative corona from an exploratory sequence are shown. The data indicate an approximately linear characteristic over a wider range of charge number.

Figure 28 presents data for carbon dioxide for both positive and negative corona. Linearity is very good over a very wide range of charge number. Significant differences of slope appear between the negative and positive conditions.

Figure 29 illustrates the effect with nitrogen. These data are very limited and are only indicative of the trend. Lines were drawn only to relate the points, and are not meant to indicate that a linear relationship necessarily exists.

The comparisons indicated in Figures 25 through 29 are made with the curves for Case III and the mean value curve for the round tube. For a comparison with the other theoretical cases, Figure 16 should be consulted. In most of the cases presented, the data indicate an approximate linear characteristic, at least in the lower ranges of corona current. Test data, however, generally fall below the theoretical lines.

EFFECTS OF MOBILITY AND NONUNIFORMITY OF CHARGE DENSITY

A possible explanation for the observation that test data fall below the theoretical values may lie in the value of mobility and in the degree of uniformity of ionization in the tube. The value of mobility affects the charge number as:

$$N_{\rho_c} \propto \kappa^{-\frac{3}{2}}$$

A small change in the value of mobility can lead to substantial changes in the magnitude of the charge number. Since precise values of mobility are difficult to obtain and since the values vary depending upon the contaminants and impurities in the gas stream, it would not be surprising to find discrepancies in the charge density. As was indicated in Reference 1, the moisture content of the gases was relatively high. In the case of air, the moisture content was approximately 1%, even though the gas was commercially dried air. The presence of water vapor could lead to ions of lowered mobility. If the average mobility was indeed lower, then the charge densities calculated using the κ values given in Table 1 could be somewhat inaccurate.

In the calculation of charge density, it was tacitly assumed that during the corona discharge the ionization would be uniform along the wire and remain uniform as the applied field and corona current increased. This is an idealized assumption which probably cannot be achieved in practice. It is the characteristic of corona discharge to tend to localize in certain discrete points as the field increases. During corona discharge in an open room, the characteristic hissing emanating from these local points can be heard quite readily. During such testing in the dark, such local points were observed at several locations along the electrode as pinpoints of light surrounded by a violet glow. At these points, the current may be considerably larger than the average for the wire. Such local discharges would result in local high charge densities and a nonuniform distribution of ions along the tube. Thus, a substantial portion of the total charge might be located in discrete narrow paths that lay radially between the electrodes. Under this condition, calculating the average charge density from the measured corona current could lead to a substantial overestimation. Such possible nonuniformities in charge density could have resulted in values of N_{ρ_c} for individual test points that were higher than actually existed over the major portion of the tube.

A second action in the test could lead to nonuniform charge distribution. There is a possibility of slight deformation and sagging of the wire. If the wire were to move out of concentricity so that it is closer to one side of the channel than the other, a more intense field would result in the region of close spacing. A greater local ionization could result which would tend to traverse the shortest lines of force to the nearest wall. Such an action could lead to undesirable nonuniformities. Prior to setting up the tests, we made a series of calculations of the droop due to gravity and electrostatic forces. The wire tension was adjusted to keep the wire straight within 1/64 inch under the action of gravity. Strength limitations of the wire did not permit reducing the deflections much below this value. If the wire were not in perfect center, then the electrostatic forces could act to move the wire further out of true concentricity. Consequently, some nonuniformity of space charge may have resulted from the deformations that can occur during test. It is considered doubtful, however, that such localized discharges could have contributed much to the increase in pressure drop and profile distortion. Consequently, it is believed that their primary effect will result in the overestimation of N_{ρ_c} as discussed above. Such nonuniformities in charge density may possibly explain why the test data did not show as large a rate of increase in t_0 as was predicted by the theory.

SUMMARY

In order to seek an explanation of the unusually high pressure drops reported in Reference 1, we conducted an analysis based upon the hypothesis that the ions in the stream tended to set up an electrical field internal to the stream. Although it is not possible to derive a unique solution for the internal field with precise mathematics, it is believed that an expression of the form

$$E_z = f \left(\frac{w}{K} \right)$$

is a valid representation of the field. Based upon the mean value approach for the charge density, field, and velocity in the channel, explicit solutions were obtained which predicted large increases in overall pressure drop when ionization is present and is confined in the tube by the applied field. The increases predicted were of the correct order of magnitude as compared to the data of Reference 1. The mean value approach is considered to be mathematically sound. The expression

$$E_z = - \frac{w}{K}$$

satisfied the electric field equations identically, and is a permissible but not a unique representation for E_z .

If some ion slippage could occur, such that the ions would not move completely against the stream velocity, an expression of the form

$$E_z = -\alpha_0 \left(\frac{w}{K} \right)$$

could be utilized, where α_0 is a constant which indicates the amount of relative slip present. If this constant is included in the equations, then the charge number is merely multiplied by the constant and we get $\alpha_0 N_{pe}$. Thus, the effect of including such an assumed slip is to reduce the effectiveness of the charge number. Inclusion of such a term will not change any of the solutions presented but would change only the magnitude of the effective charge number. It would be possible to obtain empirical values for α_0 by determining the change in effective charge number necessary to make the slopes for the theoretical curves in Figures 26, 27, and 28 agree with the test data. No analytical representation is available at this time, however, to fully justify the inclusion of such a slippage constant. The fact that theory tends to show greater pressure drops than experiment may be an indication that some slippage actually does exist in the stream.

Use of the expression

$$E_z = - \frac{w}{K}$$

in the fluid equations led to a linear equation with variable coefficients. This equation was solved for several channel geometries and various representative charge distributions. The solutions for these cases indicated increases in pressure drop and friction factor similar to those found with the mean value approach. The rate of increase with charge density for these cases was somewhat higher than predicted by the mean value approach. All the cases indicated that large changes to the velocity profile would occur in a channel with bounded charge present. The correlation of the velocity profile test data and the theoretical curves is considered to be good. In some cases, fairly close representation was achieved.

Putting the equations in nondimensional form resulted in the appearance of two new nondimensional parameters. These two parameters are the charge number, N_{ρ_c} , and the charge Reynolds number N_{R_c} . N_{ρ_c} represents the ratio of the charge forces to the viscous forces, and N_{R_c} represents the ratio of the inertia forces to the charge forces.

Appendix I presents a detailed analysis of these parameters. Based upon the kinetic theory, it was shown that the charge number is a direct function of the number charge density ratio and the inverse function of the Knudsen number squared. If any appreciable degree of ionization is present, the Knudsen number acts as an extremely large amplification factor. This term provides a fundamental explanation of the surprisingly large effects on pressure drop and profile observed.

The overall correlation achieved between the theoretical predictions and the test data is believed to be good. The linearity achieved with f_D vs. N_{ρ_c} is considered to agree with the predictions. A clear picture of the linearity can also be seen from the additional data presented in Appendix III. The analysis, however, predicted a greater increase in friction factor for all cases considered than was actually observed. The factors which can affect this include the mobility of ions, the uniformity of the charge, and the assumption that:

$$E_z = -\frac{w}{K}$$

The mobility of ions is difficult to determine exactly for a given situation and consequently can give rise to error. Nonuniformities of corona discharge in the stream can lead to an overestimation of the charge density. The form of the induced field,

$$E_z = -\frac{w}{K}$$

could be an overestimation of the influence of the charge. The term $J_z/\rho_c K$ from Equation (52a)

$$E_z = -\frac{w}{K} + \frac{J_z}{\rho_c K} \quad (52a)$$

could act to reduce the net induced field in the stream.

Following completion of the work reported herein, it was learned that a paper by Stuetzer on "Apparent Viscosity of a Charged Fluid" might be applicable to this problem. A review of that paper is presented in Appendix IV. Stuetzer utilized a similar analytical approach that produced average values identical to the mean values presented in this report. This agreement is considered to provide strong support for the concepts set forth in this analysis.

CONCLUSIONS

From the analysis carried out in this report and from a comparison of the theory with the test data of ASD-TDR-63-842, the following conclusions can be drawn.

1. The analysis using the mean value of the body force provides a solution which is sound from a mathematical standpoint. The analysis indicated that large increases in pressure drop and friction factor could be expected if ionization is present in the stream and the charge is bound to the physical system. The increases predicted by the mean value approach are of the same order as those actually observed.

2. The analysis utilizing the first order approximation, that

$$E_z = - \frac{w}{K}$$

indicated that large increases in pressure drop and large distortions to the velocity profile would occur if a bound charge existed in the stream. Good correlation with the test data was achieved.

3. The predictions of theory that the increases in friction factor and pressure should vary directly as the charge number, N_{ρ_c} , or as the square root of corona current were substantiated by comparisons with the test data.

4. Two new nondimensional parameters appeared, the charge number, and the charge Reynolds number. These two parameters control the effects of charge on flow. The charge number is a function of the square of the Knudsen number. The Knudsen number acts as an amplification factor on the charge present, and provides the key to the surprisingly large actions of charge on flow of dense gases.

5. The hypothesis that the ions set up an internal field acting to retard the flow is considered to be substantiated by the comparison of theoretical values with test data. The solutions for velocity profile, however, may not necessarily be unique, and further work is needed in this direction. Stuetzer's analysis on apparent viscosity provided further substantiation for the validity of the induced internal field.

6. The net impact of these charge phenomena depends upon further careful evaluation of the charge effects in both internal and external flow. It is necessary to define the limits of the action as dimensions vary and as flow velocities increase. Possible critical or limiting values for N_{ρ_c} and N_{R_c} must be determined. If further research indicates that the charge phenomenon is active in laminar external flows, then we can envision many ultimate practical applications. The phenomenon could conceivably be applied to the control of laminar boundary layers and heat transfer under laminar conditions. It would appear useful as a basic flow investigative technique for use in the study of boundary layers. It could possibly be used as a flow trigger in regions of transition or separation in the gas stream. It is not possible at this time to delineate explicitly the techniques of incorporating the mechanism in actual operating systems; it is believed, however, that applications will evolve as experience is gained in working with and controlling the phenomena.

REFERENCES

1. Velkoff, H. R., An Exploratory Investigation of the Effects of Ionization on the Flow and Heat Transfer in a Dense Gas, ASD-TDR-63-842, Aero Propulsion Laboratory, ASD, Air Force Systems Command, W-PAFB, Ohio. 1963.
2. Cobine, J. D., Gaseous Conductors, McGraw-Hill Book Company, New York, N. Y. 1st Ed., 1941. p. 252.
3. Pal, S., Magnetogas dynamics and Plasma Dynamics, Springer Verlag, Vienna. (Prentice-Hall, Inc. Englewood Cliffs, New Jersey). 1962.
4. Loeb, L. B., Fundamental Processes of Electrical Discharge in Gases, John Wiley and Sons, New York, N. Y. 1939.
5. Brown, S. C., Basic Data of Plasma Physics, The Technology Press, John Wiley and Sons, Inc. 1959.
6. Stuetzer, O. M., "Ion Drag Pressure Generation," Journal of Applied Physics, Vol. 30. 1959. p. 984.
7. Harney, J. D., An Aerodynamic Study of the Electric Wind, Thesis, California Institute of Technology (AD 134,400). 1957.
8. Robinson, M., Movement of Air in the Electric Wind of the Corona Discharge, Nobs 77164, Index No. NS-600-010, Technical Paper TF-60-2, Research-Cottrell, Inc. Bound Brook, New Jersey. 1961.
9. Perlmutter, M., and Siegel, R., Heat Transfer to an Electrically Conducting Fluid Flowing in a Channel with a Transverse Magnetic Field, NASA TN-D-875, Washington, D. C. August 1961.
10. Hildebrand, F. B., Advanced Calculus for Engineers, Prentice-Hall, Inc., New York, N. Y. 1949.
11. Korn, G. A., and Korn, T. M., Mathematical Handbook for Scientists and Engineers, McGraw Hill Book Co., New York, N. Y. 1961.
12. Stuetzer, O. M., "Apparent Viscosity of a Charged Fluid", The Physics of Fluids, Vol. 4, Nr 10, Oct 1961.
13. Loeb, L. B., The Kinetic Theory of Gases, 2nd Ed. McGraw-Hill Book Co., New York, N. Y. 1934.

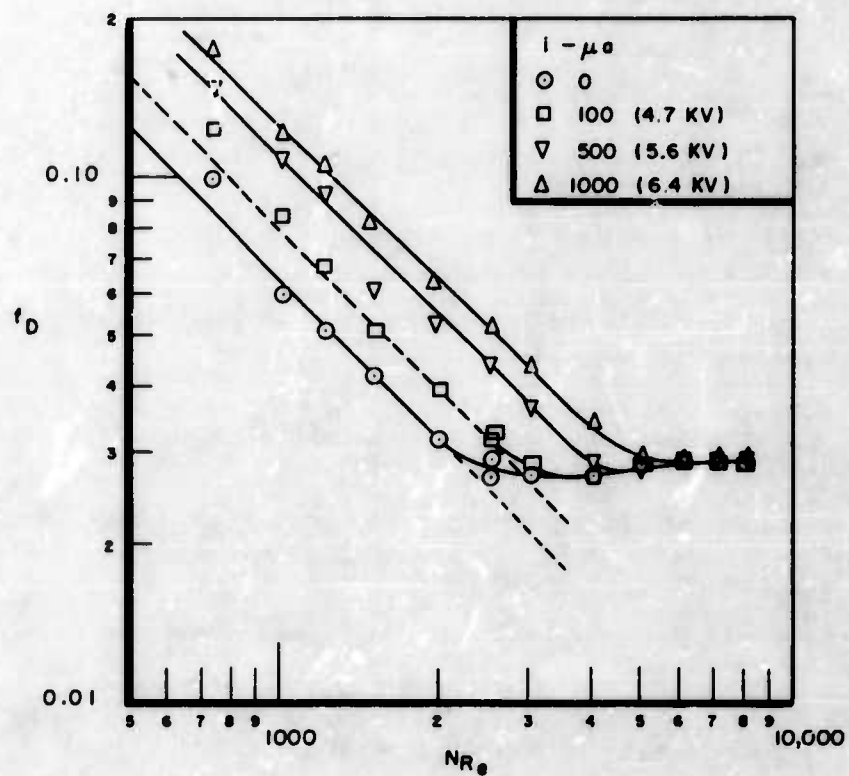


Figure 1. Effect of Ionization on Friction Factor of a Round Duct with Air at One Atmosphere, Positive Corona, Test Data

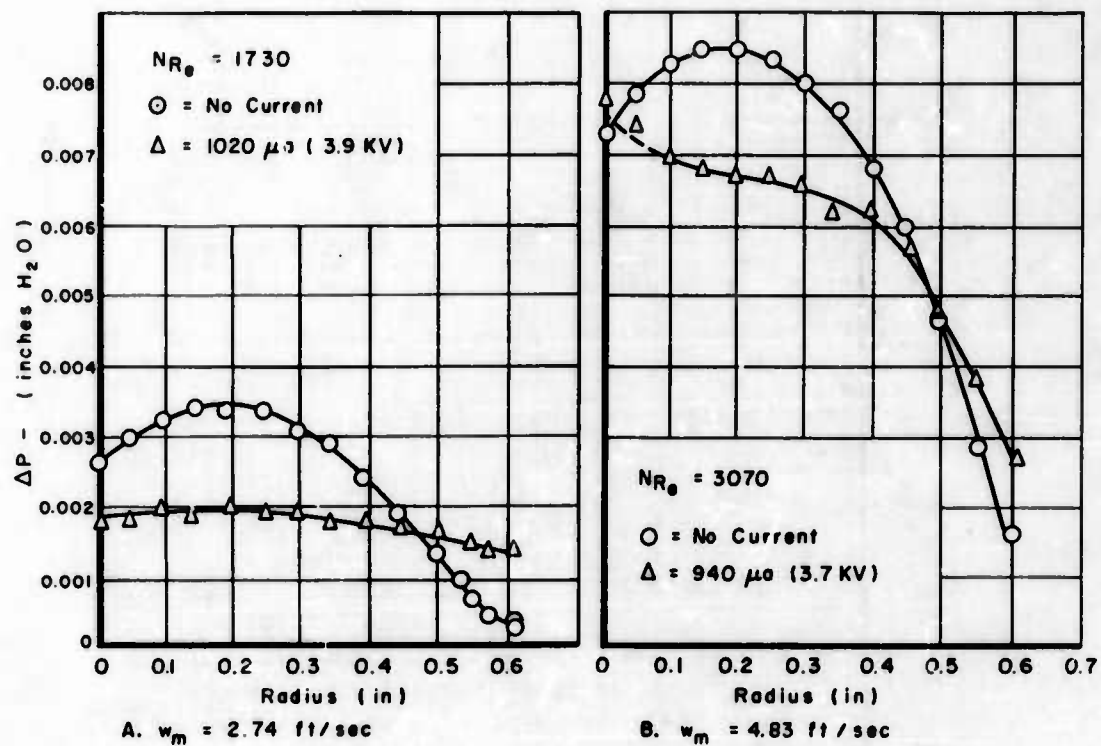


Figure 2. Effect of Ionization on Velocity Profiles in Terms of Pressure Tube with Concentric Wire, Positive Corona, Test Data

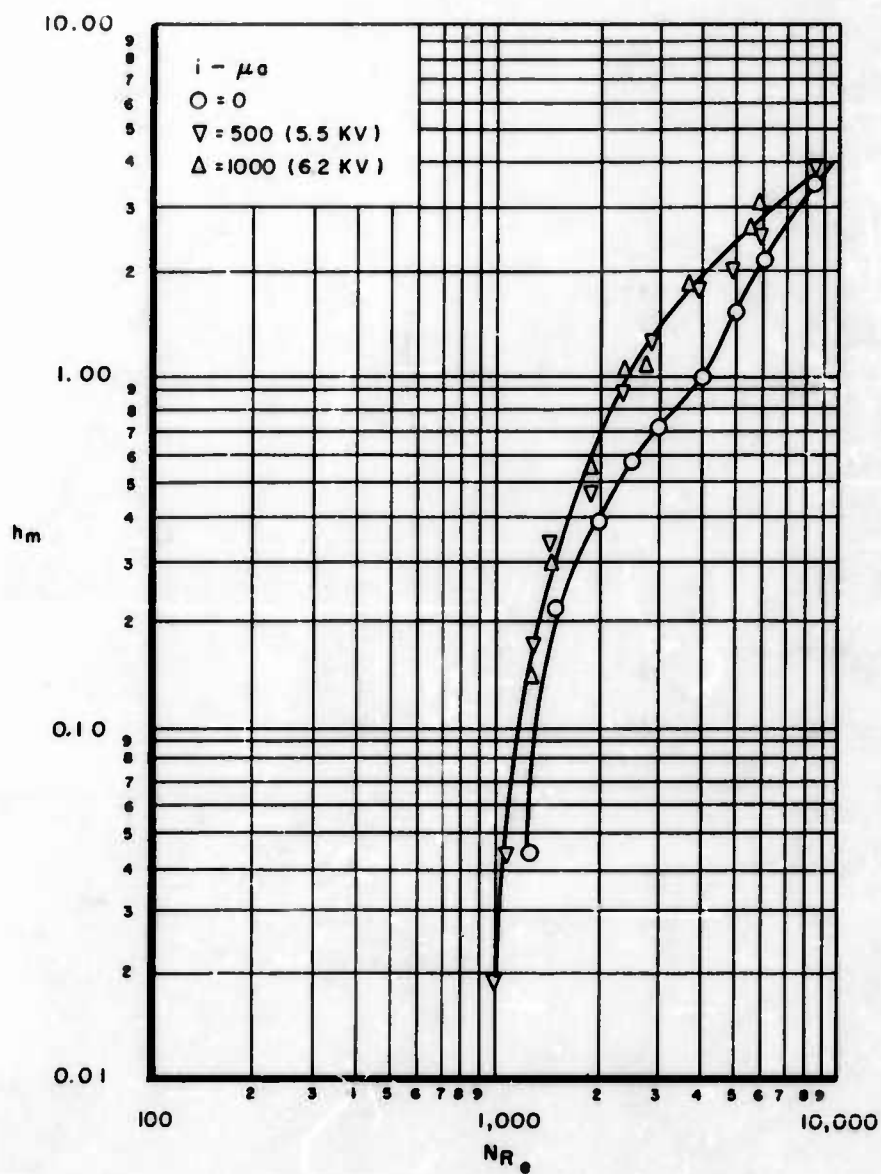


Figure 3. Effect of Ionization on Heat Transfer with Air at One Atmosphere in a Round Tube, Positive Corona, Test Data

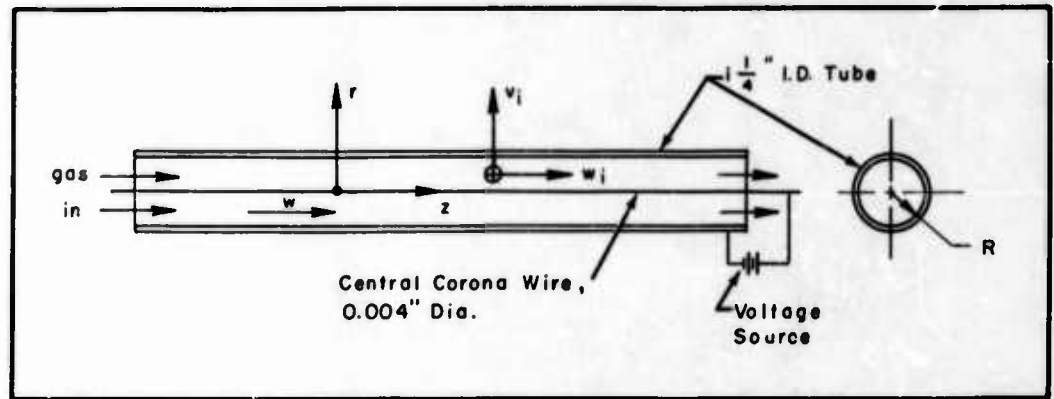


Figure 4. Round Tube Channel with Central Wire

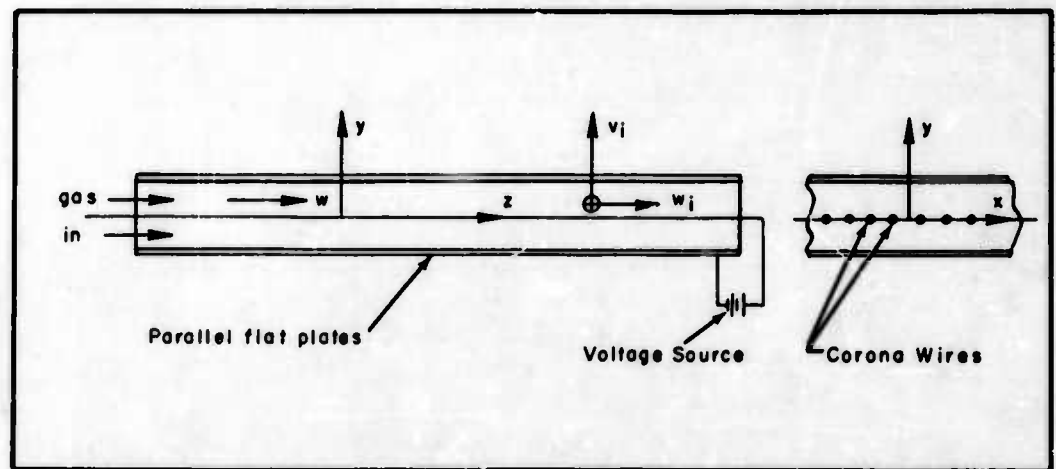


Figure 5. Parallel Plate Flow Channel

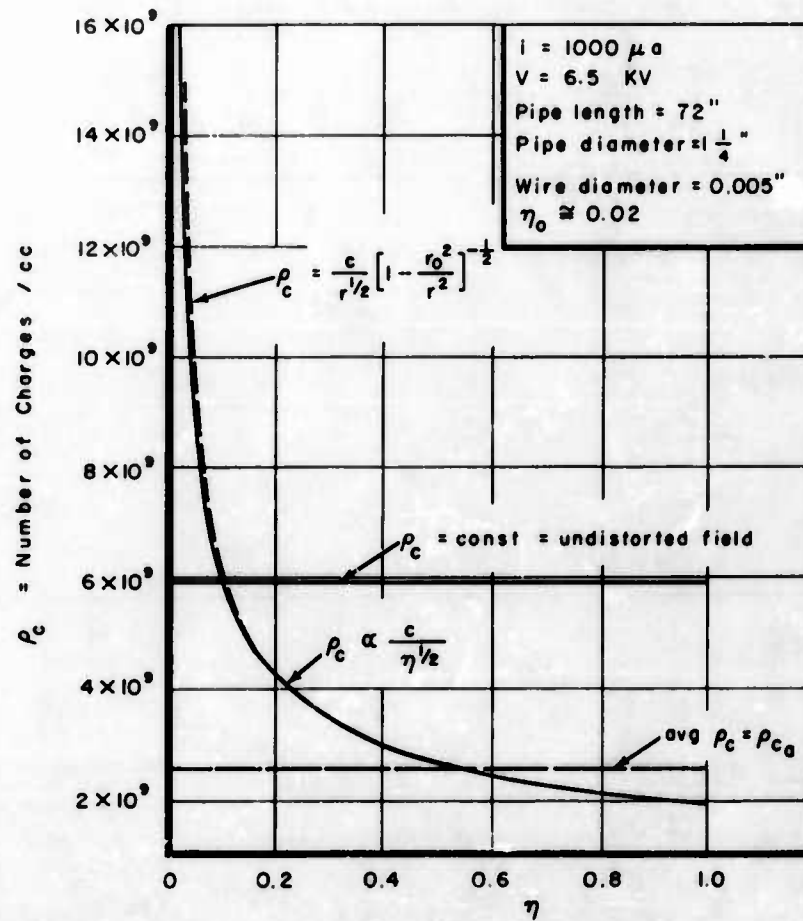


Figure 6. Charge Densities in a Round Tube

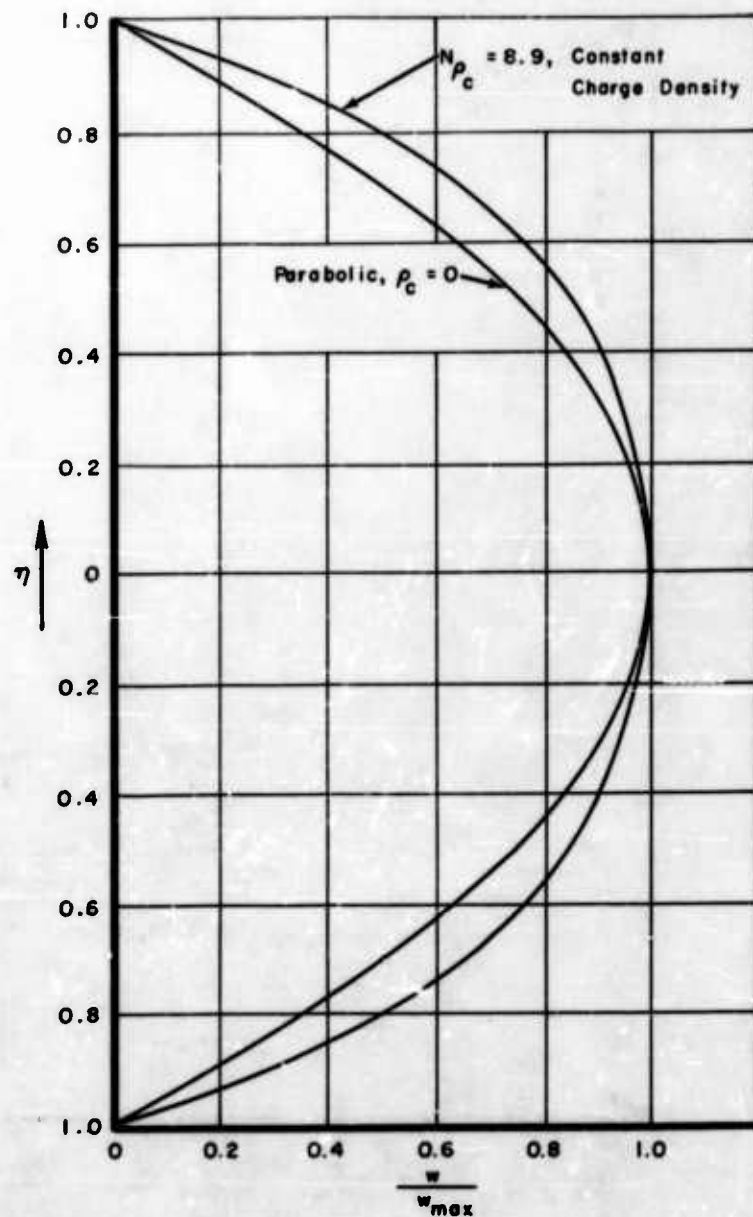


Figure 7. Case I. Theoretical Flat Plate Velocity Distribution, $\rho_c = \text{Constant}$

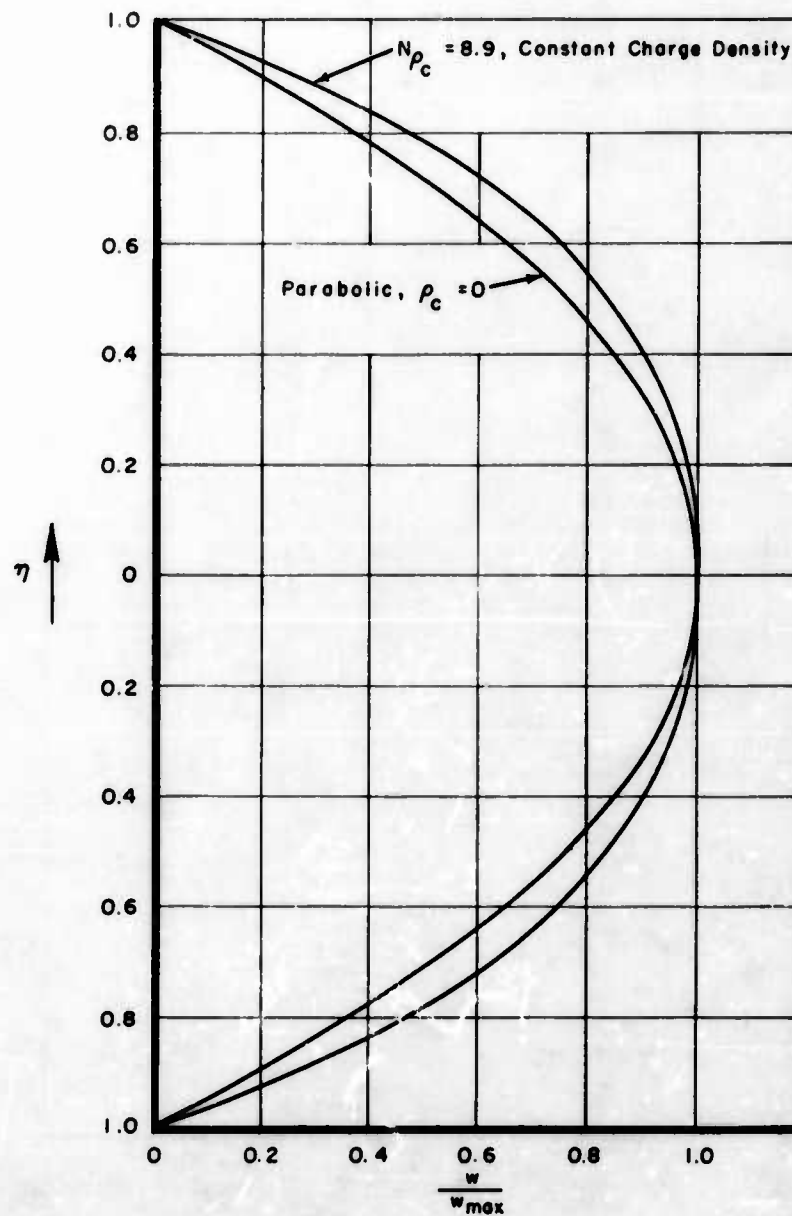


Figure 8. Case III. Theoretical Round Tube Velocity Distribution, $\rho_c = \text{Constant}$

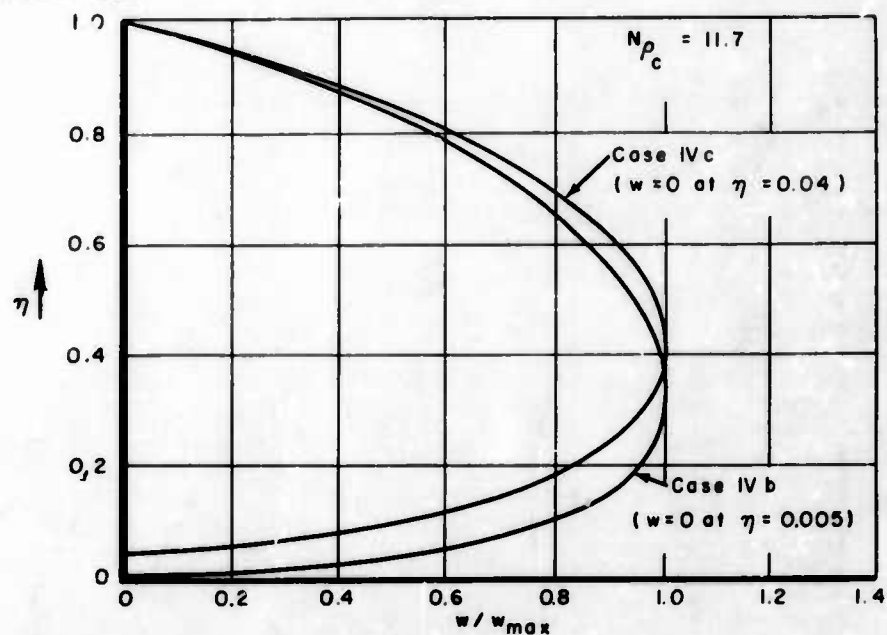


Figure 9. Theoretical Concentric Tube Velocity Distribution Case IVb and IVc, ρ_c = Constant in Tube

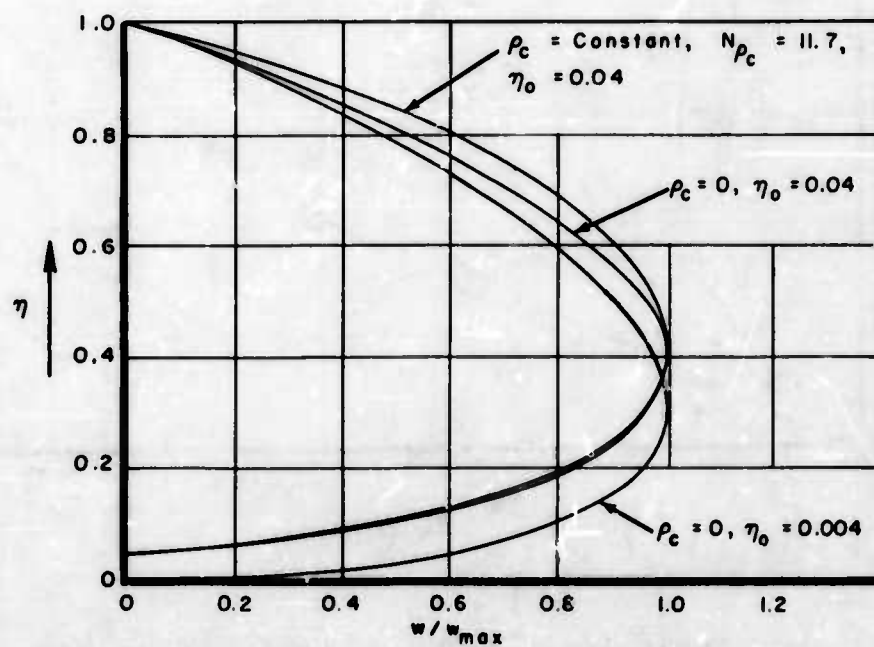


Figure 10. Theoretical Concentric Tube Velocity Distribution Case IV, ρ_c = Constant in Tube

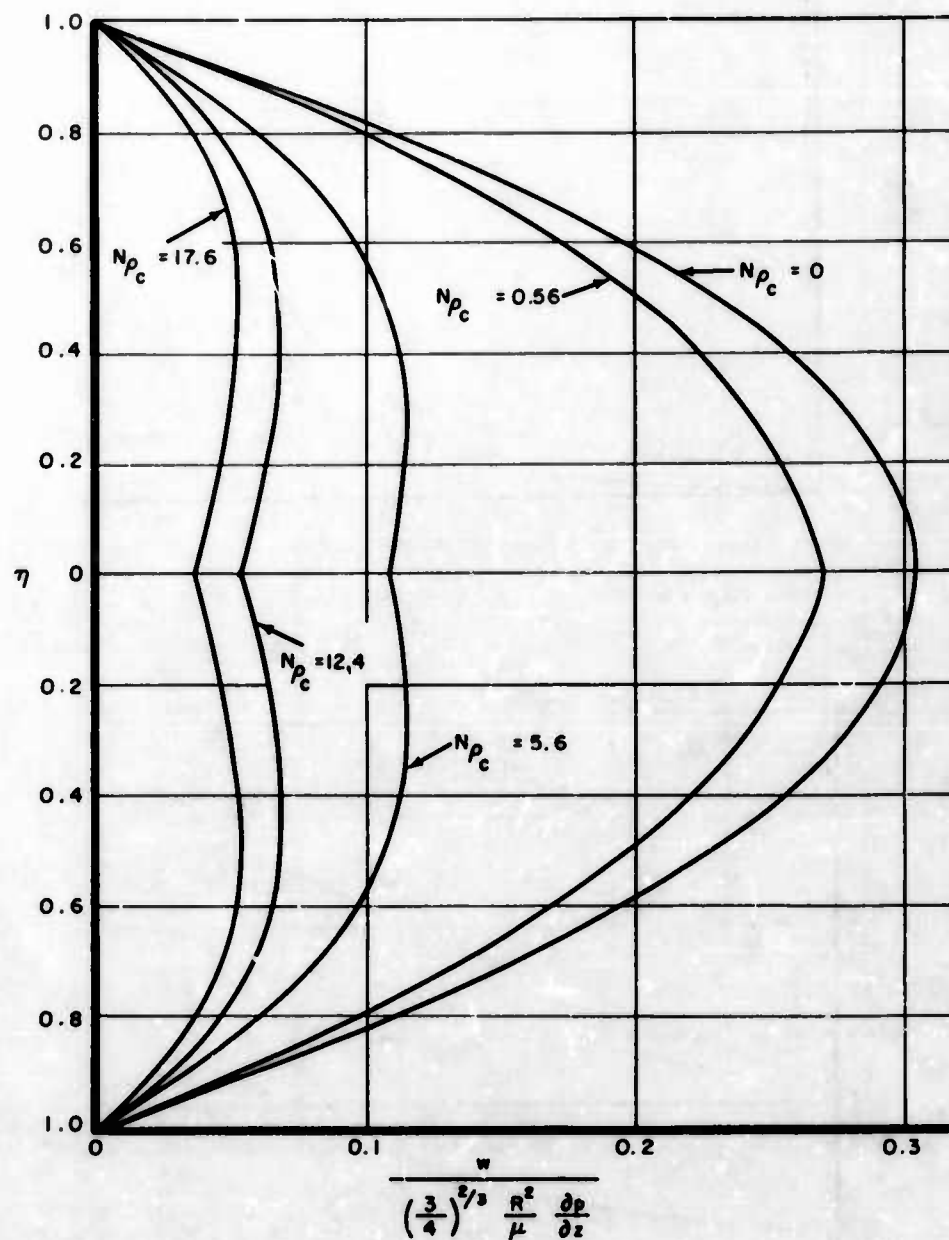


Figure 11. Case V. Variation of Velocity Distribution at Constant Pressure Drop and with $\rho_c \propto \eta^{-1/2}$

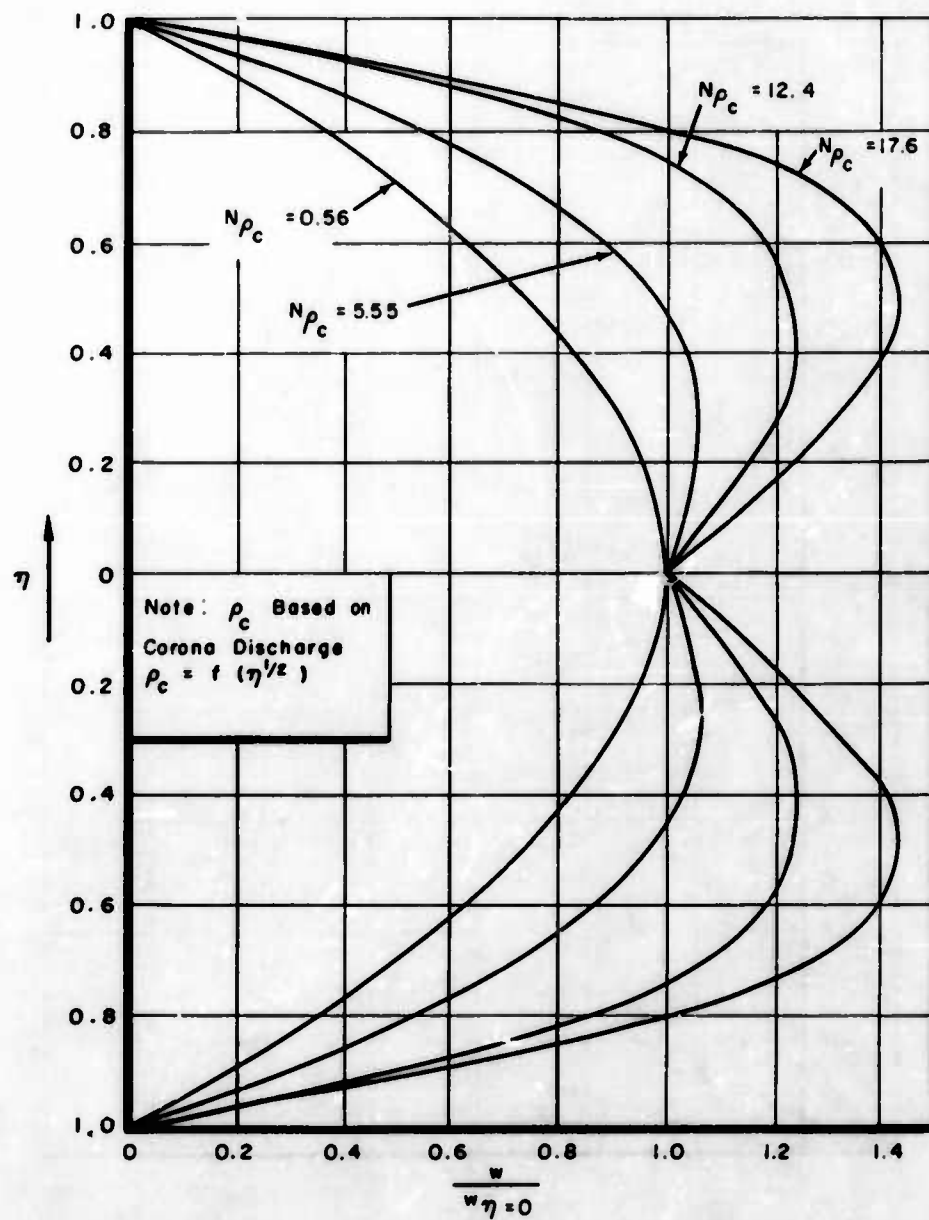


Figure 12. Case V. Velocity Profiles for Round Tube

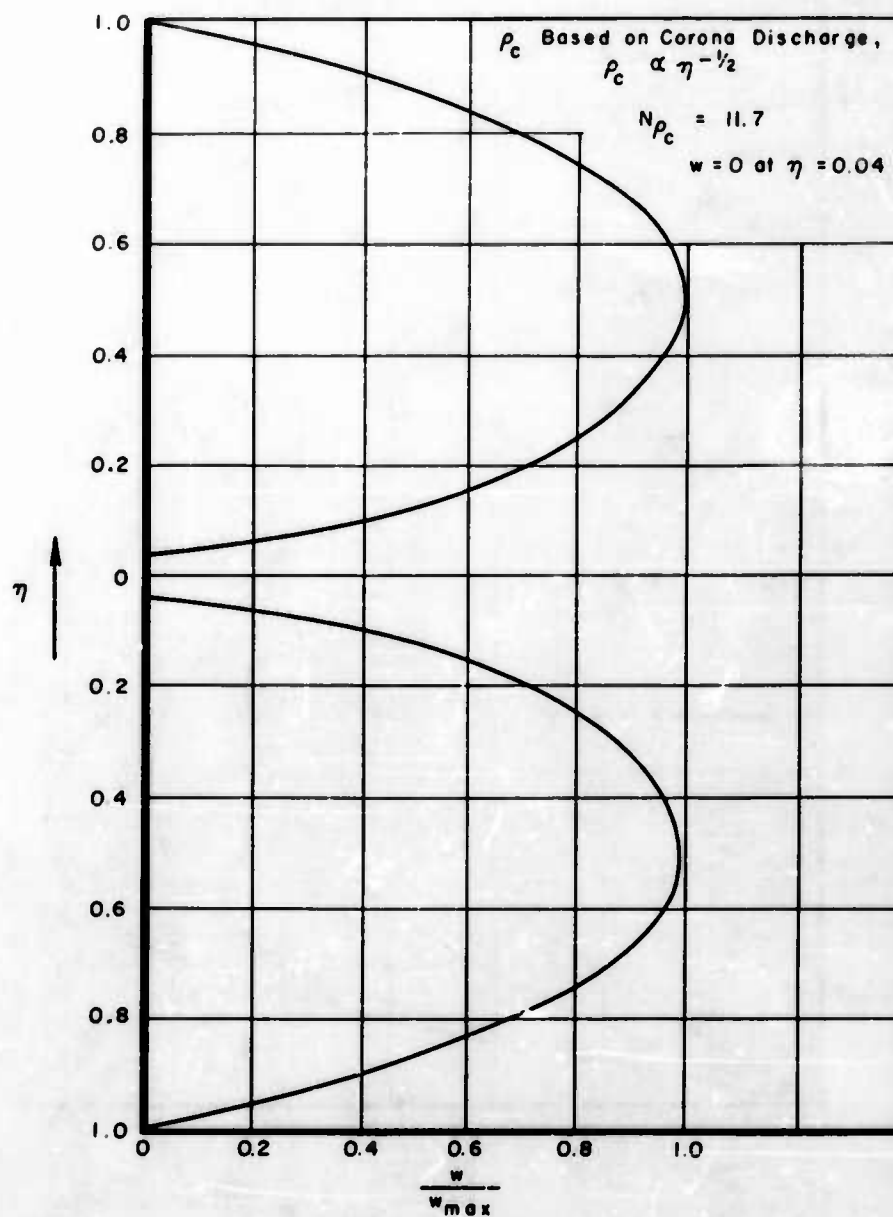


Figure 13. Case VI. Velocity Profile for Concentric Tube

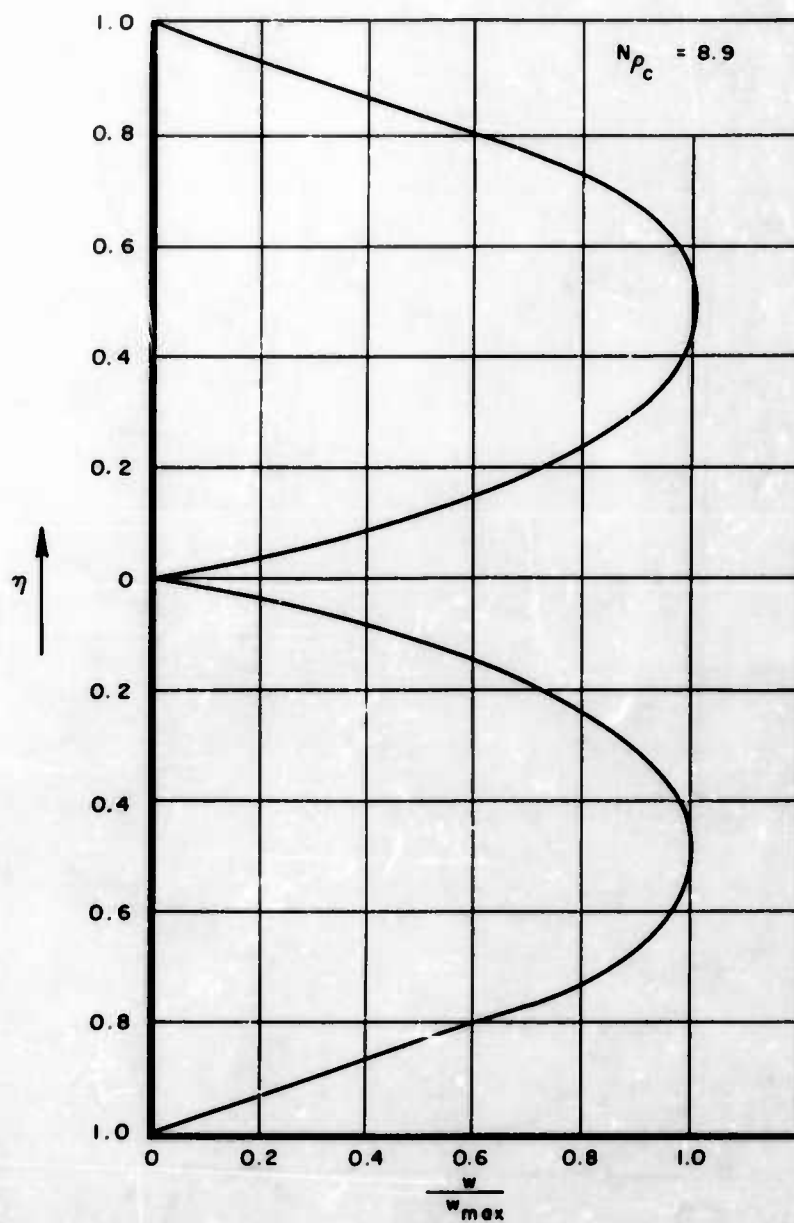


Figure 14. Velocity Profile for $\rho_c \propto \eta^{-2}$

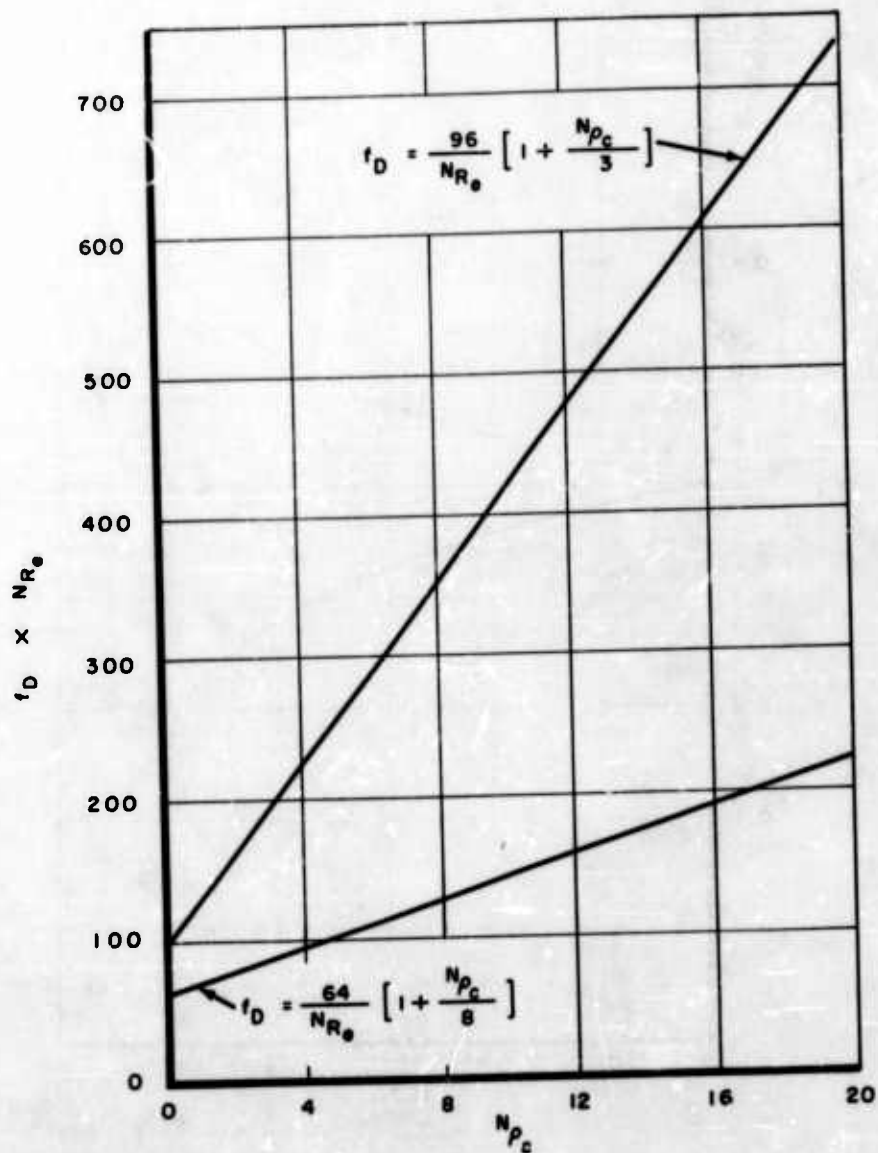


Figure 15. Effect of Charge Number on f_D . Mean Value Approach

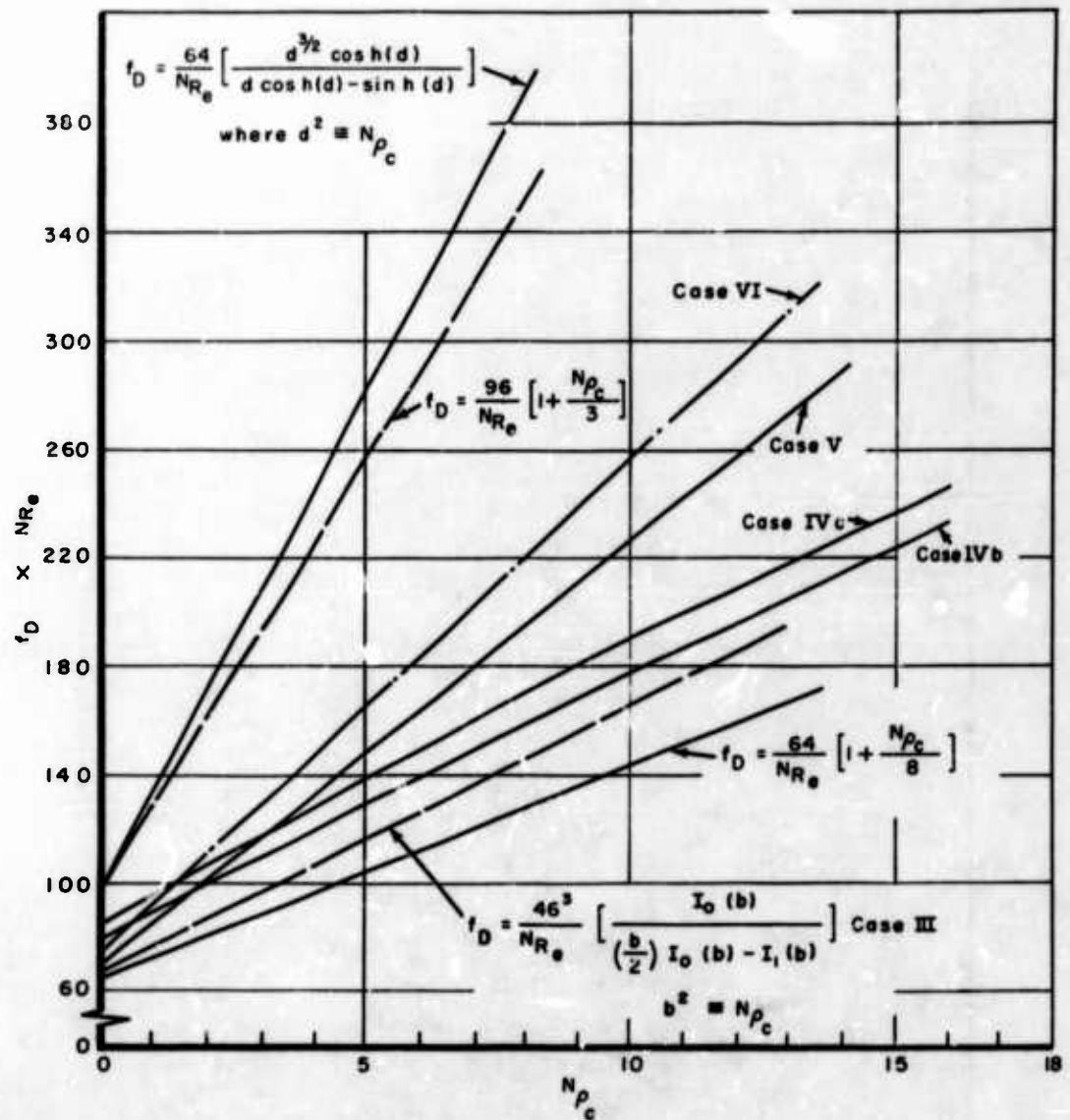


Figure 16. Variation of Friction Factor with Charge Number

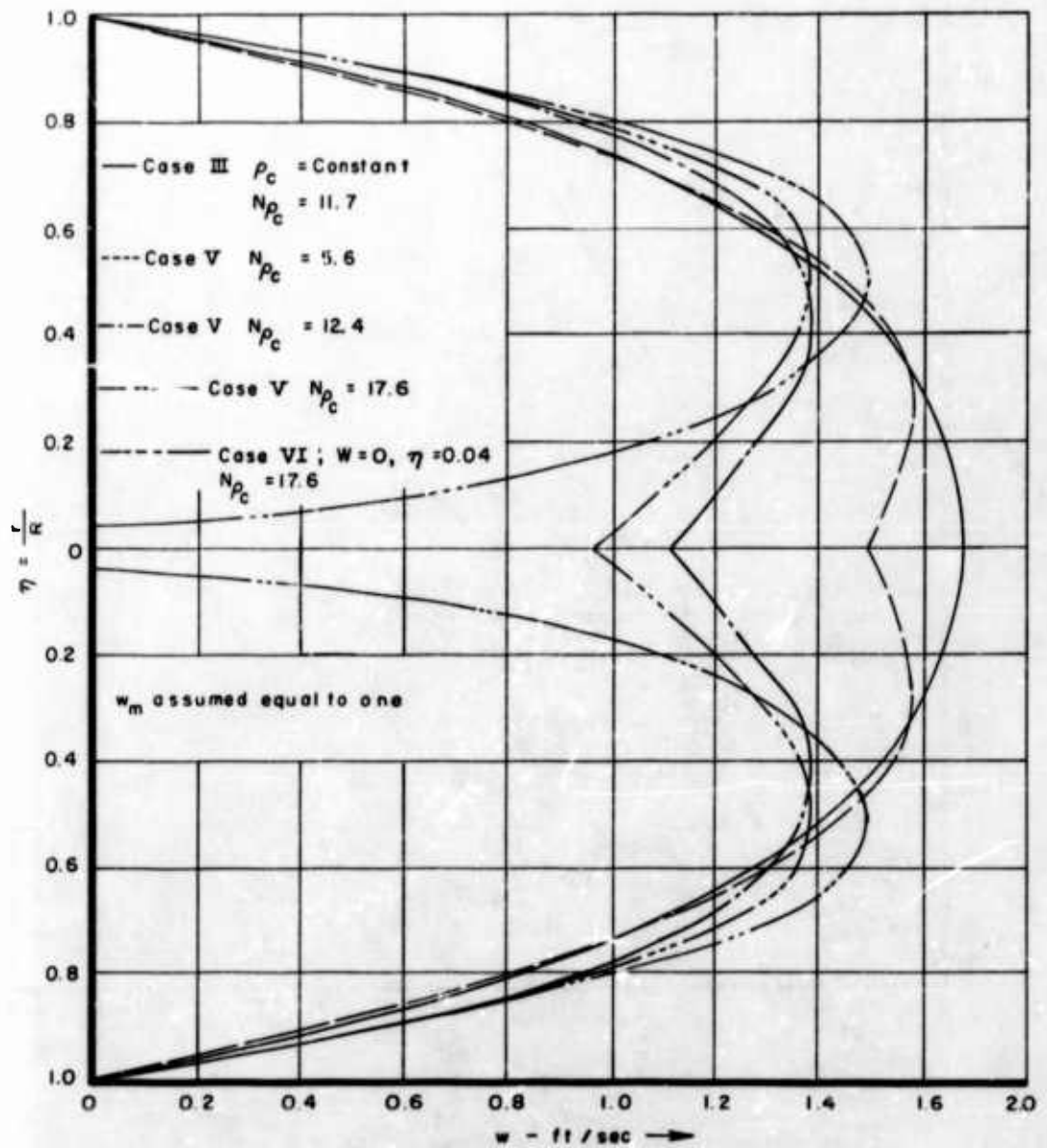


Figure 17. Typical Velocity Distributions at $w_m = 1 \text{ ft/sec.}$

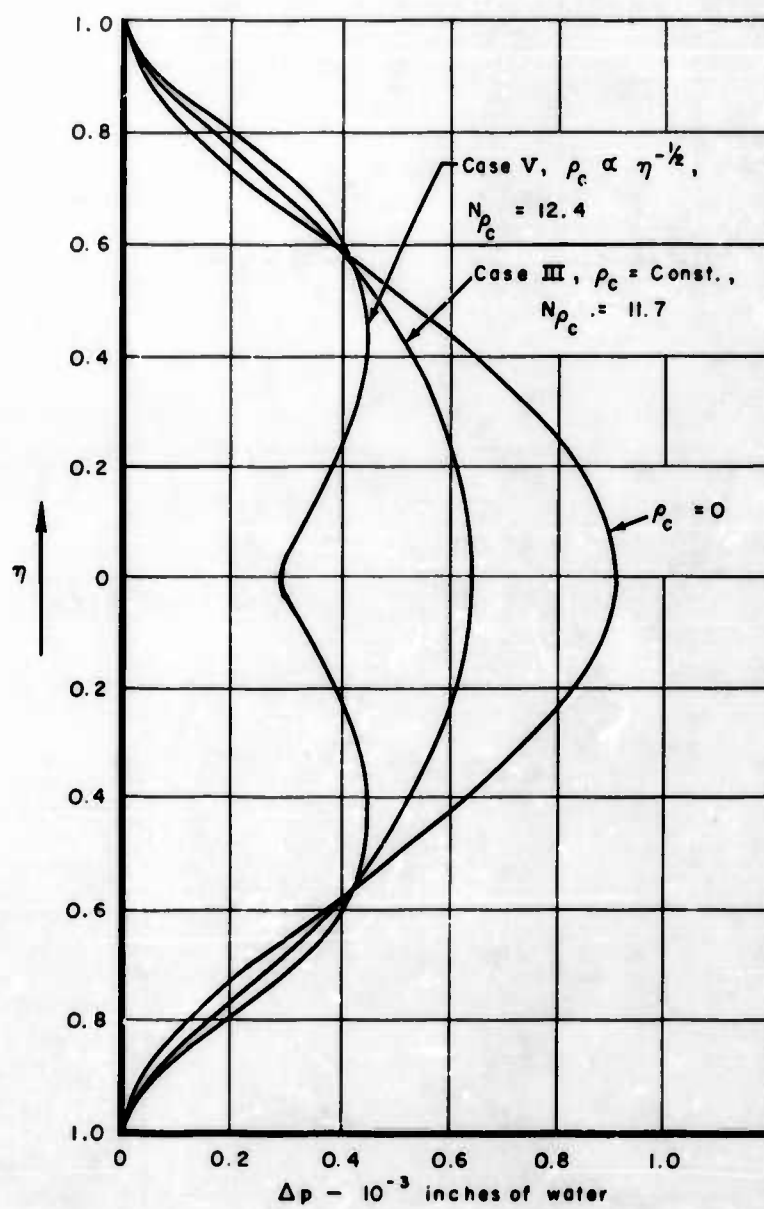


Figure 18. Typical Profiles in Terms of Pressure

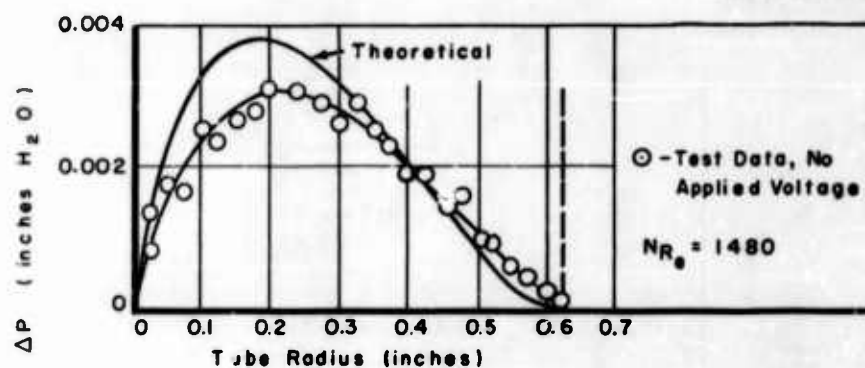


Figure 19. Velocity Profile Without Ionization. Concentric 0.005 -inch Wire, $w_m = 2.35$ ft/sec.

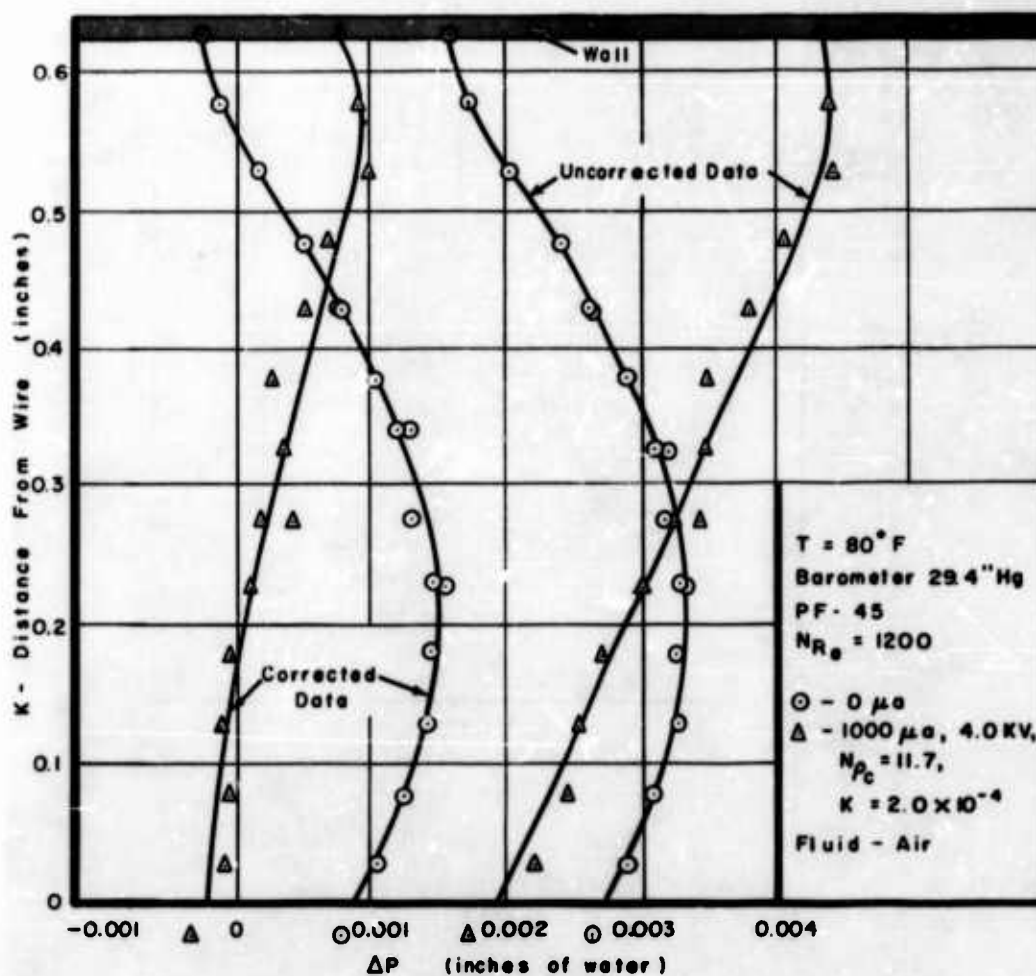


Figure 20. Velocity Profile Data, $N_{Re} = 1200$

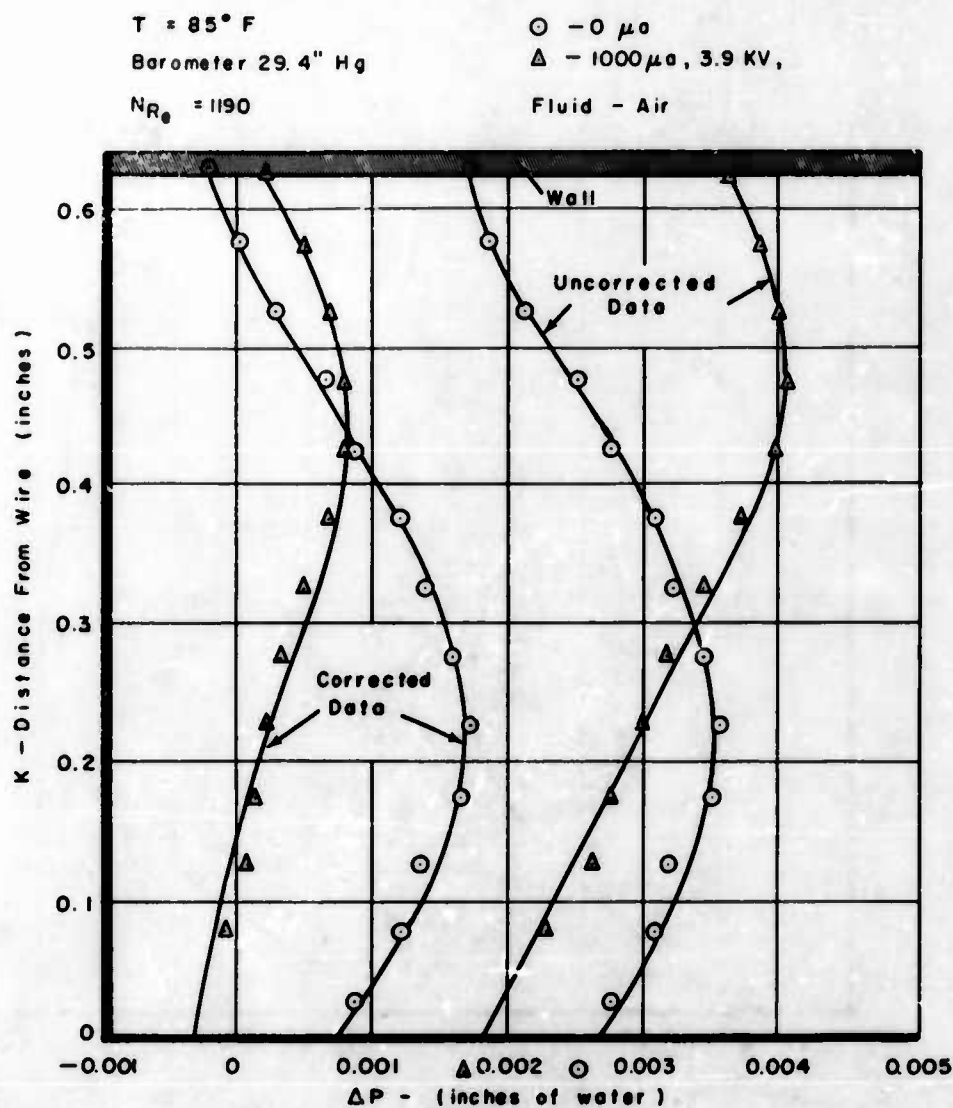


Figure 21. Velocity Profile Data, $N_{Re} = 1190$

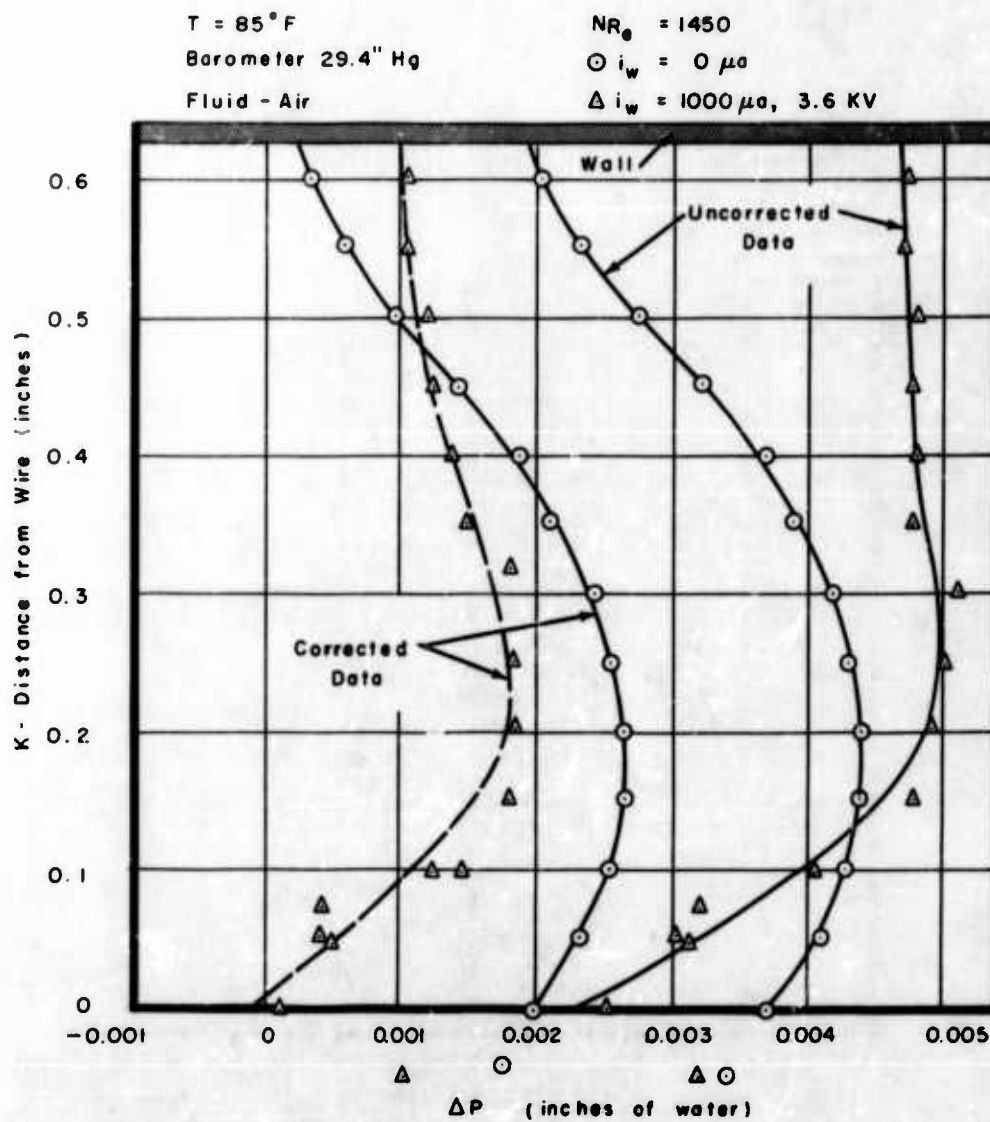


Figure 22. Velocity Profile Data, $NR_e = 1450$

$T = 86^{\circ}F$

Barometer 29.5" Hg

$N_{Re} = 1745$

$\bigcirc - 0 \mu a$

$\Delta - 1000 \mu a, 3.8 \text{ KV}$

Fluid - Air

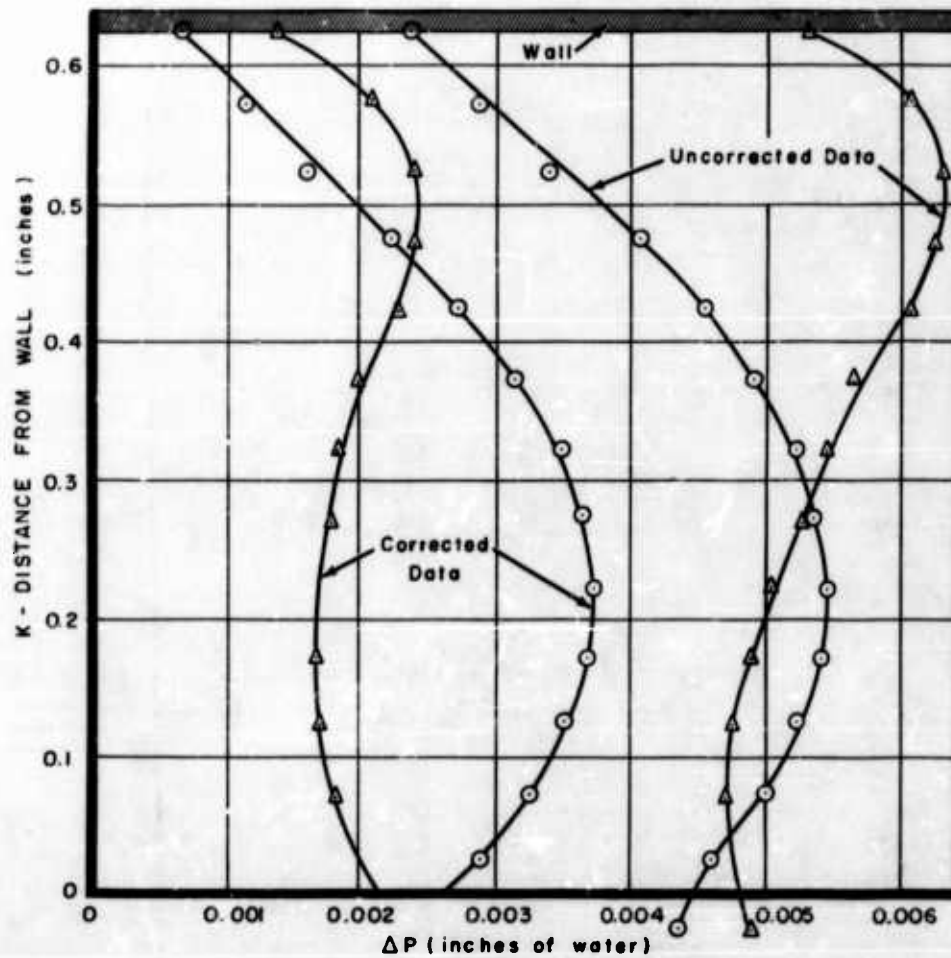
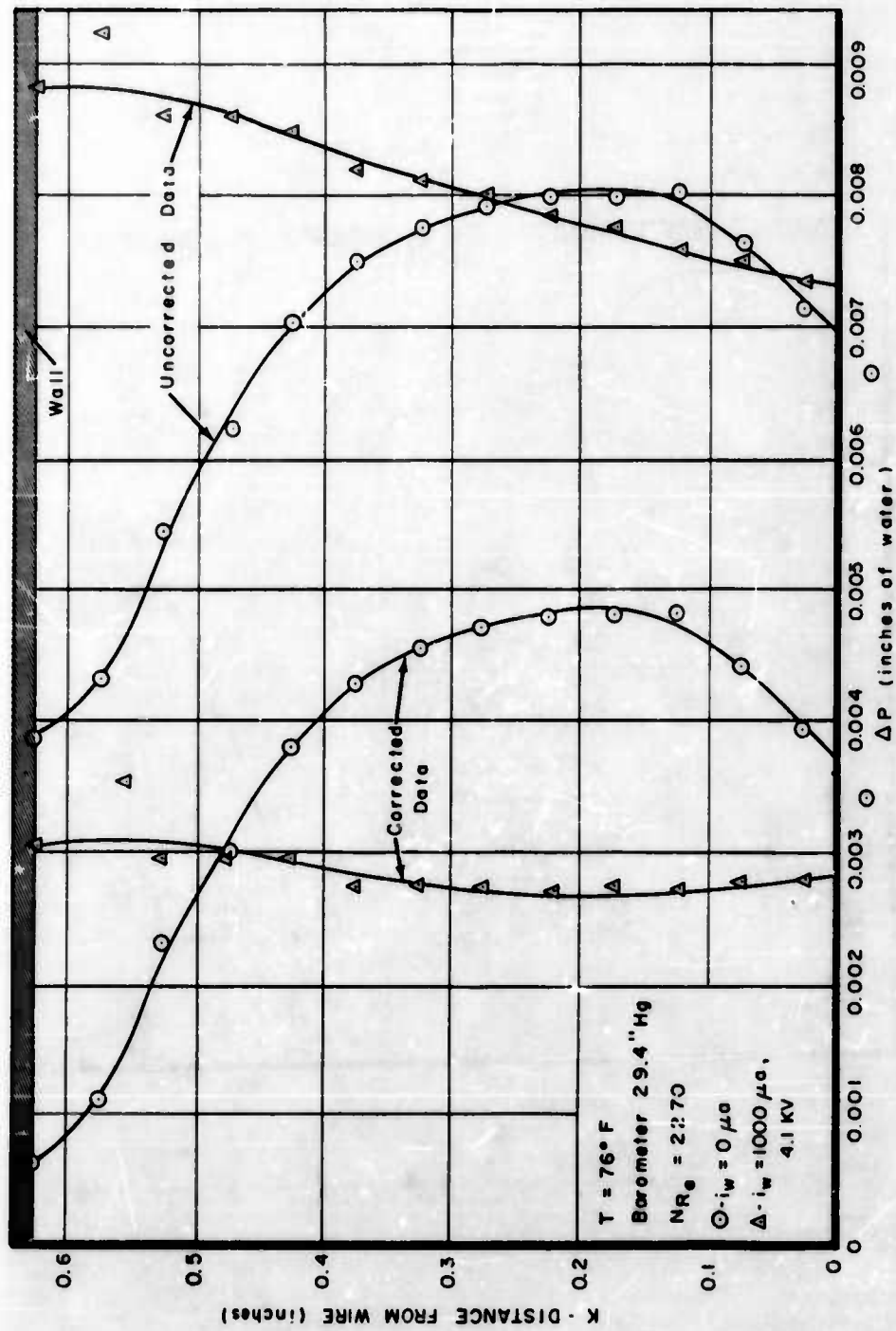


Figure 23. Velocity Profile Data, $N_{Re} = 1745$

Figure 24. Velocity Profile Data, $N_{Re} = 2070$

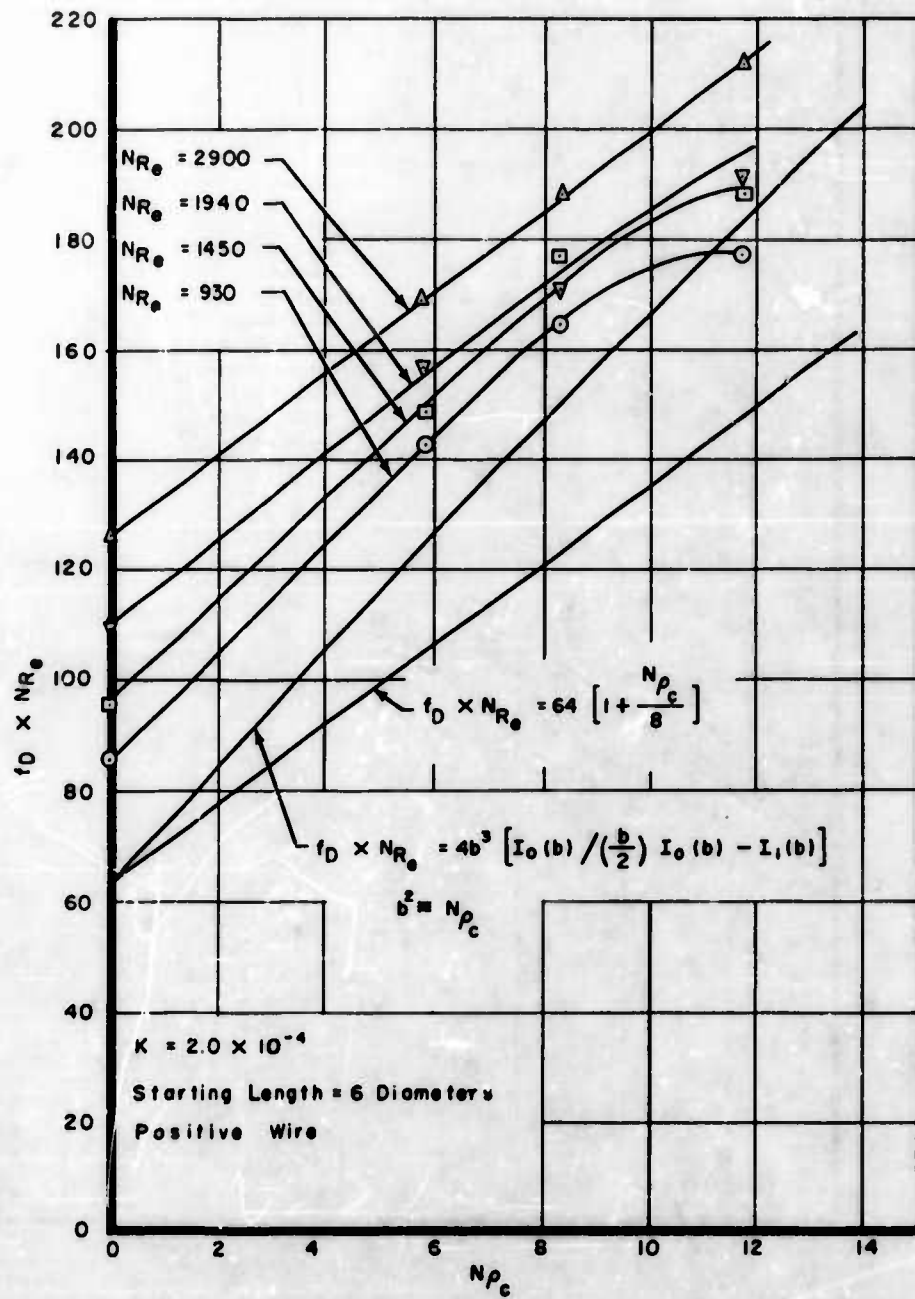
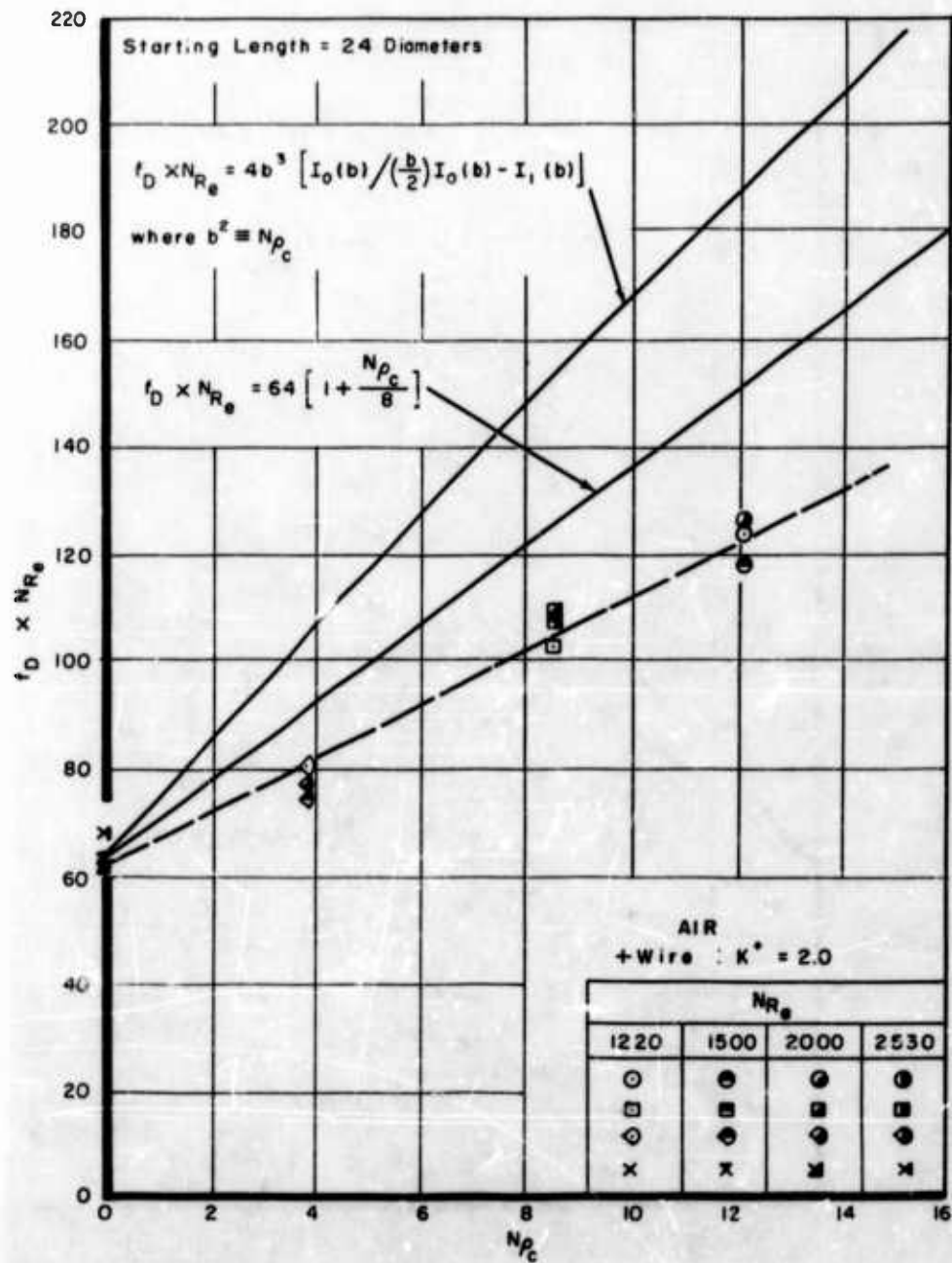


Figure 25. Exploratory Test Data Showing Variation of f_D with Charge Number for Air

Figure 26. Variation of f_D with Charge Number for Air

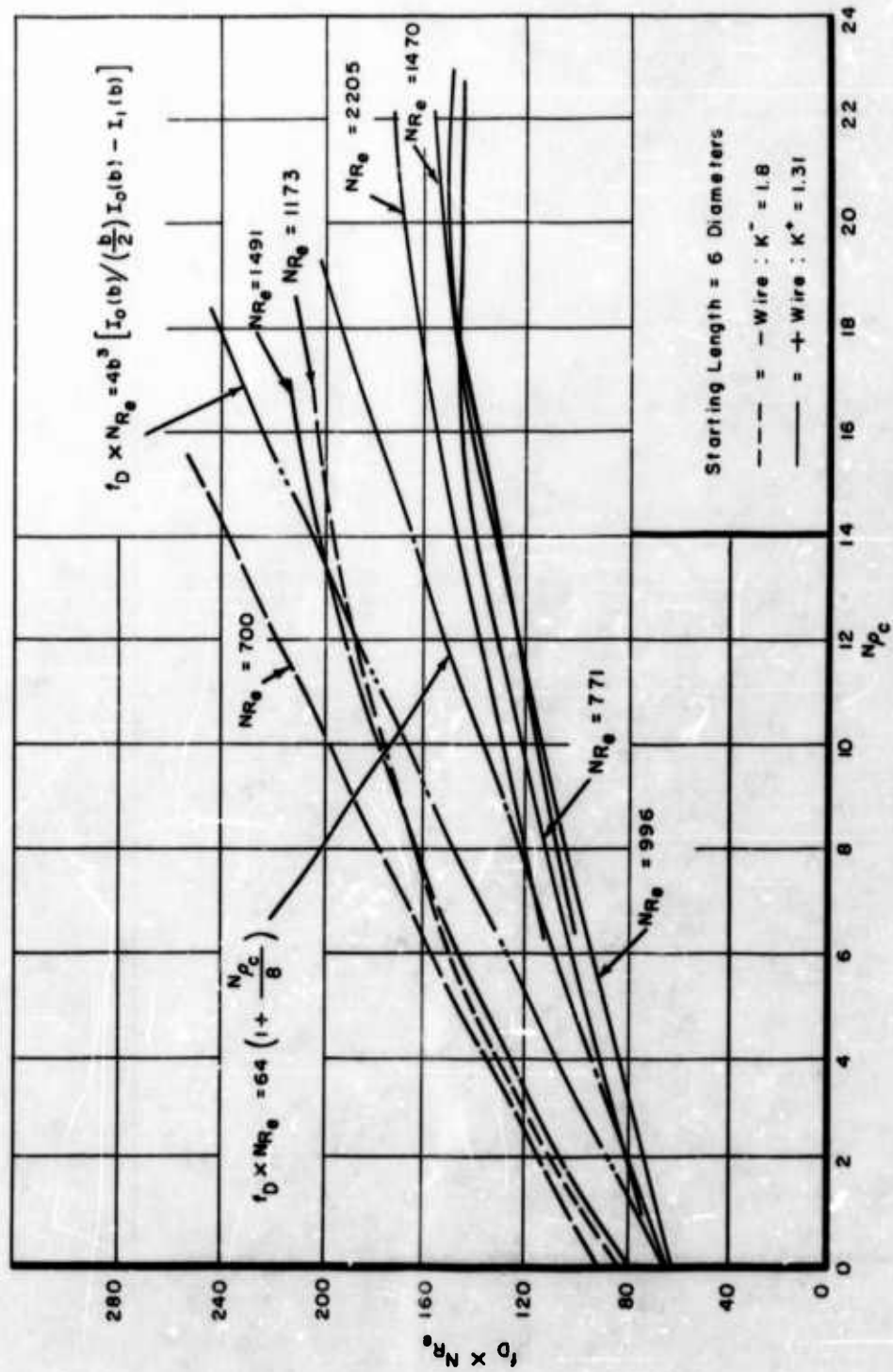


Figure 27. Variation of f_D with Charge Number for Oxygen

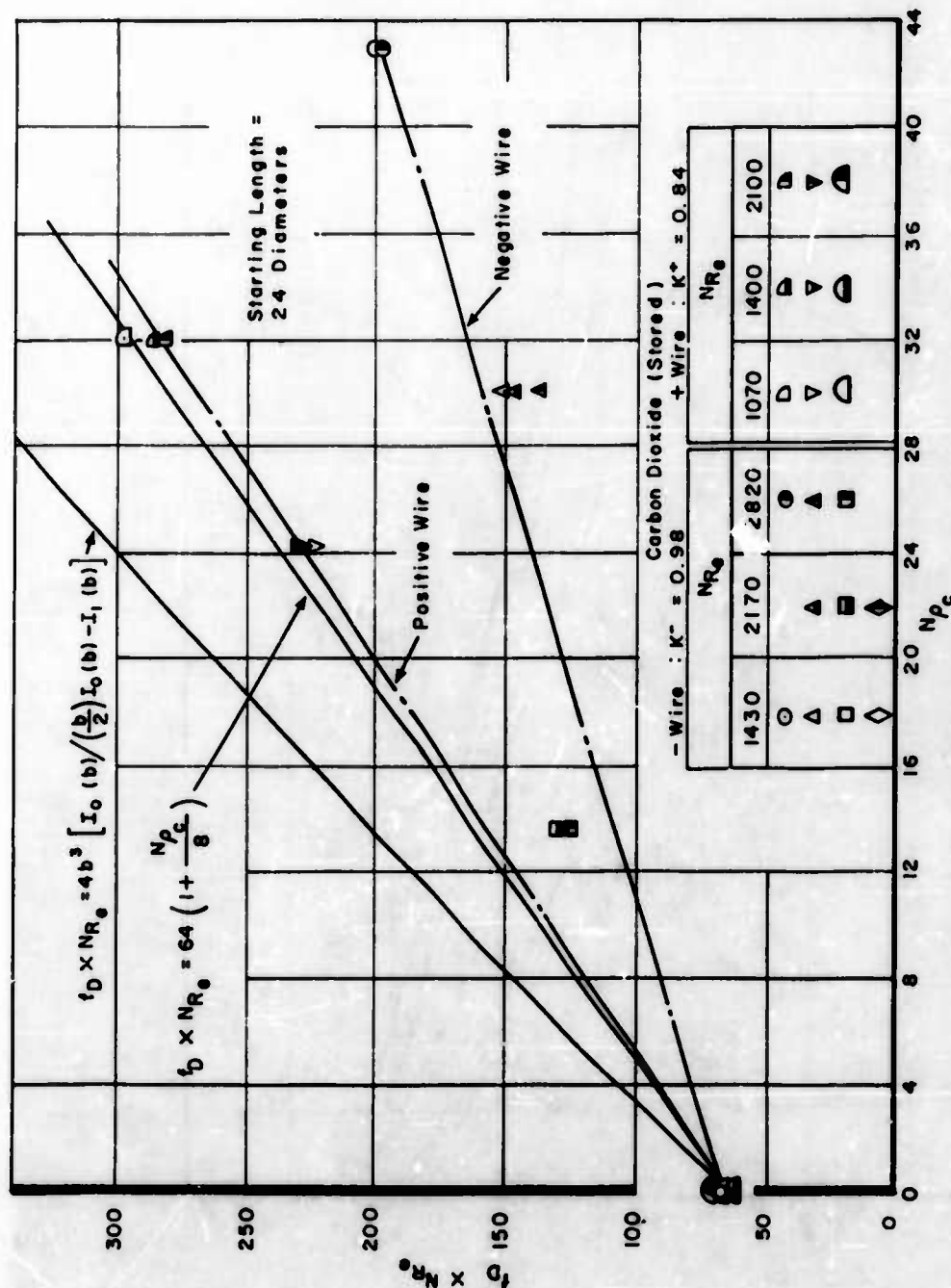


Figure 28. Variation of f_D with Charge Number for Carbon Dioxide

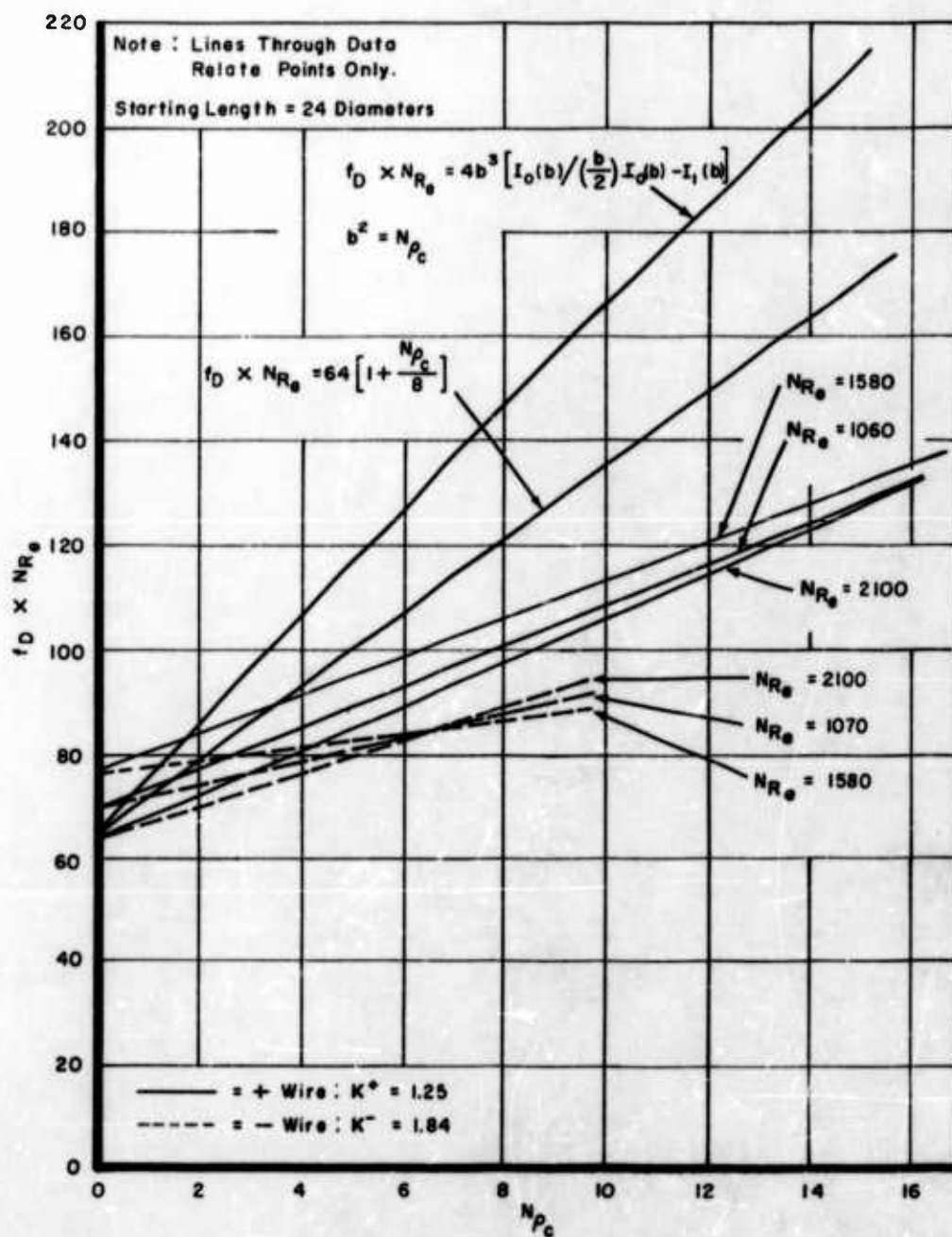


Figure 25. Effect of Charge Number on f_D for Nitrogen

APPENDIX I

NONDIMENSIONAL PARAMETERS

The analysis in the body of this report revealed a new dimensionless ratio. From Equations (64) and (75), the ratio appeared in the form:

$$\frac{\rho_c L^2}{\mu K}$$

Equation (72) put this in terms of the average charge density:

$$\frac{\rho_c L^2}{\mu K} = \frac{\rho_{cm} L^2}{\mu K} \rho_c^*$$

where

$$\rho_c^* = \frac{\rho_c}{\rho_{cm}}$$

L is a characteristic length of the flow, and

ρ_c^* is a nondimensional variable charge.

The charge number then is defined by Equation (71) as:

$$N_{\rho_c} = \frac{\rho_{cm} L^2}{\mu K}$$

This number is equivalent to the ratio of the charge forces to the viscous forces in the flow.

Another nondimensional parameter arises from consideration of Equation (100) or (101).

$$f_B = \frac{24}{N_{R_0}} \left(1 + \frac{N_{\rho_c}}{3} \right) \quad (100)$$

$$f_B = \frac{16}{N_{R_0}} \left(1 + \frac{N_{\rho_c}}{8} \right) \quad (101)$$

Equation (101) can be written as:

$$f_B = \frac{16}{N_{R_0}} + 2 \frac{N_{\rho_c}}{N_{R_0}} \quad (102)$$

The ratio N_{ρ_c} / N_{R_0} is also a new parameter:

$$\begin{aligned}\frac{N\rho_c}{NR_e} &= \frac{\left(\frac{\rho_{cm} R^2}{\mu \kappa}\right)}{\frac{\rho w_m D}{\mu}} \\ &= \frac{1}{4} \frac{\rho_{cm} D}{\rho w_m \kappa}\end{aligned}\quad (183)$$

This represents the ratio of the charge forces to the inertia forces in the stream. The inverse of Equation (183) is:

$$\frac{NR_e}{N\rho_c} = 4 \left(\frac{\rho w_m \kappa}{\rho_{cm} D} \right) \quad (184)$$

The factor in the brackets, then, becomes an effective charge Reynolds number,

$$NR_c = \frac{\rho w_m \kappa}{\rho_{cm} D} \quad (185)$$

This interesting parameter indicates that, as the charge density disappears, the charge Reynolds number becomes very large and the flow field is dominated by the inertia forces. If there is appreciable ionization in the stream and the density of the gas is low, then charge effects could appear. If the velocity is very low, charge effects could also appear. If dimensions are very large and velocity and density are relatively low, the charge could also influence the flow. The data could be plotted against the charge Reynolds number, but the plots of i_D vs. NR_e at constant corona current (constant charge density) and i_D vs. $N\rho_c$ are believed to present the data adequately.

It is of considerable interest to study the flow charge number further:

$$N\rho_c = \frac{\rho_{cm} L^2}{\mu \kappa}$$

Since both μ and κ depend upon the molecular actions in a gas, this ratio may be expressed in completely different terms.

From the kinetic theory of gases the viscosity of a gas can be given by (Ref. 13):

$$\mu = \frac{1}{3} N m \bar{c} \lambda \quad (186)$$

where N is the number of molecules per unit volume,

m is the mass of a molecule,

\bar{c} is the mean speed of a molecule, and

λ is the mean free path.

The constant, $1/3$, is from the elementary derivation of viscosity. More complete theories modify this constant. To account for this, let the viscosity of the gas be represented by:

$$\mu = a_1 N m \bar{c} \lambda \quad (187)$$

where a_1 is a suitable constant.

From the kinetic theory, the value of mobility in terms of molecular action can be obtained (Ref. 2) by:

$$\kappa = b \frac{q \lambda_i}{m_i \bar{c}} \quad (188)$$

where q is the charge per ion,

λ_i is the mean free path of an ion,

m_i is the mass of the ion,

\bar{c} is the mean speed of the neutral molecules in the gas through which the ion is moving, and

b is a constant which depends upon the theory used.

Cobine (Ref. 2) shows that for ions of the parent gas:

$$\lambda_i = 2^{1/2} \lambda \quad (189)$$

An experimental observation is that the electrical forces around an ion cause its mean free path to be much shorter than that of the neutral molecule (Ref. 4). The form for κ given in Equation (188) is sufficiently accurate for our use, since the value for the constant, b , can be chosen to account for the theory used and the mean free path. From Equations (187) and (188):

$$\mu \kappa = a_1 N m \bar{c} \lambda \times b q \frac{\lambda_i}{m \bar{c}} \quad (190)$$

Using Equation (189):

$$\mu \kappa = 2^{1/2} a_1 b q N \lambda^2 \quad (191)$$

but

$$\rho_{c_0} = q N_i \quad (192)$$

Letting $\sqrt{2} a_1 b = c_i$ and substituting Equation (192) gives:

$$\mu \kappa = c_i \rho_{c_0} \left(\frac{N}{N_i} \right) \lambda^2 \quad (193)$$

Substituting into the charge number:

$$\frac{\rho_{c_0} L^2}{\mu \kappa} = \frac{1}{c_i} \left(\frac{L^2}{\lambda^2} \right) \left(\frac{N_i}{N} \right) \quad (194)$$

The Knudsen number is defined as:

$$N_{K_n} = \frac{\lambda}{L} \quad (195)$$

It is the ratio of the mean free path to a representative dimension of the flow system. Substituting Equation (195) into the charge number:

$$N_{\rho_c} = \frac{1}{c_i} \frac{1}{(N_{K_n})^2} \left(\frac{N_i}{N} \right) \quad (196)$$

N_i/N represents the number of charges per neutral molecule and is dimensionless. c_i , a constant, is dimensionless, as is the Knudsen number.

$$N_{\rho_c} \propto \frac{1}{(N_{K_n})^2} \left(\frac{N_i}{N} \right) \quad (197)$$

This equation indicates why the ionization has such a surprisingly large effect on the flow. If ionization is present in any appreciable quantity, then the influence of the Knudsen number can be very great. Since in ordinary gas flows at standard conditions:

$$\lambda = 0.1 \text{ (} 10^{-5} \text{) cm}$$

and using $L = 1 \text{ (} 1 \text{) cm}$:

$$N_{K_n}^2 = 0.1 \text{ (} 10^{-10} \text{)}$$

Considering the constant, c_i , based upon the simpler theory:

$$a = \frac{1}{3}$$

$$b = 1,$$

$$c_i \approx \frac{\sqrt{2}}{3}$$

Therefore:

$$\begin{aligned} N_{\rho_c} &= 0.1 \left(\frac{3}{\sqrt{2}} \times 10^{10} \cdot \frac{N_i}{N} \right) \\ &= 0.1 \left(10^{10} \frac{N_i}{N} \right) \end{aligned}$$

This indicates that the charge number will be of the order of 10^{10} times the charge ratio. This large amplification effect of the Knudsen number indicates why even small charge densities can have significant effects on flow. Since typical charge densities in the tests were from 10^{-10} to 10^{-9} , the magnitude of N_{ρ_c} is of the order of 1 to 10. This value is in line with the values of N_{ρ_c} presented in the body of the report.

Other important ratios such as those relating to compressibility (Mach Number) or heat transfer can also be obtained as necessary for specific problems.

APPENDIX II

CURVES FOR CALCULATING CASE V AND CASE VI VELOCITY PROFILES

Universal curves for calculating the velocity profile for round tube geometry with variable space charge (Cases V and VI) are presented in this appendix. For these calculations, ξ is a useful coordinate defined by Equation (162):

$$\xi = \frac{4}{3} \gamma_1^{1/2} \eta^{3/4}$$

$$\gamma_1 = \frac{3}{4} N \rho_c$$

By using these parameters, Equation (161) for Case V, where the wire does not affect the flow, and Equation (167) for Case VI, where the flow is assumed at rest at or near the wire, we can use the curves to compute the profiles for specific values of corona current.

Figure II-1 thru II-10. Universal Curves for Calculating Velocity Profiles, Cases V and VI

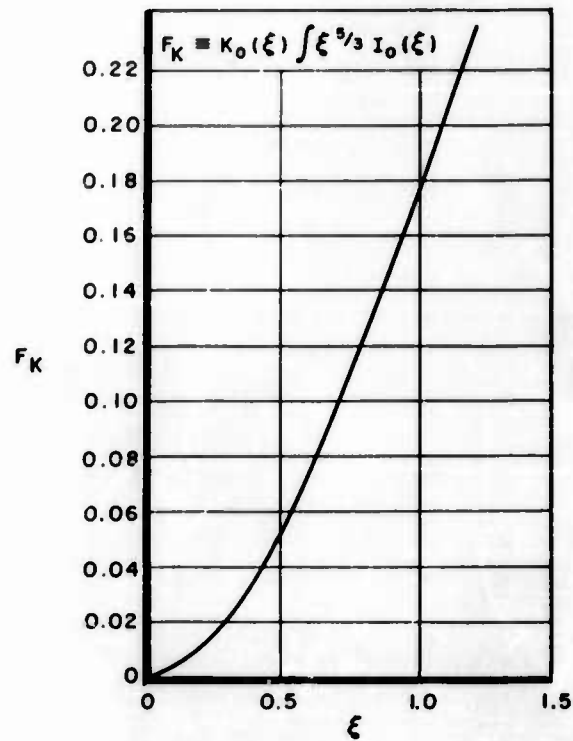


Figure II-1.

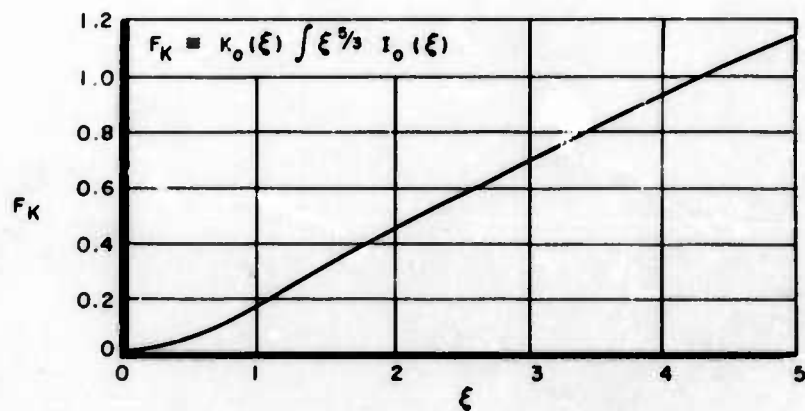


Figure II-2.

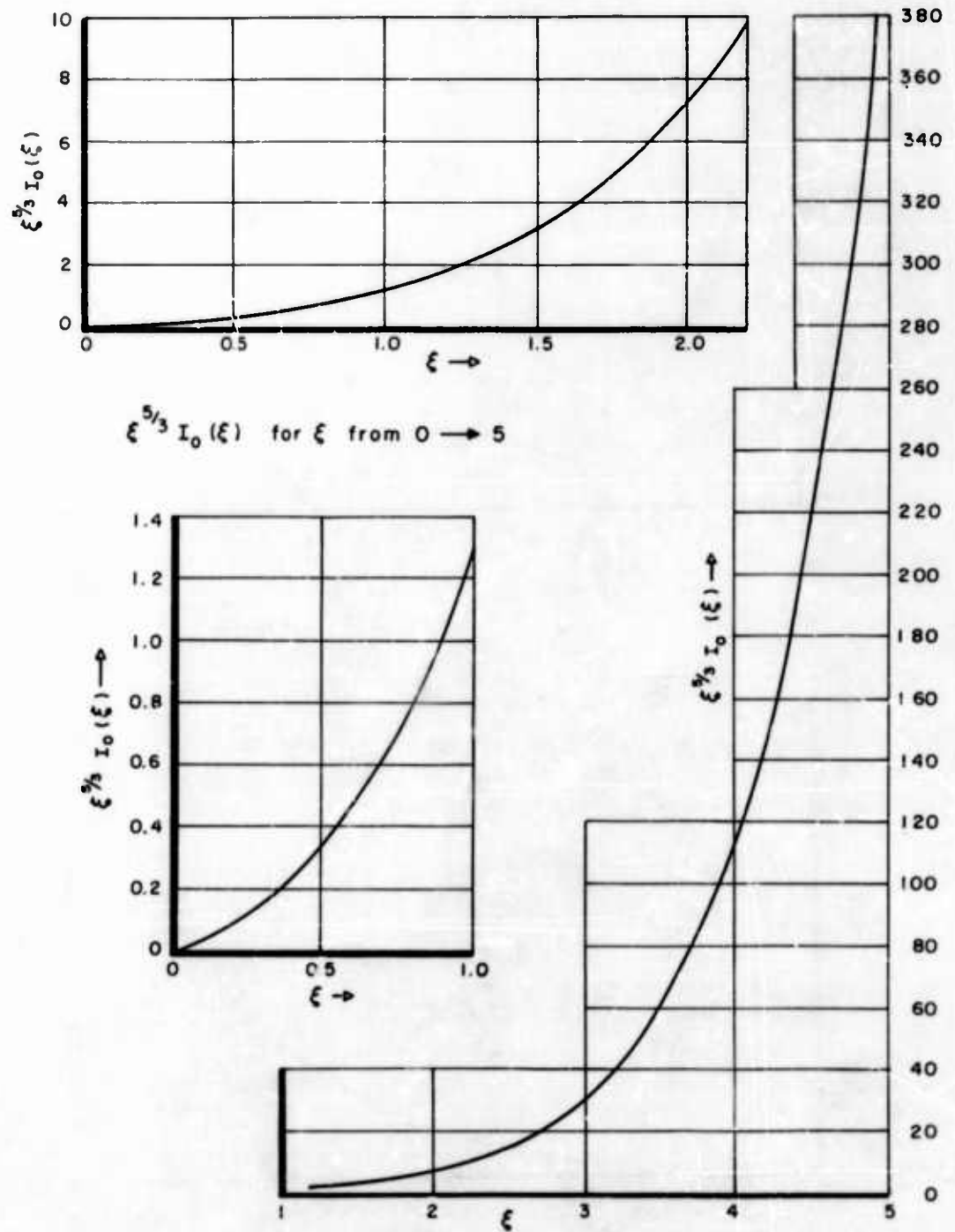


Figure II-3.

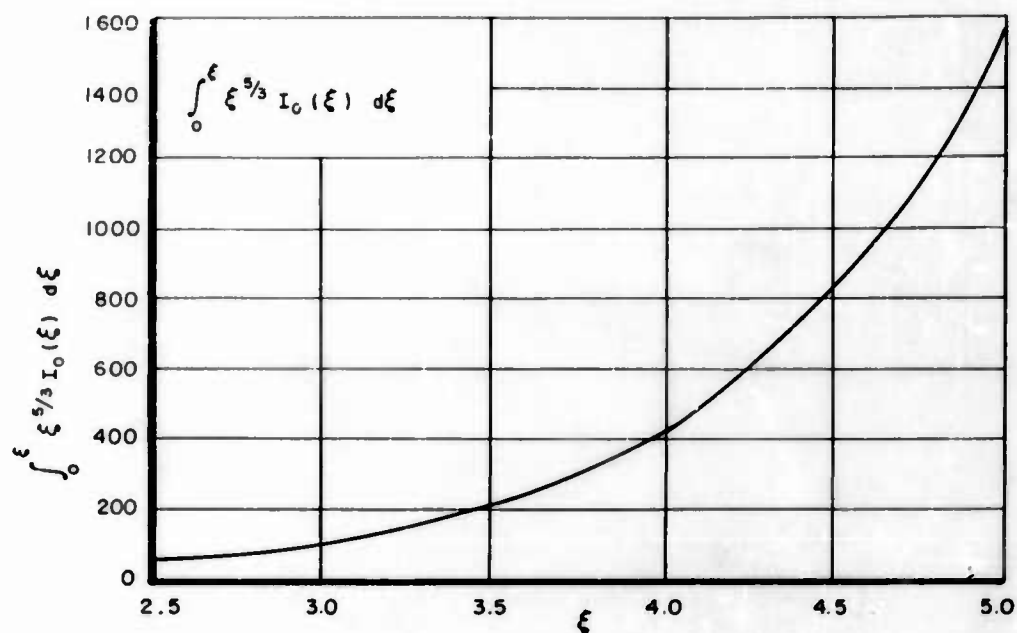


Figure II-4.

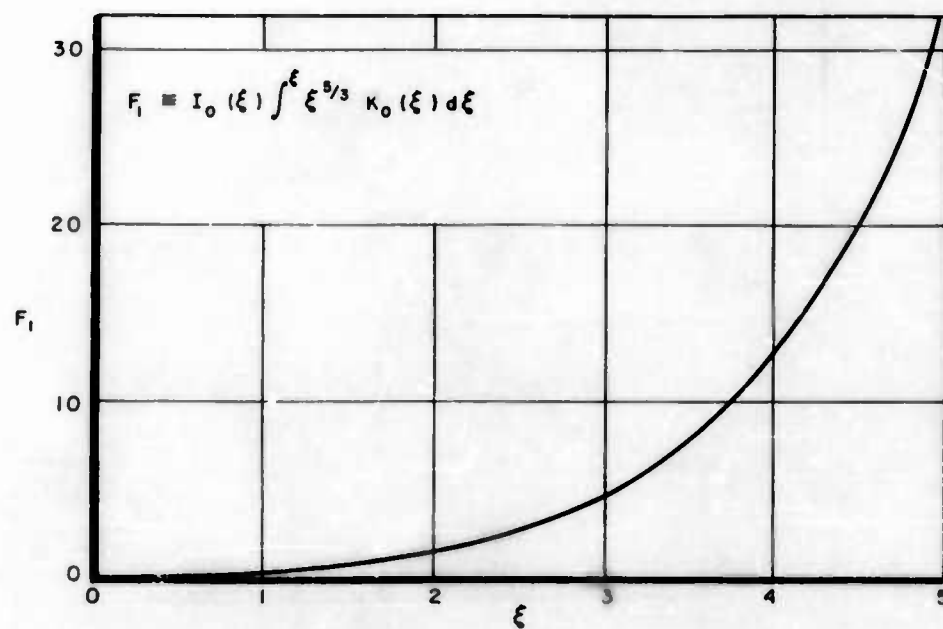


Figure II-5.

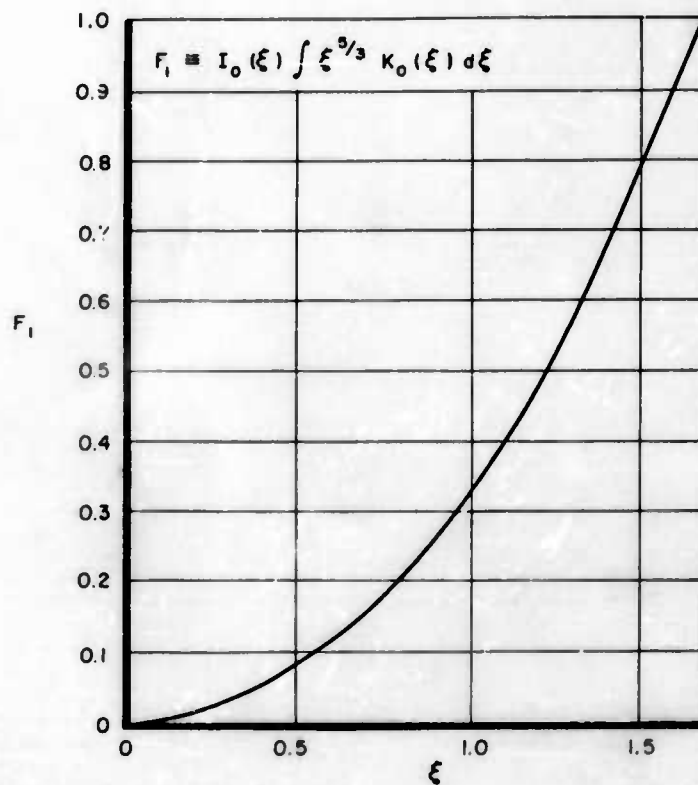


Figure II-6.

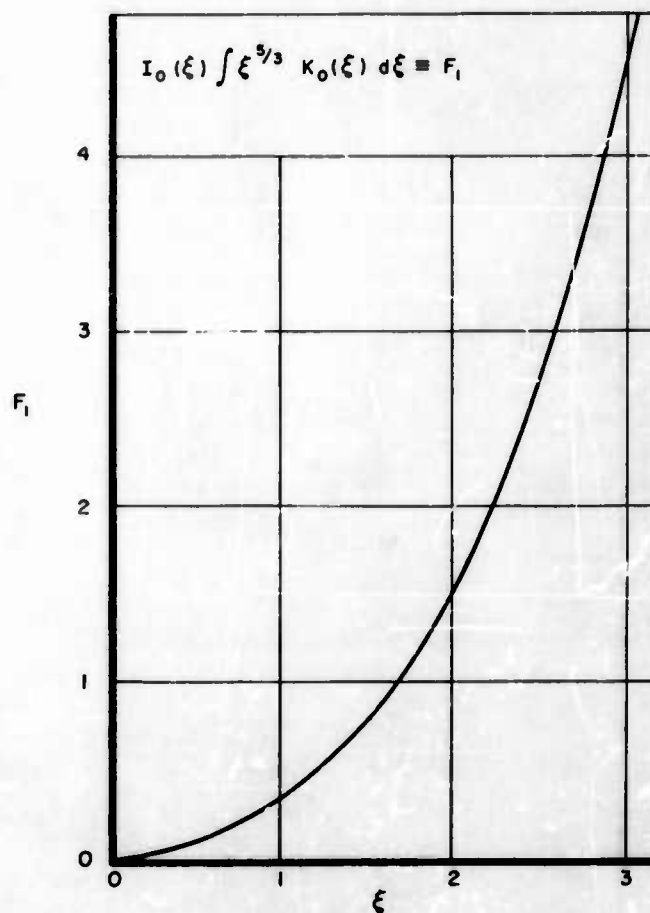


Figure II-7.

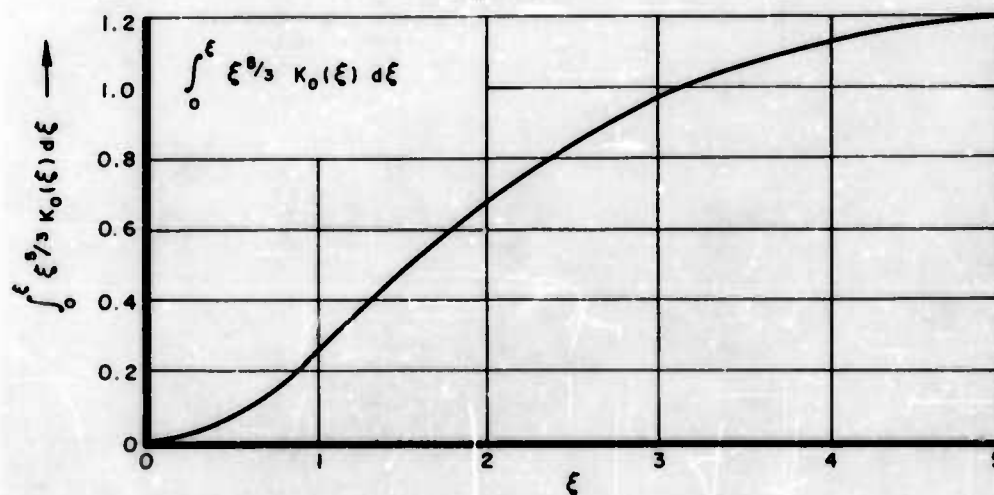


Figure II-8.

RTD-TDR-63-4009

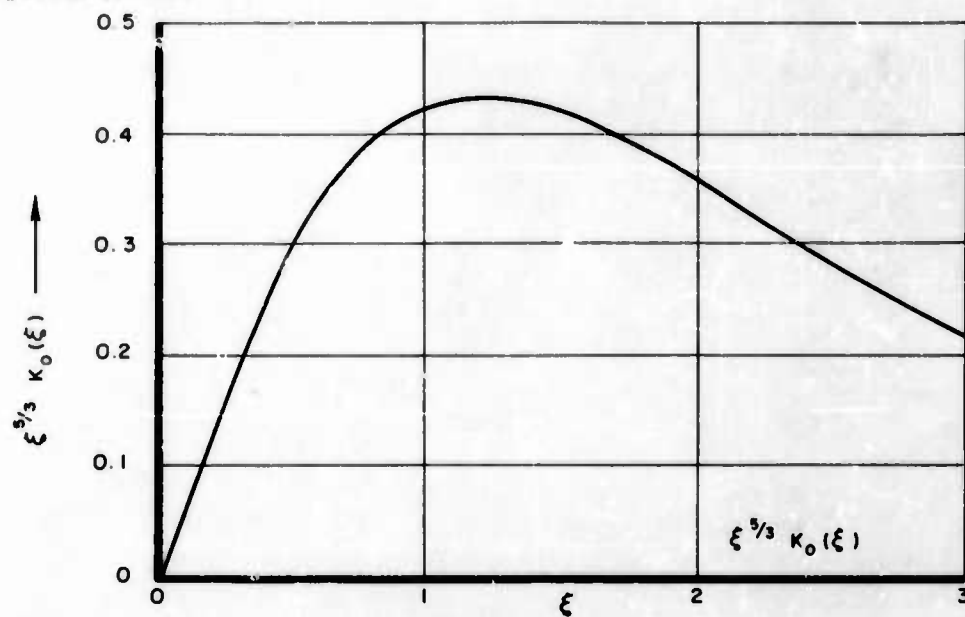


Figure II-9.

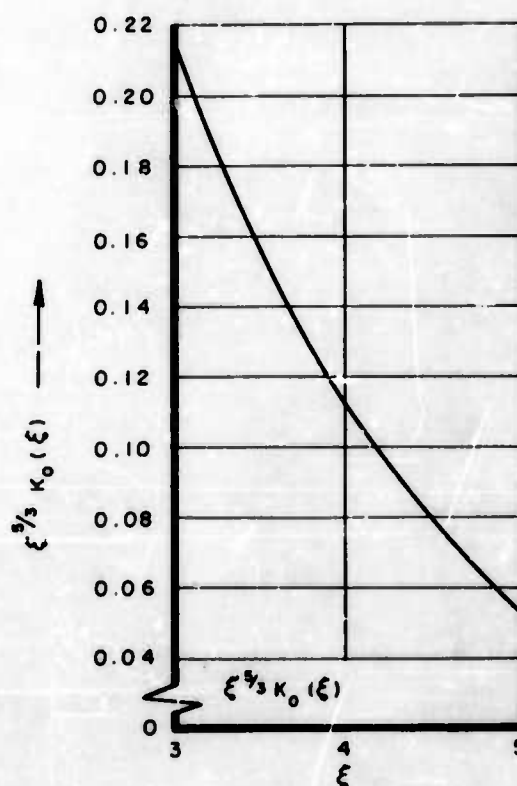


Figure II-10.

APPENDIX III

PRESSURE DROP DATA AND MODIFIED CORONA WIRE TEST

A. VARIATION OF PRESSURE DROP WITH CURRENT

In the body of this report the friction factor, f_D , was compared with the charge number, N_{ρ_c} . Agreement was shown between the theory and the test data. A clearer relationship between the ion influences on flow and the charge density can be obtained by considering the variation of pressure drop with increasing corona current. Figures III-1, -2, and -3, present typical data taken from ASD-TDR-63-842. In these figures the pressure drop is plotted against the square root of the corona current.

Figure III-1 is based upon data taken for the exploratory sequence for air with the positive corona. At the lower Reynolds numbers the data points fall on straight lines indicating good agreement with the theory. In Figure III-2 data is plotted from another test sequence, which indicates an interesting phenomenon. The linear correlation is good, but it can be noted that, at the higher Reynolds numbers, a region of very low slope occurs at low current values. As current values increase, there is a linear increase at a greater slope. We interpret this phenomenon to indicate that a much larger charge density is required at the edge of the transition zone to make its presence felt in the flow and that there may be a critical value for the charge density before the action becomes effective. In Figure III-1, the general falling off of the rate of increase at the higher values of current may be due to localized discharge effects. This lower slope at the high currents may be due to corona heating of the stream, which would cause only a slight increase in pressure drop. The magnitude of the heating effects are considered in Reference 1.

Figure III-3 presents data for CO_2 with a positive corona. At the lower flow rates the linear characteristic is evident; at the higher flow rates, however, the effect of charge shows a pronounced nonlinear characteristic. Figure III-4 presents additional data for CO_2 at two widely separated Reynolds numbers and a wider range of current. At low currents and low N_{R_0} , the data of Figure III-4 compare well with Figure III-3. At high N_{R_0} , the ion effects are still present but the curve is nonlinear throughout its range.

All of the figures indicate excellent correlation in the laminar flow regime at the lower values of current. In this region the theoretical predictions are adequately substantiated by the test data.

B. TESTS WITH MODIFIED CORONA WIRE END CONDITION

A brief retest of the corona wire was made because of considerable discussion over the drift motion of the ions. It had been suggested that the ions would merely drift downstream slightly due to the stream velocity and that a local increase in current at the outlet of the pipe at the outer electrode would occur. To determine whether the end conditions of the corona wire and pipe were significant, an insulating tubing was inserted over the corona wire and extended 1-1/4 inches in from the outlet of the pipe. Data were taken for CO_2 at a range of currents and Reynolds numbers. No changes to the charge phenomenon reported in ASD-TDR-63-842 were observed. It is concluded from this test that the exact end conditions for the corona discharge are not necessarily critical for the phenomenon to occur.

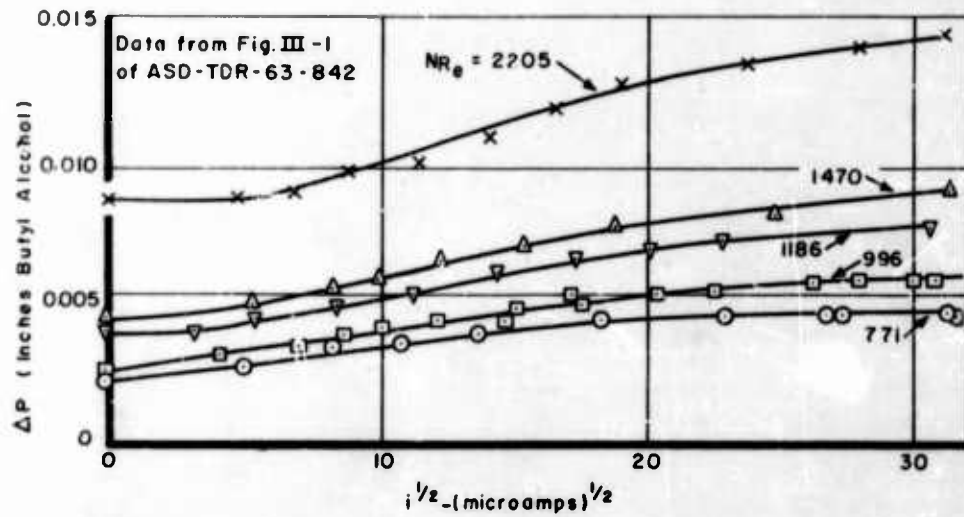


Figure III-1. Pressure Drop vs. Corona Current. Exploratory Sequence for Oxygen, Wire Positive

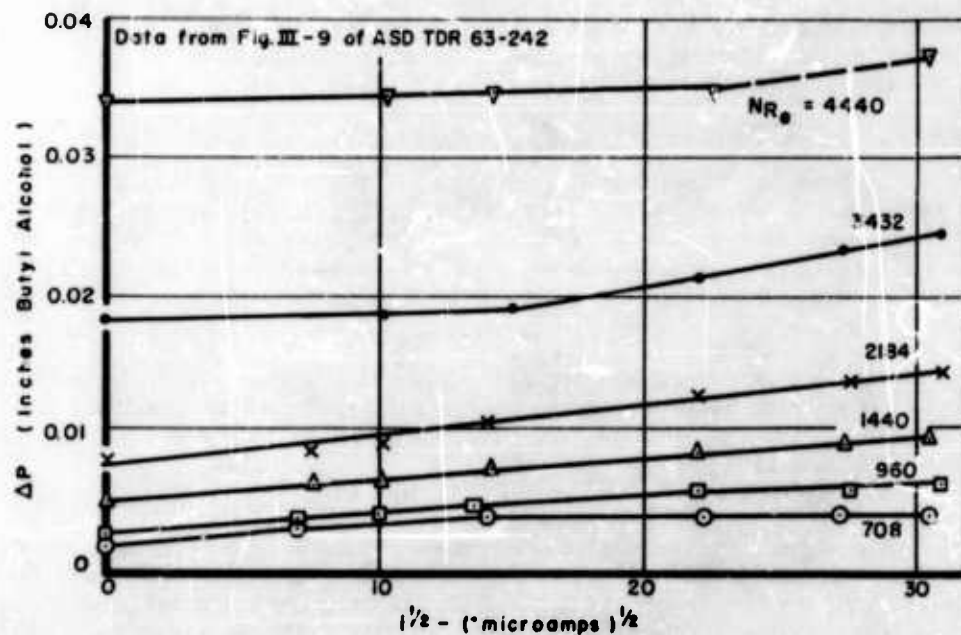


Figure III-2. Pressure Drop vs. Corona Current. Exploratory Sequence for Air, Wire Positive

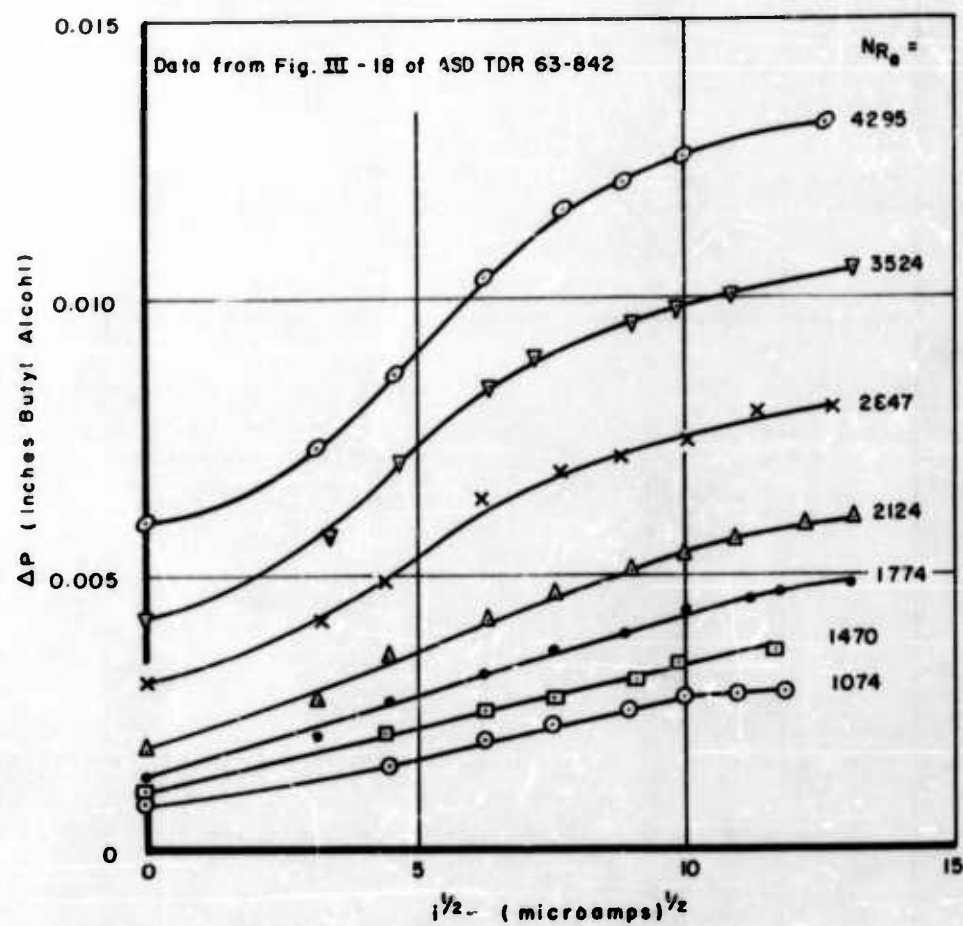


Figure III-3. Pressure Drop vs. Corona Current for CO_2 , Wire Positive

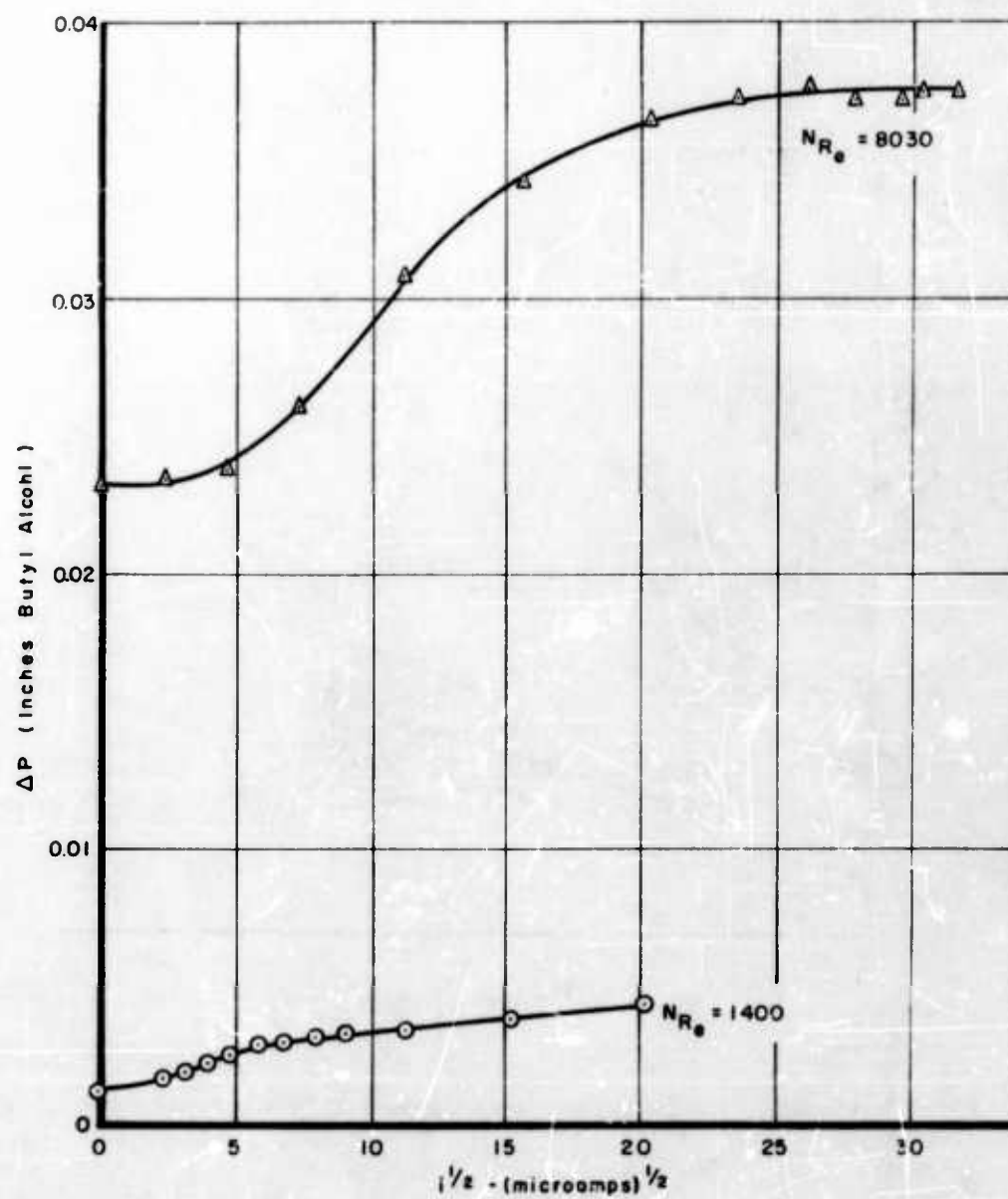


Figure III-4. Pressure Drop vs. Corona Current for Stored CO_2 , Modified Positive Wire

APPENDIX IV

COMPARISON WITH STUETZER'S PAPER

Following completion of the body of this report, the author became aware of the possible similarity between the phenomenon discussed by Stuetzer in his paper, "Apparent Viscosity of a Charged Fluid," Reference 12, and the phenomenon discussed herein. Stuetzer, in his work with ionized gases, discusses the apparent viscosity of a charged fluid. The initial stages of Stuetzer's analysis are remarkably similar to those of the analysis presented in this report, although the two research efforts were conceived and conducted completely independent of each other.

Stuetzer starts with the same basic electric field and fluid equations* and places a condition on the current that:

$$i_z = \ell \int_{-h}^h \rho_c (w + KE_z) dy \quad (198)$$

The current, i_z in Equation (198), is the net current in the axial direction. If i_z is not zero, there is a net charge flow down the tube, and a corresponding "corona-wind" pressure rise can occur along the pipe due to this charge motion.

Using Equation (49):

$$J^j = \rho_c (u^j + KE^j) \quad (49)$$

and the mean velocity defined by:

$$w_m = \frac{1}{2h} \int_{-h}^h w dy \quad (199)$$

and substituting into Equation (11):

$$\mu \nabla^2 w - \frac{\partial p}{\partial z} + \rho_c E_z = 0 \quad (11)$$

Stuetzer obtains:

$$\frac{\mu d^2 w}{dy^2} - \frac{\partial p}{\partial z} + \frac{i_z}{2h\ell K} - \frac{|\rho_c|}{2hK} \int_{-h}^h w dy = 0 \quad (200)$$

where $|\rho_c|$ is the absolute value of the charge density. Integrated, this becomes Stuetzer's Equation (11):

$$w_m = - \frac{h^2 \left(\frac{\partial p}{\partial z} - \frac{i_z}{2h\ell K} \right)}{3 \left(\mu + |\rho_c| \frac{h^2}{3K} \right)} \quad (201)$$

*The symbols used in Stuetzer's paper have been changed to conform to those used here.

The term containing i_z is the "corona wind" pressure rise term. For $i_z = 0$, this expression becomes identical to Equation (94) for parallel plates.

Likewise, Stuetzer derives two expressions for apparent viscosity for flat plates and round tubes:

Flat Plates

$$\mu_E = \mu + \left(|\rho_c| \frac{h^2}{3K} \right) \quad (202)$$

Round Tubes

$$\mu_E = \mu + \left(|\rho_c| \frac{h^2}{8K} \right) \quad (203)$$

These equations are identical to the mean value approximations given by Equations (180) and (181). Stuetzer also calls attention to the similarity of this type of flow to Hartmann flow of MHD and draws an interesting comparison with the effective viscosity increase in both types of flows.

The analysis given in the body of this report using the mean value of the body force leads to the same value of apparent viscosity as Stuetzer obtained by his method. The two approaches are similar, but the techniques used to introduce the average value are different. In discussing limitations on the effect of the ions on the flow, Stuetzer indicates that the time required for the fluid to flow down the length of the pipe must be short relative to the time required for the charge to change its lateral distribution. In the initial hypothesis, for typical values of mobility and field, Equation (1) indicated a cross channel mean speed of the order of 100 m/sec, while the speed down the pipe was of the order of 1 m/sec. Stuetzer's criteria are:

Transit time down the channel, t_z ,

$$t_z = 0 \left(\int_0^L \frac{dz}{w + KE_z} \right) \quad (204)$$

Transit time across the channel, t_y ,

$$t_y = 0 \left(\frac{\epsilon}{\rho_c K} \right) \quad (205)$$

Stuetzer states that his solution is valid only when $t_y \gg t_z$. Examining the transit time across the channel further, consider Equations (2), (3), and (30).

$$v = KE_y$$

Since

$$\begin{aligned} \frac{\partial E_y}{\partial y} &\gg \frac{\partial E_z}{\partial z} \\ \frac{\partial E_y}{\partial y} &\approx \nabla \cdot \vec{E} = \frac{\rho_c}{\epsilon} \end{aligned} \quad (206)$$

Therefore:

$$\frac{dv}{dy} = \frac{K \rho_c}{\epsilon} \quad (207)$$

Assuming a constant space charge:

$$v = \frac{K \rho_c}{\epsilon} y + c \quad (208)$$

Let:

$$v = 0, \text{ at } y = 0$$

$$v = \frac{K \rho_c}{\epsilon} y \quad (209)$$

$$\frac{dy}{y} = \frac{K \rho_c}{\epsilon} dt \quad (210)$$

$$t = \frac{\epsilon}{K \rho_c} \ln y + c. \quad (211)$$

Let:

$$t = 0, \text{ at } y = 0$$

$$t_y = \frac{\epsilon}{K \rho_c} \ln y \quad (212)$$

For the case discussed above:

$$t_z = 0 \text{ (1 sec)}$$

$$t_y = 0 \text{ (} 10^{-4} \text{ sec).}$$

Since $t_y \ll t_z$, it appears that Stuetzer's criteria may not be fully applicable. One possible explanation is that in the region between the sheaths occurring at each electrode, the local field may be low enough that the local transverse ion drift velocity is very low and the transit time in this region may be significantly longer.

From an overall comparison of Stuetzer's paper and this report, it appears that the mean value approach is similar to that presented by Stuetzer. The broader interpretation used in this study, that:

$$E_z = f\left(\frac{w}{K}\right)$$

or

$$E_z = -\frac{w}{K}$$

was not considered by Stuetzer. Consequently, he limits his work to situations where the velocity profiles do not change, whereas our test results indicated severe distortions of the velocity profiles. The Stuetzer paper is an excellent work, however, and the author regrets not recognizing its applicability to the charge phenomenon sooner since it adds solid substantiation to the hypothesis used in this report.